12-2009

IDENTIFYING THE OPTIMUM PROCESS PARAMETERS OF PRECISION GLASS MOLDING FOR ASPHERICAL LENSES

Waqas Iqbal
Clemson University, waqasi@clemson.edu

IDENTIFYING THE OPTIMUM PROCESS PARAMETERS OF PRECISION GLASS MOLDING FOR ASPHERICAL LENSES

A
Thesis Presented to the
Graduate School of
Clemson University

In Partial Fulfillment
Of the Requirements for the Degree
Master of Science
Mechanical Engineering

By
Waqas Iqbal
December 2009

Accepted by:
Dr. John C. Ziegert (Committee Chair)
Dr. Paul Joseph
Dr. Joshua Summers
Dr. Lonny Thompson

ABSTRACT

The purpose of this research is to determine the optimum process parameters for the Precision Glass Molding (PGM) Process using Manufacturing Design, Design of Experiments and Metrology (for measuring the geometry of lenses). First, a custom machine is designed and manufactured which can carry out Precision Glass Lens Molding Experiments. This machine is then modified to improve temperature, position and force control. A literature review is performed to obtain data for process parameters that have been used in previous PGM studies. The collected data is then used in Design of Experiments to create twenty seven experiments that determine the optimum process parameters. The lenses produced from these experiments are measured for surface form and surface roughness. This research also addresses the issues with PGM which include wear of mold coating, sticking of glass on mold cavities and repeatability of form of the lenses produced. This project resulted in data that could be used in validating PGM finite element simulations and the PGM experiments are able to produce good quality lenses. Three experiments are chosen for optimum process parameters. One experiment has the optimum (minimum) cycle time for PGM, the second experiment has the optimum process repeatability and the third has optimum process parameters for reducing power error on the aspherical side of the lens.

DEDICATION

This work is dedicated to my father Iqbal, my mother Farhana, my brother Wajih, my sister Misha and all of my wonderful friends. My father has been my greatest role model. His excellent academic achievements have always pushed me to unlock my potential. He has been an excellent guide for me throughout my academic career and without him none of this would have been possible. My mother, brother and sister have always been available whenever I had to relieve stress from my research. I have had a wonderful time with my friends who are mostly undergraduate students in engineering. Helping them in basic engineering courses has given me the confidence to achieve my life goals. To everyone who have helped me in achieving my goals, thank you everyone.

ACKNOWLEDGEMENTS

With great respect, I would like to thank my advisor, Dr. John Ziegert. It is an honor for me to work with him. He has always had patience and confidence in me, even when I had none. He is the most experienced and intelligent engineer I have worked with. He is also the most kind and humble professor I have known at Clemson. He has given me great inspiration and constructive criticism which has shaped the way I think and act. I have always admired the method he used for solving problems, by first making the problem simple and then solving the problem step by step. He has given me so many opportunities and I have learned so much from him and I could never thank him enough.

I would like to thank Dr. Paul Joseph. I enjoyed his elasticity course in which he taught many concepts that helped me in understanding the behavior of glass in different phases.

Also, with great admiration, I would like to thank Dr. Joshua Summers. I have learned many basic concepts regarding design and manufacturing from the courses that he taught me. I have always liked his frank attitude towards all students. I have used many of the design concepts from his courses in designing parts for the molding machine.

I would also like the privilege to thank Dr. Lonny Thompson. He has always been available whenever I need his help. His expertise in Design of Experiments gave me a better understanding of the Taguchi Method.

I am grateful to Dr. Yazid Tohme at Moore Nanotechnology who is responsible for designing and building the machines that are used in this Project. Without his expertise in machine design and his understanding in controls, this project would have been impossible. I have learned a lot about Precision Glass Molding and the Molding

Machine from him. He has always been available whenever there were any problems with the molding machine.

I am also grateful to Peiman Mosadegh. He has been a great colleague and I have enjoyed the time that I have spent with him. Our discussions about the properties of glass, glass molding and glass friction have helped me throughout my research and will also help in the future. I have also gained experience in machine design from all the modifications that we made to the Molding Machine for Peiman's glass friction experiments.

TABLE OF CONTENTS

Page

Table of Contents (Continued)

Page

LIST OF TABLES

LIST OF FIGURES

List of Figures (Continued)

CHAPTER 1

INTRODUCTION

There are many applications for aspherical optical elements, including CD/DVD players, digital cameras, cell phone cameras and many more. Most of these applications currently use polymer based lenses because they are easily manufactured on a large scale and have low cost. When the optical properties of polymer are compared with glass, then glass has superior optical properties, including stability, uniformity and lower stress induced birefringence. For this reason the demand for precision glass optics is increasing. Polymer based lenses have three major disadvantages [1]. The first disadvantage is that they are sensitive to scratches. Another disadvantage is that polymer based lenses are soft and there is no practical method to clean them. The greatest disadvantage of polymer based lenses is that they expand and contract more than glass when exposed to temperature changes. When the lenses expand and contract the user has to adjust the focal length repeatedly to reduce any aberrations. Since, glass lenses are superior to polymer lenses, a new method for manufacturing precision optical lenses has been devised which is called Precision Glass Molding (PGM). In PGM, the finished lens is compression molded to final dimensions and requires no subsequent finishing or polishing. However, due to differences in thermal expansion between the mold material and glass, combined with the time and temperature dependent material properties of glass, the geometry of the molded lens is generally different from the geometry of the mold used to produce it. The primary disadvantage to PGM is the difficulty involved in determining a mold geometry that will give the correct geometry for the finished lens. This is currently done in an iterative process that requires many molds to be produced in order to find the proper geometry. The ultimate goal is to solve this problem by creating simulation software which will

eliminate the iterative process of obtaining the correct mold geometry. To predict the final shape of the optic the simulation will need the mold geometry, process parameters and glass material. The objective of this project is to determine the process parameters needed for the simulation when mold geometry and glass material is given.

1.1 Motivation

The motivation for this project comes from the fact that traditional lens manufacturing methods are expensive and time consuming. The traditional method for lens manufacturing includes a series of material removal processes [2, 3, 12, 13, 16, 19]. First a glass blank is ground to the desired lens geometry. After this the lens goes through hand polishing and small pad zonal polishing. This is a time consuming process and requires constant inspection and evaluation of the lens. The typical cycle time for producing a lens using this method ranges from two to three hours. This method also produces varying degrees of surface deviation which affects the overall performance of the lens. Figure 1.1 (next page) shows the difference in the traditional and glass molding method for manufacturing glass lenses.

1.2 Benefits of PGM

Traditional methods for glass lens manufacturing have been successful, but molding of lenses is a superior method for obtaining large volumes of lenses with minimal surface deviations [2, 3, 14, 17]. Standard cycle times for aspheric molded lenses are in the range of 15 to 25 minutes. This lower cycle time potentially enables a high volume manufacturing method. In addition to this multiple optical elements can be molded simultaneously, enabling even higher production volume compared to the traditional manufacturing process.

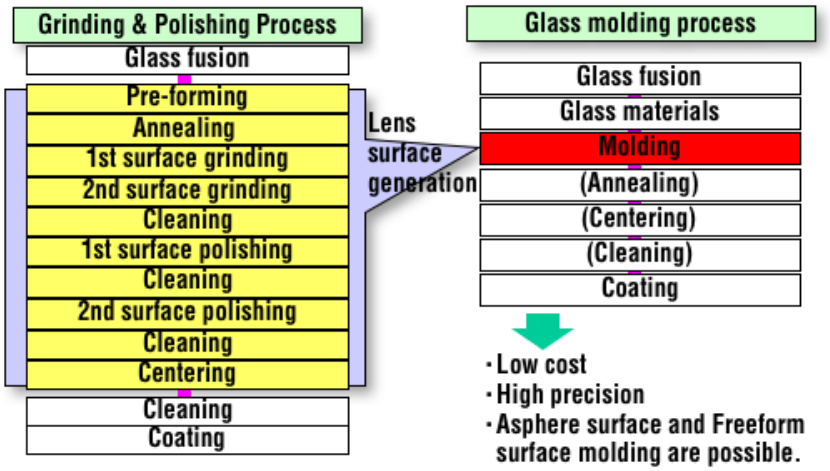

Figure 1.1: Comparing Traditional (Grinding & Polishing) and Molding Method for Manufacturing Glass Lenses [2]

1.3 Steps involved in PGM Process

The precision glass molding procedure can be divided into five main steps as shown in Figure 1.2.

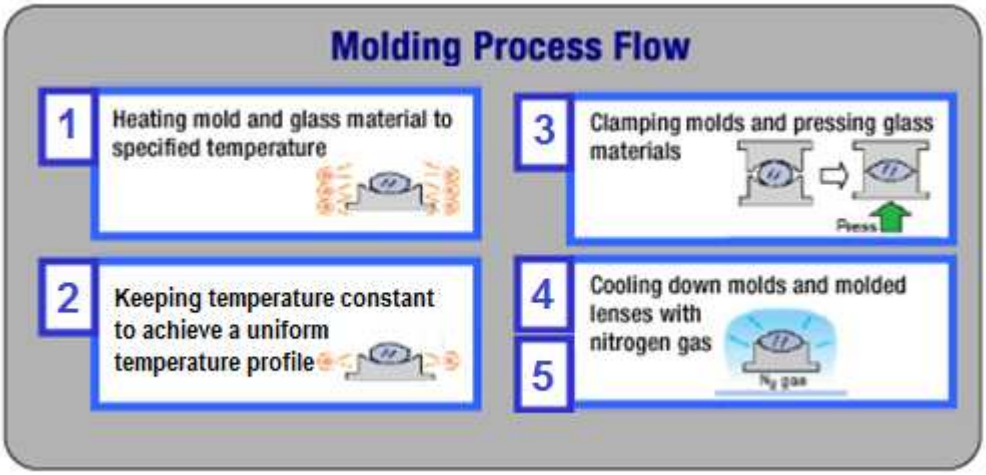

Figure 1.2: Steps Involved in PGM [2]

The first stage is the heating stage [3, 8, 10, 11, 12, 13, 15, 16, 17, 20]. First the glass ball is placed in position. Then, the chamber is vacuumed and the remaining oxygen is removed by purging the chamber with nitrogen gas. The goal of this step is to remove oxygen gas from the chamber to prevent oxidation of the mold at high

temperatures. After purging with nitrogen, the glass gob and mold are heated until their temperature reaches slightly above the glass transition temperature of the glass material. Nitrogen is purged at a slow rate throughout all five steps of the molding process to prevent oxidation of molds.

The second stage is the soaking cycle [3, 8, 10, 11, 12, 13, 15, 16, 17, 20]. During this stage the temperature of the glass is kept constant to ensure that the entire glass gob is at the same temperature and has consistent material properties throughout. After reaching the soaking temperature the glass becomes visco-elastic, which means that it becomes moldable.

The third stage is the compression cycle [3, 8, 10, 11, 12, 13, 15, 16, 17, 20]. During the compression cycle a constant force is applied to the mold halves and the glass gob is compressed until it takes the shape of the cavities of the top and bottom mold. The temperature during the compression stage is the same used for the soaking cycle.

Once the compression stage is over, the cooling cycle begins. The cooling cycle is divided into two parts. First there is a slow cooling cycle (fourth stage), and then there is a fast cooling cycle (fifth stage) [3, 8, 10, 11, 12, 13, 15, 16, 17, 20]. The slow cooling cycle helps to prevent any internal stresses in the lens that might cause distortion or cracking. This slow cooling process is also called annealing. If glass is not annealed then it may be liable to crack or shatter due to a small temperature difference or mechanical shock. Nitrogen gas is used to facilitate convective heat transfer during the slow cooling cycle and the heating elements may also be activated during this cycle to help in maintaining a constant cooling rate during the slow cooling stage.

The final stage is the fast cooling stage. In this stage nitrogen is introduced to the chamber at a high flow rate and the heating elements are turned off. The goal of this stage is to return the mold and lens to a temperature where the lens can safely be removed from the mold. The PGM process changes the index of refraction of glass due to the thermal treatment but the cooling stages help in bringing the value of the refractive index close to the original value.

1.4 Issues with PGM

The main issue with PGM is the difficulty involved in producing molds which will result in geometrically correct optics. The reason for this difficulty is the deformation that occurs in the mold and the glass at high temperatures. During cooling, the dimensions of both the mold cavity and glass change due thermal expansion. In addition to this the mechanical properties of glass, i.e. elastic modulus, visco-elastic parameters, etc., change with temperature. The main result is that a mold cavity with a given geometry will normally not produce an optical element of that exact same geometry. Currently, the technology for predicting the geometry of a glass lens is not available when the mold geometry, lens material and processing parameters are given. For this reason, the current method for determining the correct mold geometry is an iterative process where an initial mold geometry is used to mold optical elements. Then, the form error between the mold geometry and the molded optical element is measured. New molds are produced to correct for these form errors until a satisfactory mold shape is discovered.

1.5 Objective of this research

This research is part of a larger project in which the objective is to create simulation software that will predict the glass lens geometry when the mold geometry, lens material and process parameters are given. The objective of this research is to

determine the process parameters that can be used for compression molding of BK-7 glass, and to create a database of how molded lens geometry changes with changes in the processing parameters to be used to verify the simulation models. For the selected optimal process parameters, we will also quantify the process repeatability.

To determine the process parameters a literature review was performed to find any available data on the cycle times, temperatures and forces used for PGM. Once all of the data was assembled, a set of experiments were generated using design of experiments. All of the experiments were performed to determine process parameters that would provide the minimum form error between the mold and geometry of the molded optic. The data from these experiments are then used for the development of the computer simulation program. Other objectives of this project are to study issues with PGM including the wear of the coatings used on the molds, sticking of the glass on the molds, and the repeatability of the form of lenses produced by the molding process.

CHAPTER 2

LITERATURE REVIEW

This chapter will review the current knowledge available in Precision Glass Lens Molding, and gather information about the process parameters used in glass lens molding that will help in designing experiments to determine optimum cycle time for glass molding and get repeatable results.

2.1 Recent research in PGM

Yi designed a machine to provide the flexibility to run a variety of molding experiments for scientific research [3]. He used a 2 KW furnace for the heating system and the entire machine was built around the thermal heating source. The frame of the machine is fully symmetric about the molding axis so that heat is transferred into the mold symmetrically during the heating process. Yi mentions that typically the molding temperature for molding is slightly above the glass transition temperature where the viscosity of the glass is decreased to a value in between $10^{7.6}$ Poise and 10^{9} Poise [4]. The glass transition temperature for BK7 is 557 ˚C [5]. Figure 2.1 shows the viscosity (log scale) of BK7 glass at different temperatures. According to the figure the molding temperature for BK7 glass can be in the range of 670 ˚C to 695 ˚C. If the molding temperature is above 700 ˚C then the mold material (tungsten carbide) might face oxidation.

In another paper Yi mentions that he used a molding temperature of 685 ˚C for BK7 and a cooling rate of approximately 1.5-2 ˚C per second [4]. Using these parameters he was able to get a maximum form deviation of 5 microns between the mold and lens. He also found scratches on the surface of the lens that were 30 nanometers deep, that were reproduced from the mold surface onto the lens surface.

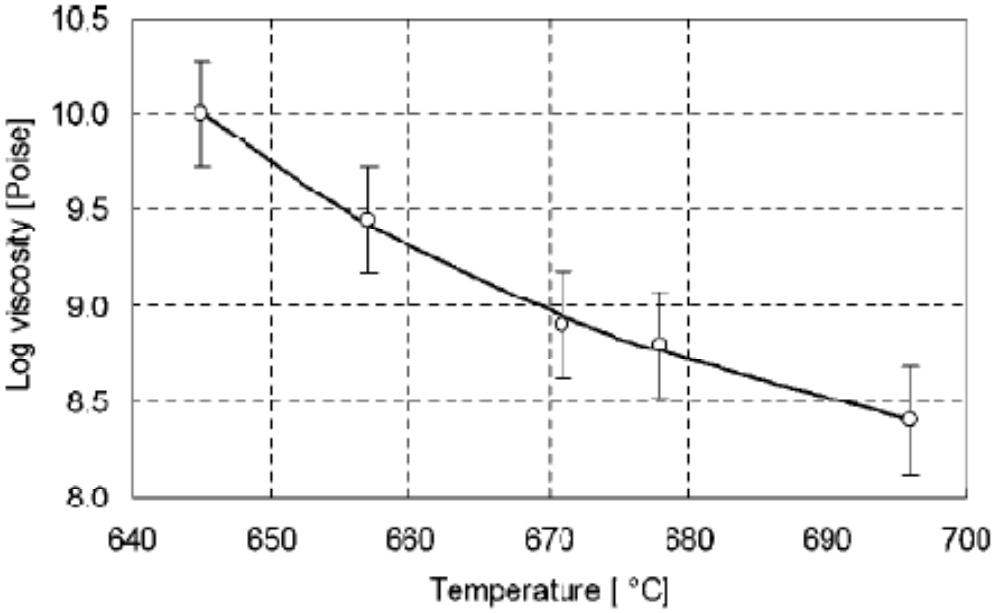

Figure 2.1: Viscosity of BK-7 Versus Temperature, [3]

Tsai concludes that a sufficient molding temperature would be 30-50 ˚C above the glass transition temperature [4]. In his experiments he did not use BK7 glass, but he used S-FPL52 glass which has a lower glass transition temperature of 445 ˚C. For S-FPL52 glass he used a molding temperature of 475 ˚C. This lower molding temperature gave him slower wear on the surface of the molds being used. Since the glass transition temperature for BK7 is 557 ˚C, according to Tsai its molding temperatures should be in between 587 ˚C and 607 ˚C.

Yi and Huang performed molding experiments using K-GP 325 glass, which has a glass transition temperature of 285 ˚C [7]. Figure 2.2 shows the process parameters that were used for the molding experiment. Since K-GP 325 has a lower glass transition temperature, the molding temperature used was 325 ˚C, which is 40 ˚C above the glass transition temperature. It can be seen that forces were applied at two different stages of the process. First, the force is applied during the pressing cycle, and then the slow

cooling stage starts. Another force is applied during the fast cooling stage and the magnitude of the force is half of what was used in the pressing cycle.

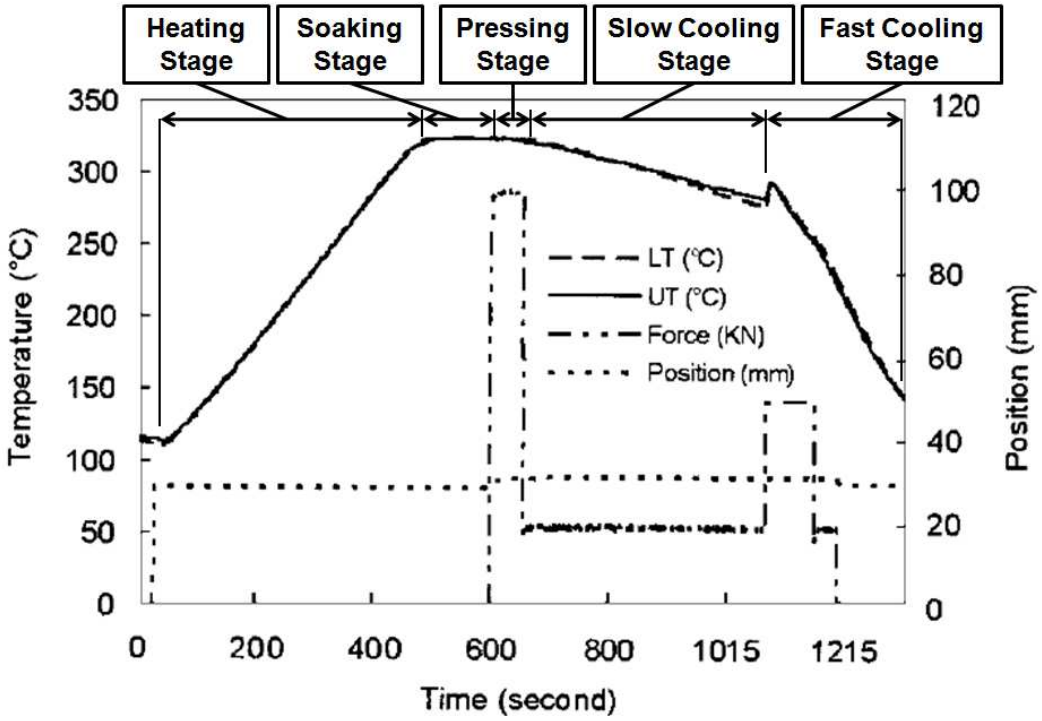

Figure 2.2: Lens Molding Process Parameters for KG-P 325, [7]

Klocke created a 3D simulation for PGM using finite element analysis to predict the shape of the lens after the molding process. In the simulation he used the process parameters as shown in Figure 2.3 [8]. It can be seen that the second force is not applied during the 2nd fast cooling cycle [8], but instead the second force is applied during the 1st slow cooling cycle. Therefore, depending on the characteristics of the glass being used, the second force can be applied in either the 1st slow cooling cycle or the 2nd fast cooling cycle.

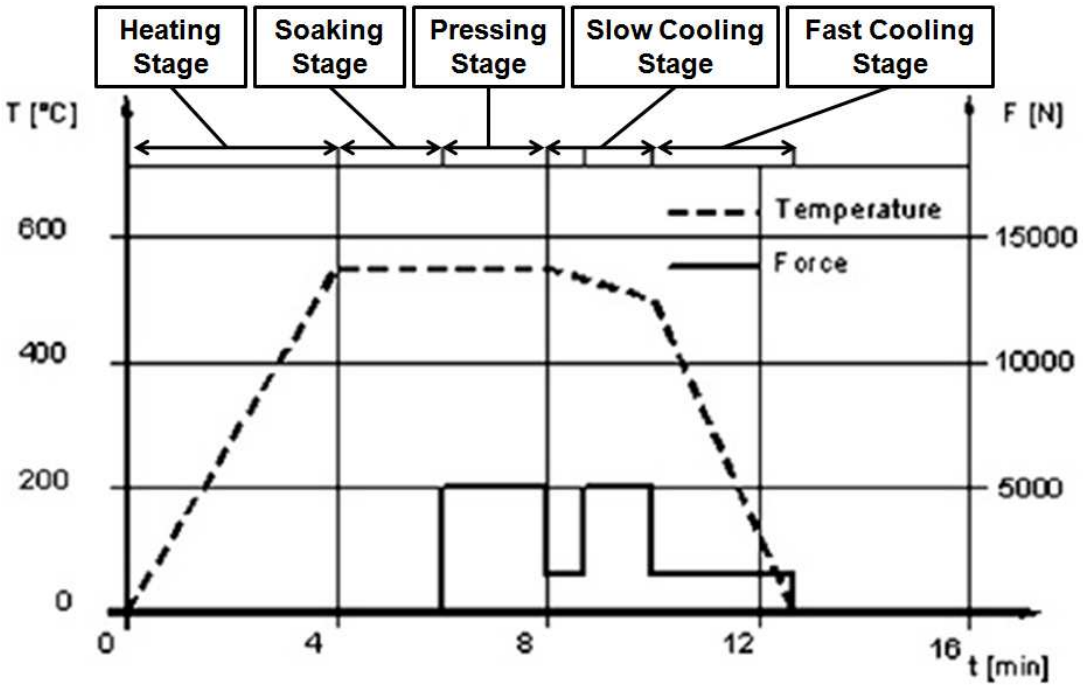

Figure 2.3: Molding Process Parameters used for FEA, [8]

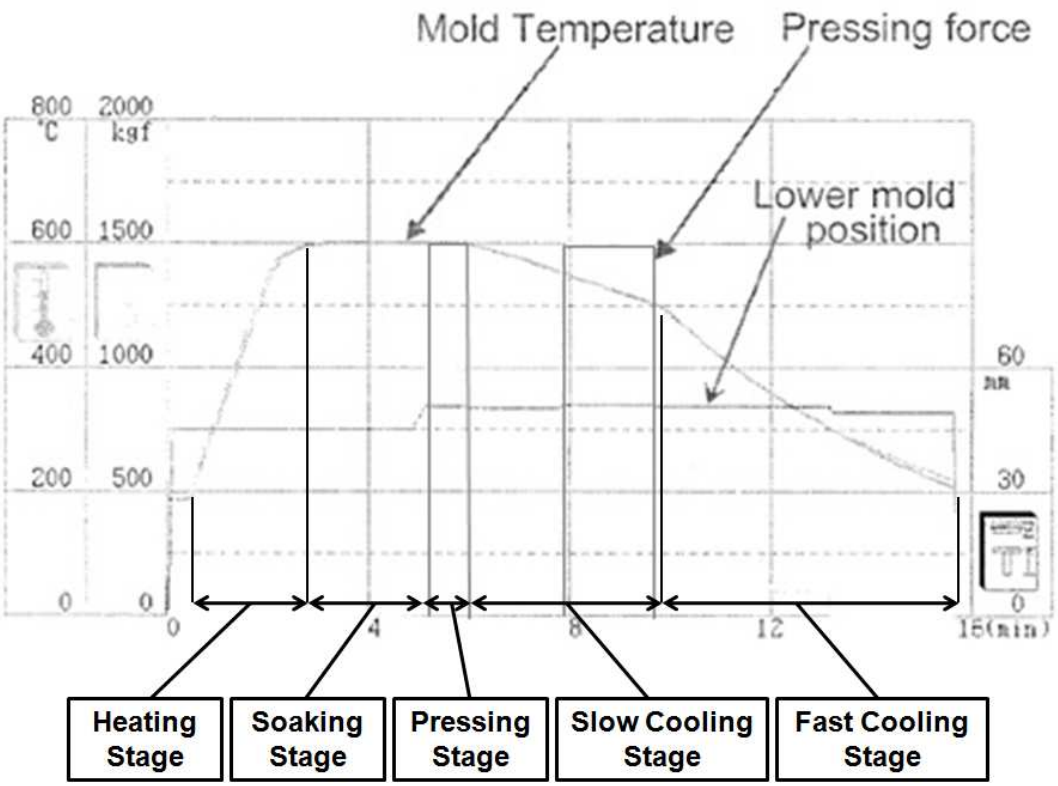

Figure 2.4: Molding Process Parameters used by Toshiba, [9]

Figure 2.4 is a plot of process parameters for PGM that was taken from a presentation of a Toshiba Molding Machine [9]. The second force in this case is applied in the end of the 1st slow cooling cycle. This plot also shows the position of the lower mold which increases as the force is applied. And as soon as the force is removed the position of the lower mold decreases in position.

Figure 2.5 shows the viscosity of BK-7 glass versus the temperature. The recommended molding temperatures are shown in the plot. According to Yi the molding temperature depends on the viscosity of glass [6]. If Yi's method is followed, then the molding temperature of BK-7 should be in the range of 650-720 ˚C. A few molding experiments were performed using BK-7 at these temperature, but bubbles would appear inside the glass. In PGM, if the molding temperature is high, then it would affect the life of the mold coating and if the molding temperature is low, then pressure will be applied on the molds during the pressing stage. Therefore, it was decided to use lower molding temperatures in the range of 587-607 ˚C.

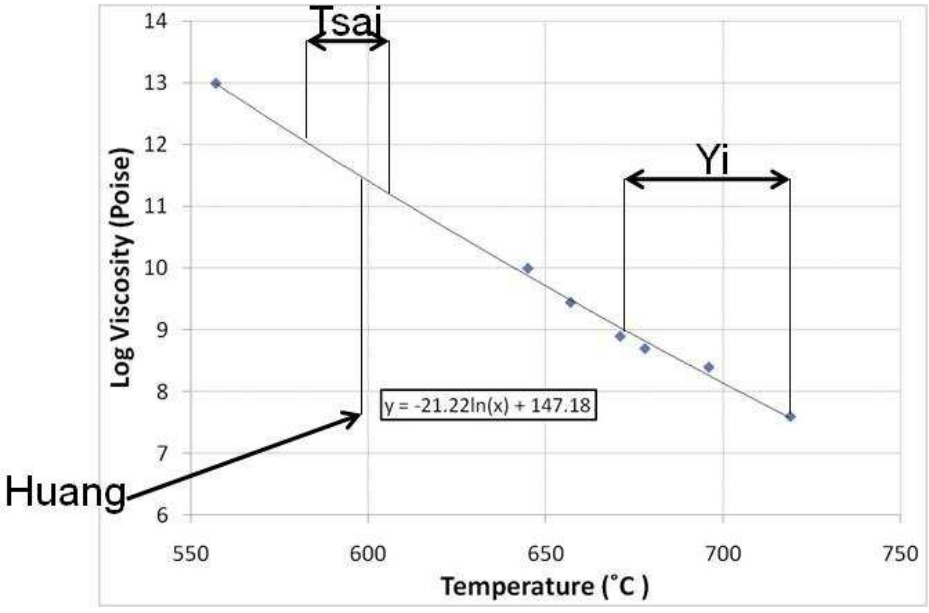

Figure 2.5: Determining Temperature Range for Molding Experiments

2.2 Process Parameters for PGM Process

Figures 2.2, 2.3 and 2.4 all show different process parameters because different glass materials, mold material and geometry and different molding machines are being used for each scenario. The glass material being used for this PGM project is BK-7 and tungsten carbide is the mold material. Therefore, the process parameters for molding BK-7 glass lenses need to be determined. First, the process parameters were defined by a set of variables. Figure 2.6 shows how these variables are defined. According to the data obtained from studying previous papers, a range for each variable was developed as shown in Table 2.1.

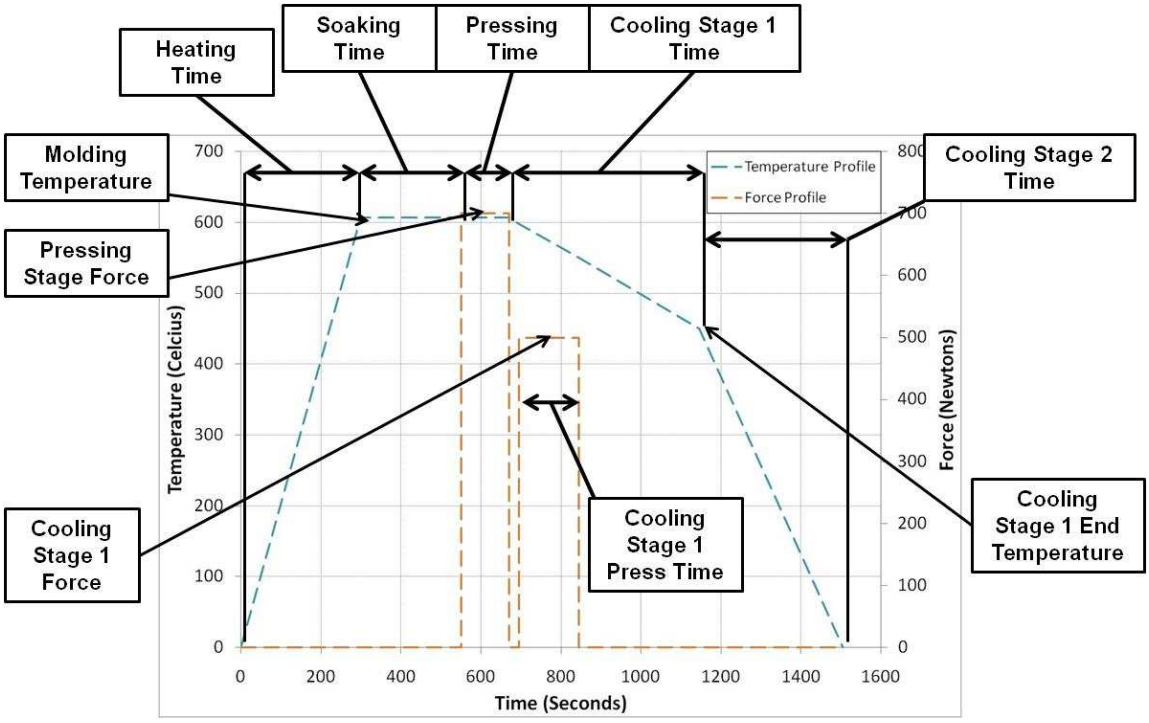

Figure 2.6: Variables to Define Process Parameters

It can be seen from table 2.1 that there are 10 different process variables that are used in the PGM. In this work, each of the variables is assigned three different values which cover a wide range of molding conditions. From these values a set of experiments was designed and conducted to determine how the lens geometry is affected when

process variables are changed. These experiments will also allow the determination of process parameters that give the lowest cycle time and process parameters that result in the least form error in between the mold geometry and the resulting lens geometry. Before further description of the experiments it is important to understand the design of the machine and how it functions. That is described in chapter 3.

Table 2.1: Process Parameters for Each Variable

	Minimum	Medium	Maximum
Heating Time (seconds)	200	250	300
Soaking Time (seconds)	120	185	250
Pressing Time (seconds)	60	90	120
Cooling Stage 1 Time (seconds)	120	210	300
Cooling Stage 2 Time (seconds)	180	270	360
Heating Temperature (degC)	587	597	607
Cooling Stage 1 End Temp (degC)	400	425	450
Pressing Stage Force (N)	300	500	700
Cooling Stage 1 Force (N)	100	300	500
Cooling Stage 1 Press time (seconds)	50	100	150

CHAPTER 3

DESIGN AND MODIFICATIONS OF PGM MACHINE

In order to run the required molding experiments a molding machine had to be designed that would have the flexibility and capacity for scientific research. A prototype glass molding machine was designed and constructed by Moore Nanotechnology Inc., sponsors of this work, and was used for this research. The machine provided by Moore did not provide all of the functionality required for this research, and therefore some modifications were implemented on the machine to enable more precise control of the process variables. Modifications were also made to the molding tools to improve the PGM process.

3.1 Machine Design

The objective of this machine is to have precise control over mold position, temperature and force so that a variety of molding experiments can be performed. The prototype machine was designed to have comparable performance to commercially available products and also have the flexibility for laboratory testing and process research. Figure 3.1 shows the glass molding machine and also an internal view.

The machine has a base dimension of 1 x 1 meter, a height of 1.8 meters and a mass of 998 Kg. In Figure 3.1, it can be seen that all the components of the machine are supported by four main beams. The upper portion of the machine includes the load cell, heating system, chamber and press actuator. The lower portion of the machine includes the motor, controllers and PLCs. Figure 3.2 shows an exploded view of the main components of the machine. The load cell being used in this machine has a capacity of 20,000 Newtons and is located at the top of the assembly. The chamber is made out of glass and is connected to the press actuator. There is a rubber sealing on top of the

glass chamber which seals the chamber when it is raised to the closed position. The press actuator moves up and down with the help of the motor.

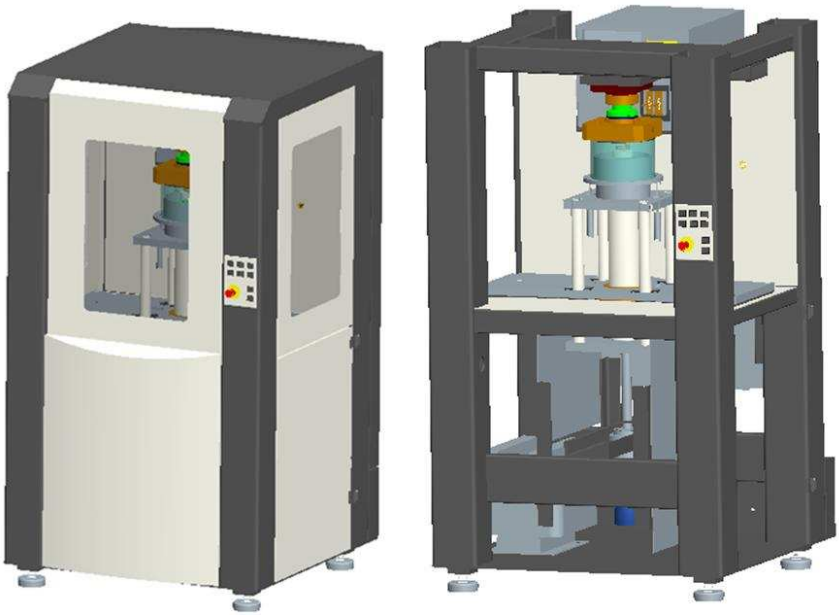

Figure 3.1: PGM Machine [21]

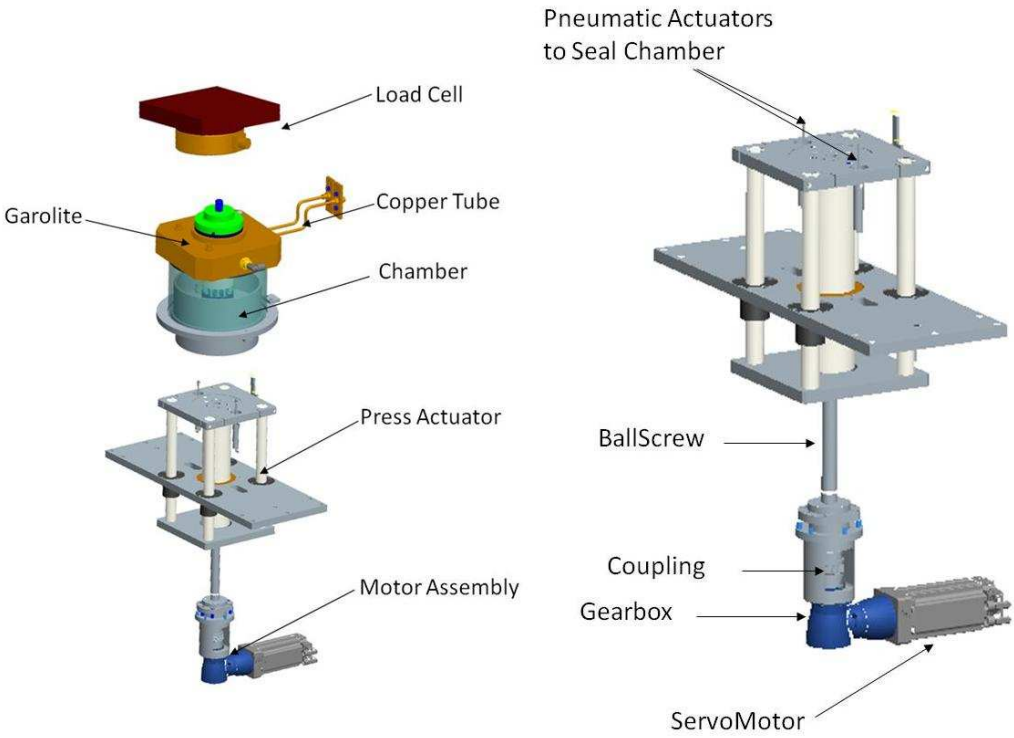

Figure 3.2: Exploded View of Main Components [21]

The pneumatic cylinders on the press actuator are used for closing and opening the glass chamber against the garolite part.

3.1.1 Position and Force Control

The servo motor is capable of delivering 6 Nm of torque. The gearbox has a ratio of 5:1 and the gearbox is attached to a 6 mm lead ball screw. The resolution of the encoder used for the position feedback is 0.12 micron. The resolution of the load cell is 0.3 Newtons and it is capable of measuring a maximum load of 22,000 KN. The machine is capable of applying a constant amount of force during the pressing stage of the PGM process. The force is controlled using a position controller with a PID (Proportional-Integral-Derivative) loop, which is closed with a force loop on top of the position loop. With this control architecture, the force error is transformed into a command to the position loop.

3.1.2 Temperature Control

The heat is supplied using an induction heater. An induction heater consists of an electromagnetic coil through which a high-frequency alternating current (AC) is passed. The induction coil is made of copper tubes and water is passed through them to keep them from melting during the heating process. Induction heating is the process of heating an electrically conducting object by electromagnetic induction, where a time-varying electromagnetic field induces eddy currents within the metal and resistance leads to resistance heating of the metal. In our case the electrically conducting objects are the molds.

The temperature is controlled using a PI loop. If the temperature error (commanded temperature minus measured temperature) is positive then the induction heater turns on and supplies heat to the system as the temperature error approaches

zero. If the temperature error is negative then the induction heater is turned off and the part cools by natural conduction, convection, and radiation.

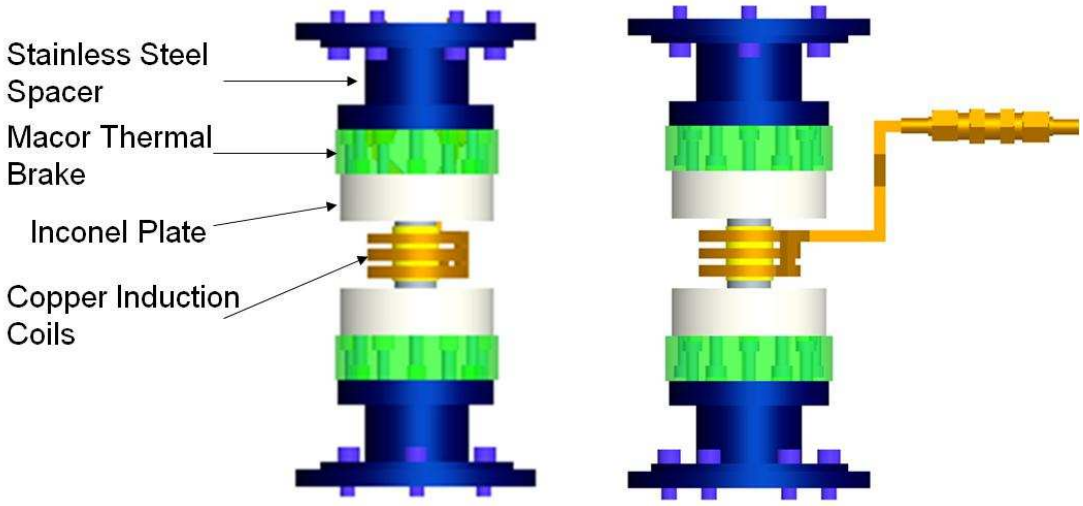

Figure 3.3: Front and Side View of Upper and Lower Plates and Induction Coils [21]

3.2 Issues with Preliminary Design and Solutions

The prototype machine delivered by Moore had many issues which prevented successful molding experiments. Several modifications to the machine were carried out to enable it use for this research.

3.2.1 Temperature Measurement

Initially, mold temperature was measured using thermocouples that were placed at an incorrect position. The temperature is measured using two K-type thermocouples. Each thermocouple is placed in the center of the upper and lower inconel plates and is able to measure temperatures up to 1000 ˚C. The thermocouples were placed such that they contacted the back surface of the top and bottom molds approximately 7.4 mm away from the glass that was being pressed as shown in figure 3.4. During initial testing of the machine, a third thermocouple was used to directly measure the temperature of

the glass and compare to the mold back temperatures. It was found that a substantial temperature gradient existed through the mold, creating a temperature difference between the top and bottom surface of the molds of more than 100 ˚C. Since one goal of this research is to study the effect of glass temperature on the molding process, it was necessary to obtain better temperature measurements closer to the glass being molded.

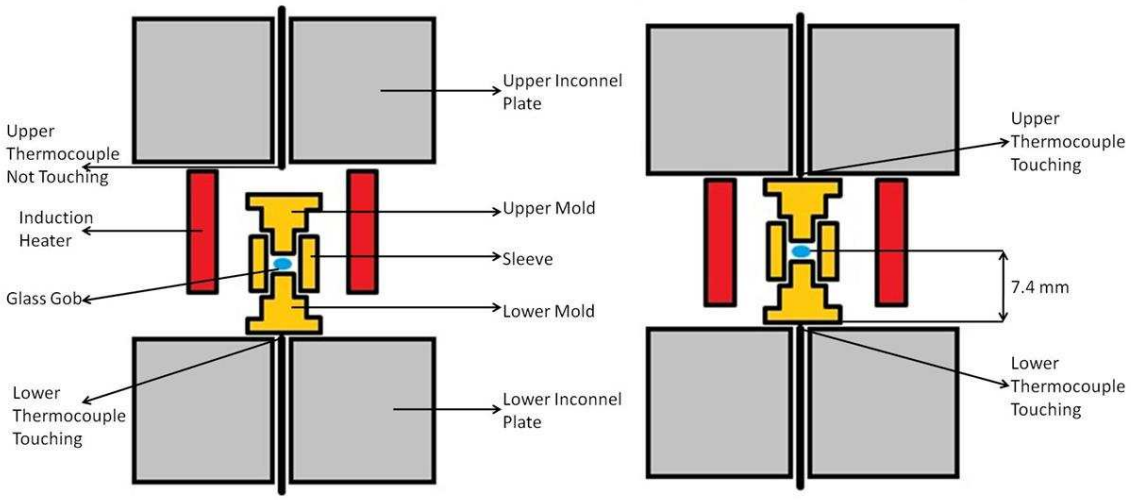

Figure 3.4: Cross Sectional View during Heating and Soaking Stages (left), Cross Sectional View during Pressing Stage (right), (not drawn to scale)

3.2.2 Solution for Temperature Measurement

The temperature measurement issue was solved by designing and fabricating a spring loaded thermocouple system that would touch the molds at all time throughout all the molding stages. To more accurately measure the correct glass temperature, blind holes were made in the center of the molds as shown in figure 3.5, to decrease the distance in between the glass and thermocouple to 4 mm.

The fixture holding the stationary thermocouple was replaced by a spring loaded thermocouple assembly. The spring pressed against the inconel plate and a ceramic tube with two holes was used to allow the thermocouple leads to pass without contacting

the surrounding metal surfaces. These modifications to the original design enable the thermocouples to measure temperatures more accurately and closer to the glass.

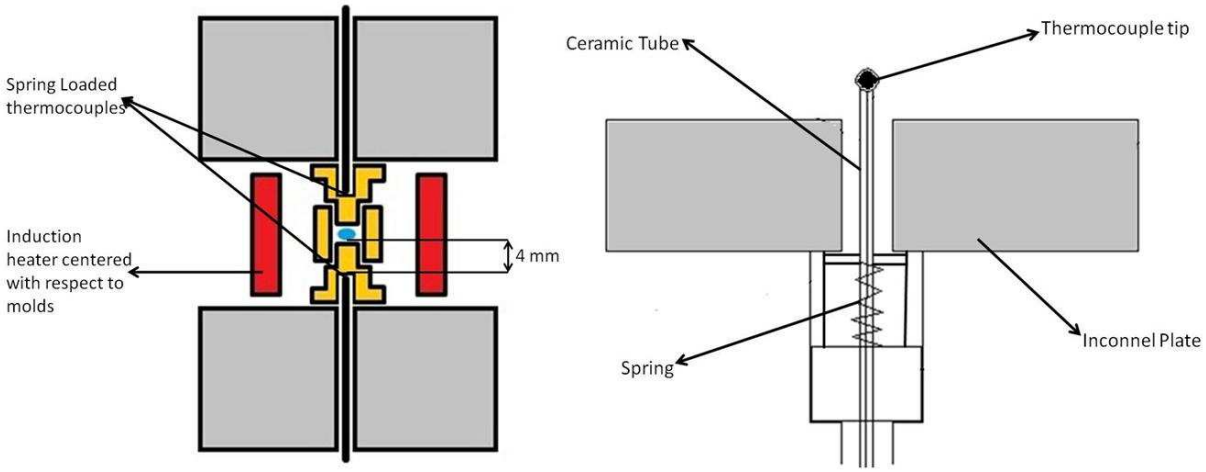

Figure 3.5: Cross sectional view for entire molding experiment (left), Concept behind spring loaded thermocouple (right), (not drawn to scale)

3.2.3 Induction Heater Position

Another issue was the position of the molds during the heating and soaking stages and the position of the induction heater. As shown in figure 3.4 (left), it can be seen that during the heating cycle the upper thermocouple is not touching the upper mold. This gap (0.25 mm) was provided to allow for thermal expansion of the molds. If there was no gap then the molds would expand due to heat and press against the upper plate resulting in large uncontrolled forces on the glass during the heating and soaking stages. A gap of 0.25 mm was found to be sufficient to avoid pre-mature pressing of the glass before the pressing stage. Due to this gap, the upper thermocouple was not touching the mold during the heating and soaking stages, and therefore the thermocouple would give an incorrect temperature measurement that was substantially less than the actual mold temperature. At the start of the pressing cycle the top thermocouple would come into contact with the upper mold resulting in rapid changes in the upper thermocouple reading.

Another issue during the pressing cycle is the vertical position of the induction coils. It can be seen in figure 3.4 (right) that the induction heaters are not symmetric with respect to the parting line of the molds. The mid-plane of the induction coils is above the mold parting line. Since the electromagnetic field within the coil is highly non uniform, this asymmetry results in more energy directed to the top mold, causing it to have a higher temperature than the bottom mold. These effects make it difficult to accurately estimate the glass temperature, and may result in non-uniform heating of the glass gob.

Another issue that can be seen in figure 3.4 (left) is that due to the gap provided to allow for thermal expansion, the upper mold is not touching the upper plate during the heating and soaking stage, while the lower mold is in contact with the lower plate. Therefore, there is a conduction path for heat to flow from the lower mold into the lower plate. However, during the heating stage, there is no conduction path for the upper mold to transfer heat. This effect also contributes to the temperature of the upper mold being much higher than the temperature of the lower mold.

3.2.4 Solution for Induction Heater Position

The position of the induction heater was changed by surface grinding 2 mm from the steel part that holds the upper inconel part, which resulted in shifting of the whole mold assembly upward by 2 mm. The copper tube which holds the induction heater was also bent to position the induction coil and achieve uniform temperature distribution though out both the upper and lower molds.

In figure 3.4 the upper mold was not touching the upper inconel plate, which also contributed to higher temperatures to the upper mold. This problem was solved by operating the machine in force control mode during the heating and soaking stages and commanding the machine to apply a small 5 Newton force, to provide a conduction path

for heat in between the upper mold and upper inconel plate similar to the lower mold and lower inconel plate.

3.3 Second Generation Molding Machine

While the modifications described above were being undertaken, engineers at Moore Nanotechnology were designing and building a second generation Precision Glass Molding Machine (Figure 3.6). This effort was undertaken because of the difficulties in obtaining uniform heating of the mold assembly with the induction heater. In the second generation machine, the induction coil was replaced by two ring infrared heaters which result in a much more uniform temperature profile on the molds.

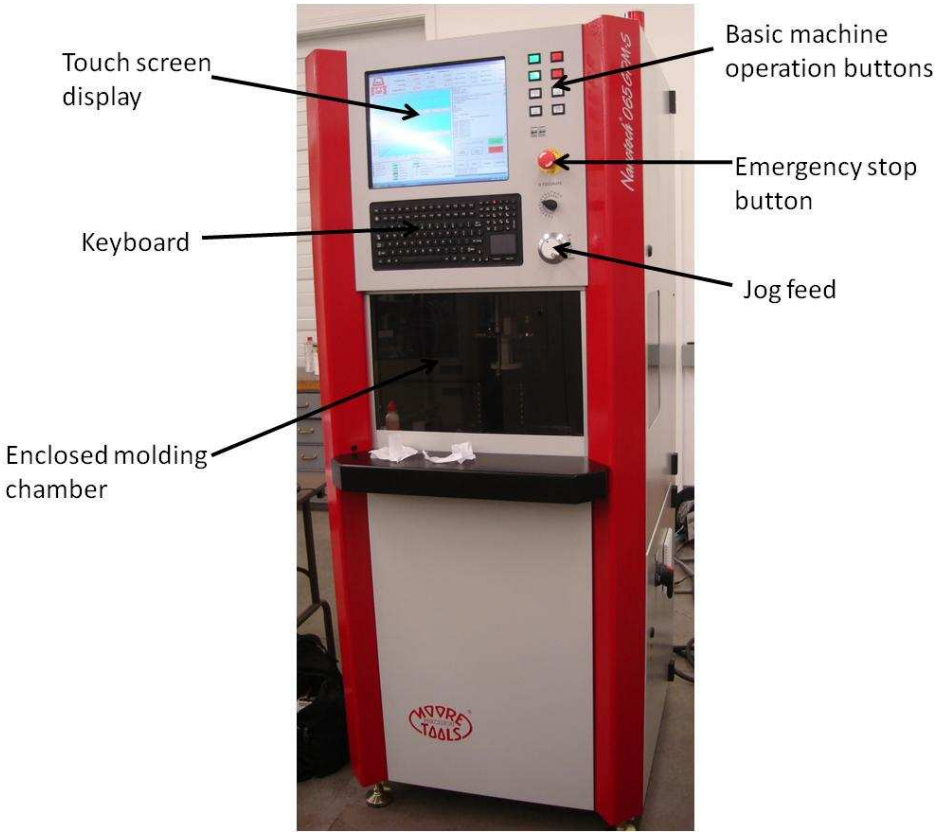

Figure 3.6: Second Generation Moore Nanotechsystems Molding Machine [21]

An additional problem with first generation machine was an inability to create a strong vacuum to remove oxygen from the chamber. Without sufficient vacuum, coatings on molds tend oxidize after only a few molding cycles due to the high temperatures (up to 700 C). In the new machine a strong vacuum pump is combined with improvements to the chamber design, and allows oxygen to be removed from the chamber and prevents the coatings on the molds from oxidizing.

Instead of using a glass chamber, an aluminum chamber (Figure 3.7) is used which has pipes within through which cold water is continuously circulated. The aluminum base also has pipes through which cold water is circulated. This cold water passing through the chamber and base allows the operator to cool down the molds at a faster rate after each molding experiment. The load cell used in this machine is similar to the previous machine.

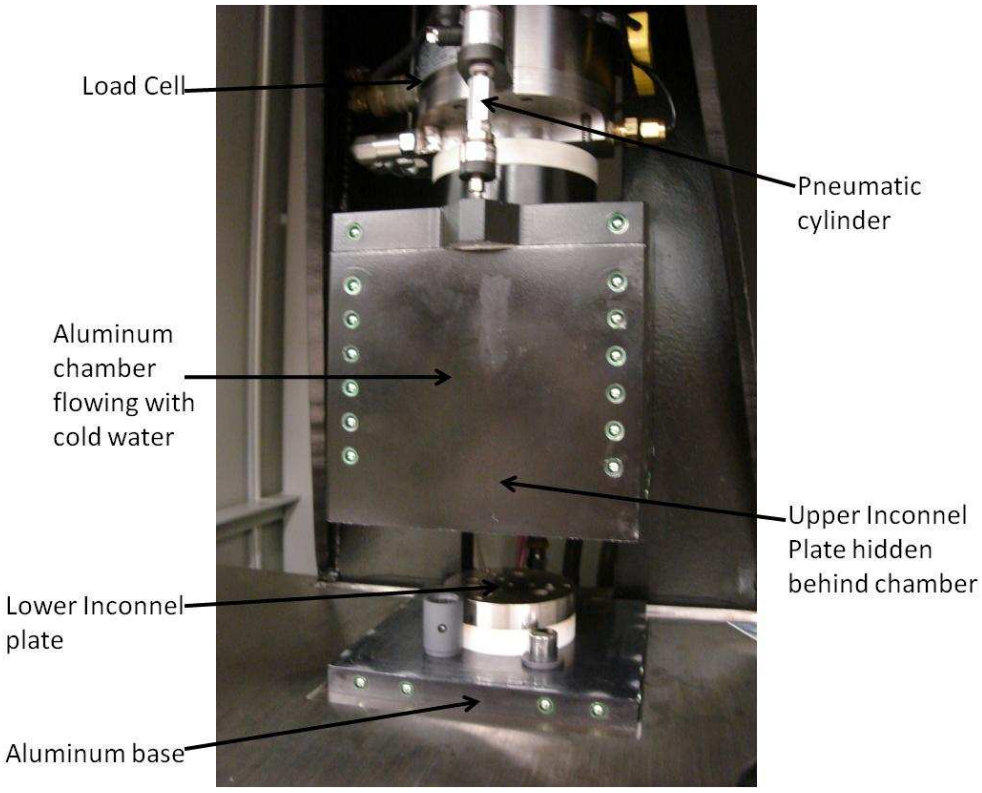

Figure 3.7: Chamber of Second Generation Molding Machine [21]

The position, force and temperature control of this machine are similar to the first generation machine. The new machine does not incorporate the thermocouple modifications that were made to the previous machine. These modifications include the spring loaded thermocouples and upper mold being in contact with the upper inconel plate during the heating and soaking stage. Even though these modifications were not made to this machine it was still able to produce lenses.

CHAPTER 4

THE TAGUCHI METHOD AND DETERMINATION OF SLEEVE DIMENSIONS

A set of experiments was created to help in finding the best possible combination of process parameters that would result in the minimum cycle time and best repeatability required for PGM (Precision Glass Molding).

4.1 Orthogonal Arrays

The basic tool that is used for deciding which experiments to run is called an orthogonal array. An orthogonal array is a matrix that shows what experiments should be run in certain cases to get the information desired [22]. Choosing the appropriate array from the library of arrays is one of the key steps in using orthogonal arrays for design of experiments. In our case there are ten experimental variables that are being used and each variable has three levels which are low, medium and high. The orthogonal array, which is taken from “Orthogonal Arrays and Linear Graphs” by G. Taguchi and S. Konishi, will be used for designing the experiments for PGM [23].

Using the L27 matrix (Table 4.1), thirteen variables can be used and twenty seven experiments are created. Table 2.1 shows the ten variables that are being used for design of experiments. In orthogonal arrays, each column conveys information different from that of any other column in the sequence which means that each column conveys unique information therefore avoiding redundancy. The individual sum of each column is the same value as shown in Table 4.1. The benefit of orthogonal arrays is that it provides uniformly distributed coverage of the test domain. It creates a concise test set with fewer test cases created. One limitation of orthogonal arrays is that it does not guarantee full coverage of the test domain. Table 4.2 shows the process parameters that are used for the twenty seven experiments. All of the experiments shown below were run

on the second generation PGM machine located at Moore Nanotechnology Inc. in Keene, NH, and the results are presented in chapter 5.

Table 4.1: L27 Matrix Array [23]

Experiment	V1	V2	V3	V4	V5	V6	V7	V8	V9	V10	V11	V12	V13
1	1	1	1	1	1	1	1	1	1	1	1	1	1
2	1	1	1	1	2	2	2	2	2	2	2	2	2
3	1	1	1	1	3	3	3	3	3	3	3	3	3
4	1	2	2	2	1	1	1	2	2	2	3	3	3
5	1	2	2	2	2	2	2	3	3	3	1	1	1
6	1	2	2	2	3	3	3	1	1	1	2	2	2
7	1	3	3	3	1	1	1	3	3	3	2	2	2
8	1	3	3	3	2	2	2	1	1	1	3	3	3
9	1	3	3	3	3	3	3	2	2	2	1	1	1
10	2	1	2	3	1	2	3	1	2	3	1	2	3
11	2	1	2	3	2	3	1	2	3	1	2	3	1
12	2	1	2	3	3	1	2	3	1	2	3	1	2
13	2	2	3	1	1	2	3	2	3	1	3	1	2
14	2	2	3	1	2	3	1	3	1	2	1	2	3
15	2	2	3	1	3	1	2	1	2	3	2	3	1
16	2	3	1	2	1	2	3	3	1	2	2	3	1
17	2	3	1	2	2	3	1	1	2	3	3	1	2
18	2	3	1	2	3	1	2	2	3	1	1	2	3
19	3	1	3	2	1	3	2	1	3	2	1	3	2
20	3	1	3	2	2	1	3	2	1	3	2	1	3
21	3	1	3	2	3	2	1	3	2	1	3	2	1
22	3	2	1	3	1	3	2	2	1	3	3	2	1
23	3	2	1	3	2	1	3	3	2	1	1	3	2
24	3	2	1	3	3	2	1	1	3	2	2	1	3
25	3	3	2	1	1	3	2	3	2	1	2	1	3
26	3	3	2	1	2	1	3	1	3	2	3	2	1
27	3	3	2	1	3	2	1	2	1	3	1	3	2
Sum	54	54	54	54	54	54	54	54	54	54	54	54	54

Table 4.2: Experiments Created from Taguchi Method

Experiment	Heating Cycle Time (sec)	Heating Temp (degC)	Soaking Cycle Time (sec)	Pressing Cycle Time (sec)	Pressing Cycle Force (N)	Cooling Cycle 1 Time (sec)	Cooling Cycle 1 End Temp (degC)	Cooling Cycle 1 Press Time (sec)	Cooling Cycle 1 Force (N)	Cooling Cycle 2 Time (sec)
1	200	515	120	60	300	120	400	50	100	180
2	200	525	120	60	500	120	425	100	300	270
3	200	535	120	60	700	120	450	150	500	360
4	200	515	185	90	500	210	400	100	300	180
5	200	525	185	90	700	210	425	150	500	270
6	200	535	185	90	300	210	450	50	100	360
7	200	515	250	120	700	300	400	150	500	180
8	200	525	250	120	300	300	425	50	100	270
9	200	535	250	120	500	300	450	100	300	360
10	250	525	120	90	300	300	450	150	300	180
11	250	535	120	90	500	300	400	50	500	270
12	250	515	120	90	700	300	425	100	100	360
13	250	525	185	120	500	120	450	50	500	180
14	250	535	185	120	700	120	400	100	100	270
15	250	515	185	120	300	120	425	150	300	360
16	250	525	250	60	700	210	450	100	100	180
17	250	535	250	60	300	210	400	150	300	270
18	250	515	250	60	500	210	425	50	500	360
19	300	535	120	120	300	210	425	100	500	180
20	300	515	120	120	500	210	450	150	100	270
21	300	525	120	120	700	210	400	50	300	360
22	300	535	185	60	500	300	425	150	100	180
23	300	515	185	60	700	300	450	50	300	270
24	300	525	185	60	300	300	400	100	500	360
25	300	535	250	90	700	120	425	50	300	180
26	300	515	250	90	300	120	450	100	500	270
27	300	525	250	90	500	120	400	150	100	360

4.2 Determination of Sleeve Height and Glass Ball Diameter

The upper and lower molds are aligned using a cylindrical sleeve (Figure 3.8) made out of tungsten carbide, the same material as the molds. The tolerances between the inner diameter of the sleeve and the outer diameter of the molds are tight to make sure that both the molds are accurately aligned.

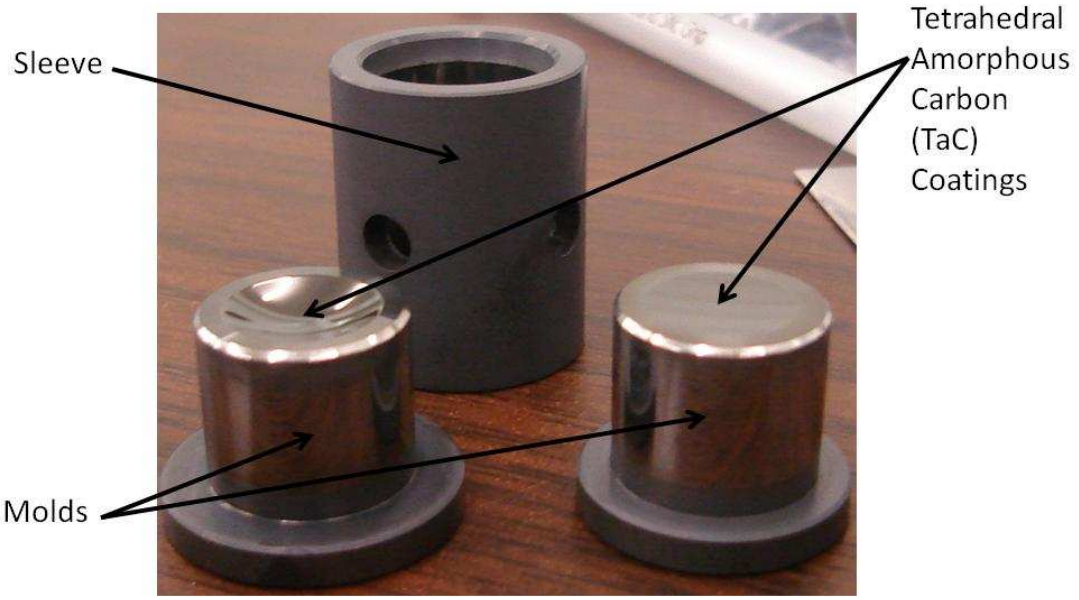

Figure 4.1: Molds and Sleeve [21]

The length of the sleeve controls how close the top and bottom mold surfaces can become, and depends upon the diameter of the glass ball being pressed, the areas of the mold cavities and the desired thickness of the lens. In our case the diameter of the glass ball is known (5 mm).The volume of the 5 mm glass ball is 65.42 mm^3. The sum of the volumes of both the mold cavities is 52.94 mm^3. Since the volume of the glass ball is greater than the volume of the mold cavities, more distance needs to be created in between the molds so the lens can form. If a distance of 0.5 mm is given in between molds, then the glass will have a volume of 92.19 mm^3 which is greater than 65.42 mm^3 and gives the glass ball enough space to form into a lens. In Figure 4.2 the distance given in between the molds is the lens edge thickness. Also, in Figure 4.2, the height of

the sleeve is H2 which is the sum of the lens edge thickness and twice the height of the mold's first step (H1).

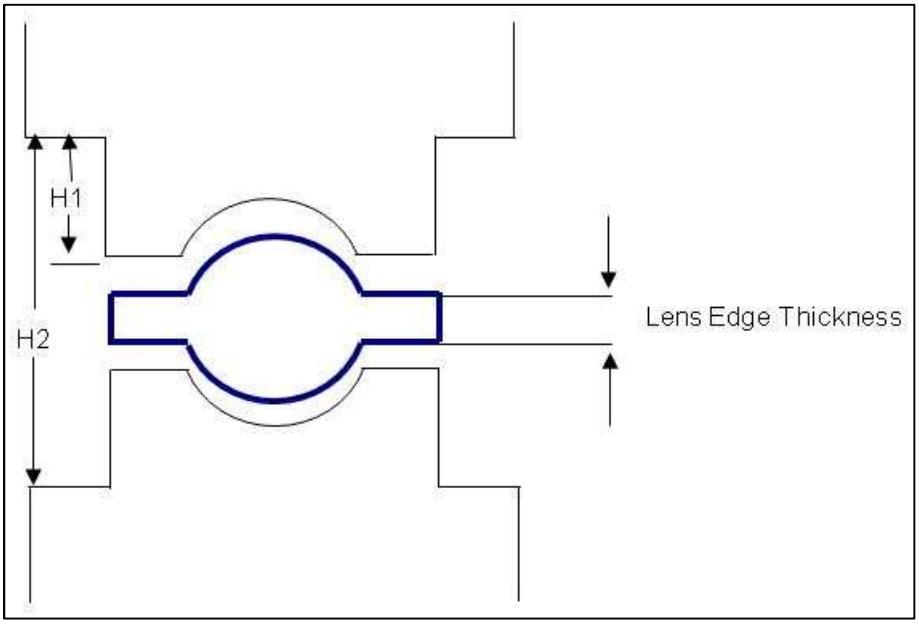

Figure 4.2: Drawing for Determining Sleeve Height [21]

CHAPTER 5

RESULTS AND DISCUSSION

The twenty seven experiments that were created using orthogonal arrays were performed on the second generation machine and twenty seven lenses were created. The same upper and lower molds were used for all the experiments. The upper mold has a spherical profile with a radius of 54.135 mm and lower mold has an aspherical profile with a R_{asp} value of 9.384 mm. The aspherical shape cannot be defined by a radius because it is not spherical, but instead it is defined using the equation:

$$H = \frac{x^2 / R_{asp}}{1+\sqrt{1-((1+K)*x^2/{R_{asp}}^2)}} + B*x^4 + C*x^6 + D*x^8 + E*x^{10} \quad (1)$$

Where x is the horizontal distance of the lens and H is the height of the lens. K, B, C, D and E are all constants. The form (radius and R_{asp} value) for all the lenses was measured using a Taylor-Hobson Form Talysurf surface profiler. The form was measured on both the spherical side and aspherical side by passing a sharp stylus over the surface along a single line and measuring the vertical deflection of the stylus. The surface roughness of the lenses was measured using a Zygo New View Scanning White Light interferometer.

5.1 Profile Form Measurements

The form is measured using the method shown in Figure 5.1. A fixture is used on which the lens is attached using wax. The probe is then centered with the lens and measures the lens profile from one end to the other. The probe has a 2 micron conical diamond tip. The system is calibrated to remove the errors due to the geometry of the measurement tip. It uses a laser interferometer to measure displacement and height

across the scan. All of the data was collected from the Taylor-Hobson and a program called Omnisurf was used to calculate the radius of both sides of the lenses.

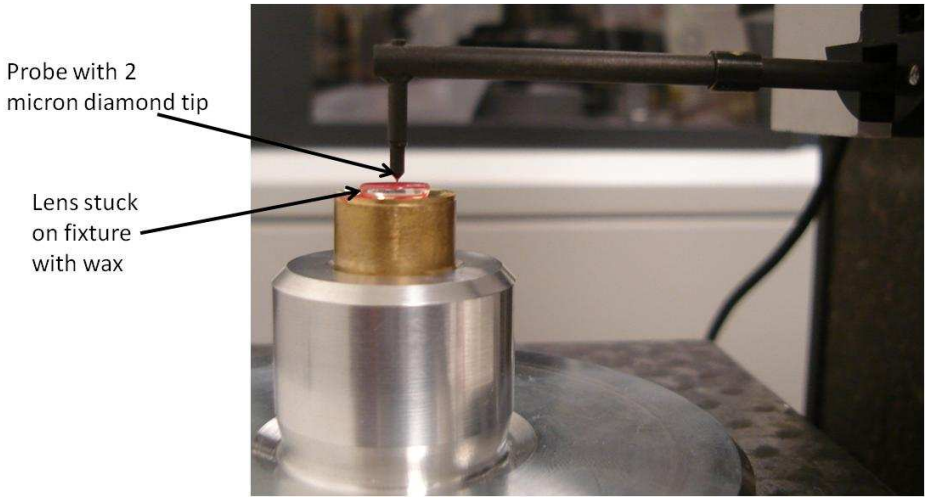

Figure 5.1: Measuring Form on Taylor Hobson Form Talysurf Machine [21]

The molds were also measured using the Form Talysurf and radius of the lenses was then compared to the radius of the molds. Figure 5.2 shows the power error which is calculated by Spherical Power Error = Absolute Value of (Radius of Lens – Radius of Mold) and the Aspherical Power Error = Absolute Value of (R_{asp} Value of Lens – R_{asp} Value of Mold). It can be seen that the power error of the spherical side of the lens is higher than the power error of the aspherical side. The reason for this high power error on the spherical side of the lens is discussed later in this section. Experiment numbers 5, 11 and 13 have the lowest combinations of the power errors on both sides of the lenses. Experiment number 27 has the lowest power error of 2 microns for the aspherical side, but the spherical side of that lens has a power error of 68 microns. Detailed results from orthogonal arrays and repeatability experiments including plots of process parameters and tables are included in the appendix A and B. In appendix B, the plot for the process parameters of experiment number 25 are incomplete because the machine started to vibrate when force were applied during the pressing stage. Experiment number 25 was

repeated again but vibrations started occurring, the instance force was applied. This experiment was abandoned and not repeated again.

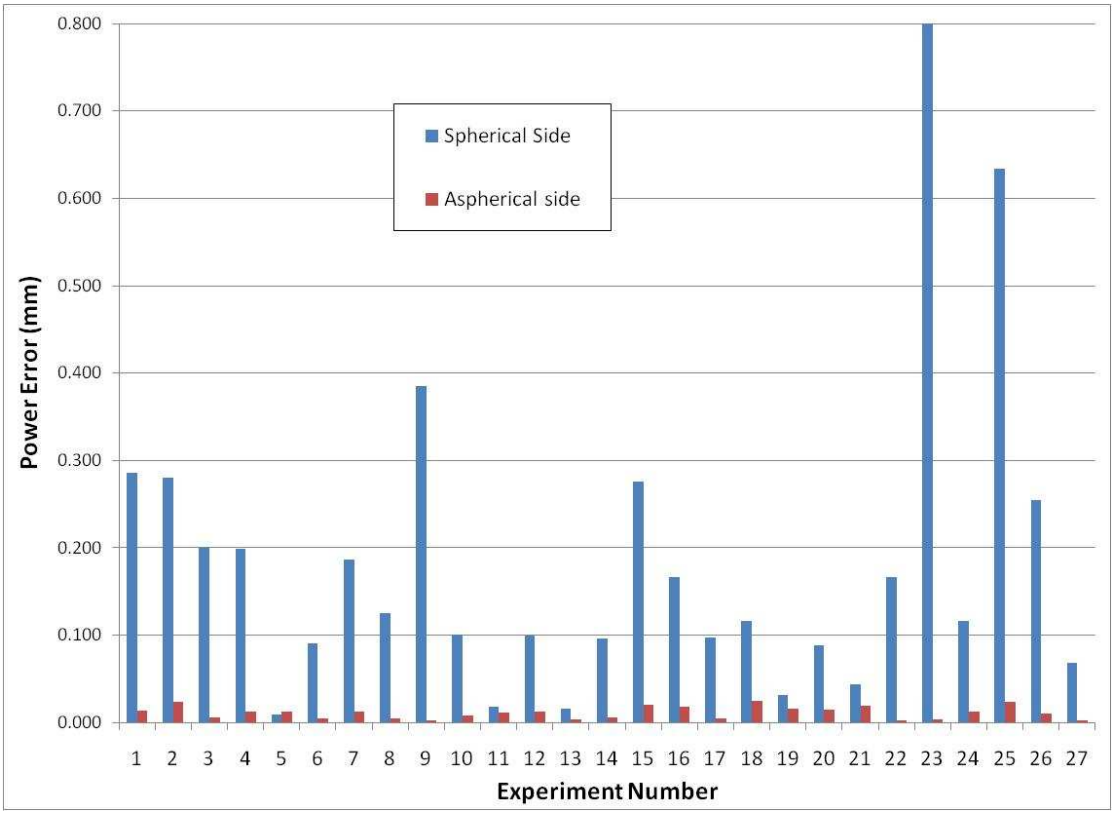

Figure 5.2: Power Error of Lenses when Compared to Radius of Molds

After performing all the experiments created from the Taguchi Method, the repeatability of the PGM process was evaluated. For the repeatability tests experiments with lower power errors and higher power errors were chosen. The process parameters from experiment numbers 13, 15 and 27 were chosen for repeatability tests. Experiment numbers 13 and 27 were chosen due to the low aspherical power error and experiment number 15 was chosen to check if a higher power error will have good repeatability. Ten lenses were molded using each of these parameter sets, and the resulting lenses were all measured on the Form Talysurf. The results are shown in Table 5.1. It can be seen that experiment numbers 15 and 27 had the lowest standard deviations.

Table 5.1: Repeatability Test Results

	Spherical Side		Aspherical Side	
Exp. #	Average Power Error (microns)	Std. Dev. (microns)	Average Power Error (microns)	Std. Dev. (microns)
13	125	±130	12	±6
15	228	±33	18	±2
27	82	±56	8	±3

The results from the repeatability test on the spherical side are substantially higher than for commercially available lenses made by other means. Commercially available lenses currently offer power errors that have a standard deviation lower than 0.3 microns. The lowest power error standard deviation for the spherical side was 33 microns and for the aspherical side was 2 microns.

The source of this variability is unknown. Investigations were undertaken to quantify what portion of it is attributable to the metrology process. First the repeatability of the form measurement was quantified by taking five form measurements on the same lens. A lens from experiment number 15 was chosen for this repeatability test. For each measurement, the lens was removed from the instrument and then reattached to the fixture. Results are shown in Table 5.2, where it can be seen that the aspherical side only had a standard deviation of 1 micron for the power error. Whereas, the standard deviation of power error on the spherical side is 21 microns. Therefore, it can be concluded that approximately 64% of the uncertainty of the spherical side power error for experiment number 15 comes from the measurement instrument itself.

Table 5.2: Repeatability Results for Same Lens Measurement

	Spherical Side		Aspherical Side	
Measurement #	**Curve Fit Radius (mm)**	**Power Error (mm)**	**Curve Fit Radius (mm)**	**Power Error (mm)**
1	53.909	0.230	9.366	0.018
2	53.861	0.278	9.364	0.020
3	53.890	0.249	9.364	0.020
4	53.923	0.216	9.366	0.018
5	53.892	0.247	9.366	0.018
Average	53.895	0.244	9.365	0.019
Std. Dev.	0.021	0.021	0.001	0.001

The issue is that since the lens has a radius of around 54 mm and the length is only 5 mm, then it becomes difficult for the curve fitting algorithm to calculate a radius that fits the measured data points. Figure 5.3 shows scale view of a 54.135 mm circle and how a lens with a length of 5 mm fits into the circle. The lens almost seems like a short straight line, and since such a small included angle of the arc is measured, small deviations in the raw data may lead to large variations in the estimated radius.

Figure 5.4 show's that a lens with a radius of 54.135 mm would have a small curvature if the scanned length of the profile is 5 mm. A Monte Carlo algorithm was created using Matlab in which the data points shown in Figure 5.4 were used and a small amount of random noise was added to the data and then the curve fitting algorithm was used to calculate the radius of the data points with the noise. The noise that is added to the data points is randomly generated from a normal distribution with a specified standard deviation.

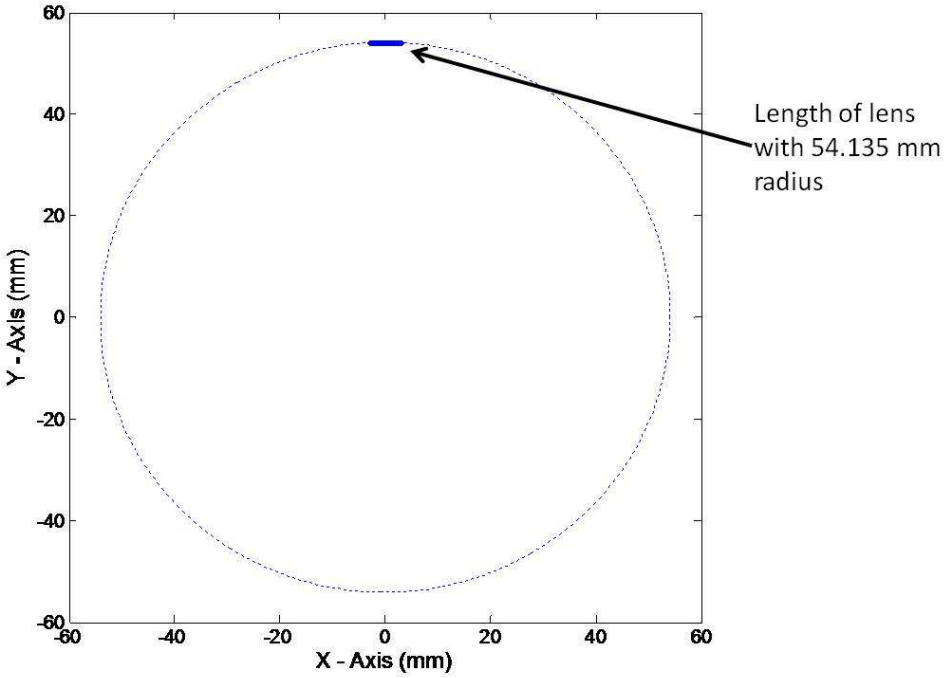

Figure 5.3: Circle Compared to Length of Lens

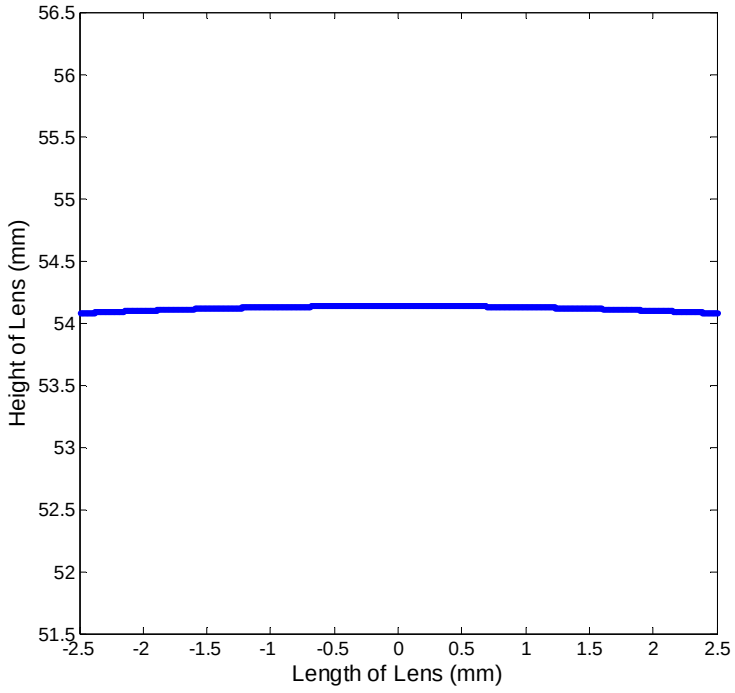

Figure 5.4: Raw Profile Data for Spherical Side of Lens

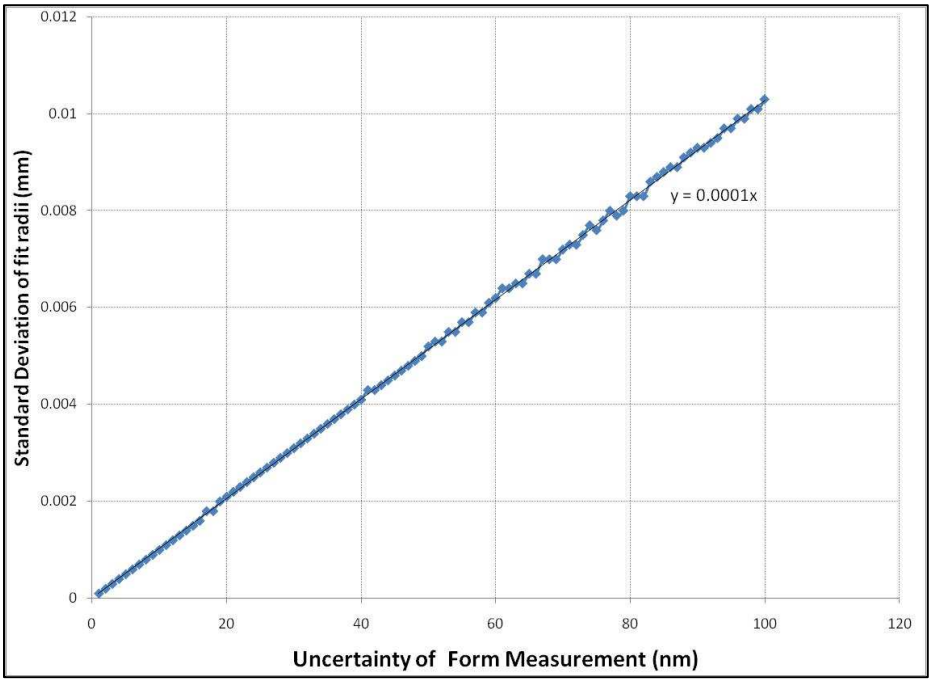

Figure 5.5: Standard Deviation of Fit Radii Based on Uncertainty of Form Measurement

Figure 5.5 shows the standard deviation of the noise that was added to the data on the x-axis. This noise was added 10,000 times to the same data for each nanometer of uncertainty. Then the standard deviation of all the 10,000 radii was calculated and plotted in the y-axis of Figure 5.5. This algorithm was repeated for noise ranging up to 100 nm. It can be seen from the data that if there is a linear trend, and the variability in the estimated radius is approximately 100 times the uncertainty of the vertical height measurements of the profilometer. For an uncertainty of 100 nm in profilometer height data, there will be an uncertainty of 10 microns in the radius fitting calculations. In our case, we observed an uncertainty in the power error of 21 microns from repeatedly measuring the same lens. Extrapolating the Monte Carlo simulation data suggest that an uncertainty on the order of 210 nm in the profilometer data could cause this. Therefore, the fact that the spherical side has a large radius of around 54 mm and a small arc length is a probable source of the repeatability error. Additionally, the profiles of both the

molds and a standard calibration sphere (radius = 21.9983 mm) were measured using the Taylor Hobson profilometer.

Table 5.3 shows that for a fixed profile length, as the radius increases the uncertainty in measuring the radius also increases. The molds and calibration ball were fabricated using precision tools and were cleaned using methanol before the measurements.

Table 5.3: Form Measurements of Different Radii with 5 mm Profile Length

Measurement #	Aspherical Mold Radius (mm)	Calibration Ball Radius (mm)	Spherical Mold Radius (mm)
1	9.385	21.997	54.119
2	9.385	21.994	54.142
3	9.384	21.991	54.139
4	9.385	21.992	54.144
5	9.383	21.995	54.130
Average	9.384	21.994	54.135
Std. Dev.	0.001	0.002	0.010

Figure 5.6 shows results from the Monte Carlo algorithm in which profile lengths of 1 mm, 3 mm, and 5 mm are used with a radius of 54.135 mm. The graph shows that as the profile length decreases then the error in measuring the radius increases. At an uncertainty of measurement of 100 nm the standard deviation is 10 microns, 24 microns and 180 microns for profile lengths 1 mm, 3 mm and 5 mm, respectively. Figure 5.6 shows that extremely high precision measurements are required to accurately fit a radius to a curve when the radius is high and the profile length is very small.

The results from the form measurements conclude that it is very difficult to measure the form of lenses with high radii and small profile lengths. Therefore, these types of lenses may not be suitable for mass manufacturing due to the repeatability issues. It may be more feasible to focus on glass press molding of lenses that have

larger profile lengths and radii which would improve inspection uncertainty and make it possible for the molding process to be used in manufacturing of high volumes of glass lenses.

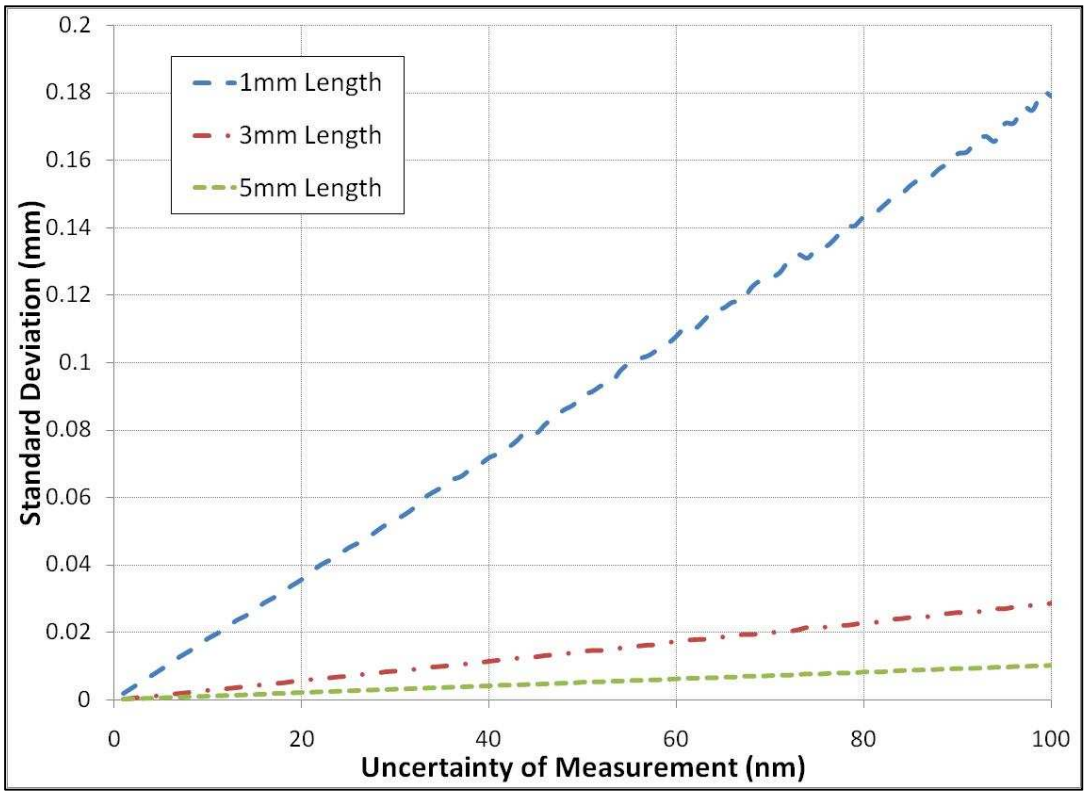

Figure 5.6: Standard Deviation of Fit Radii for 54.135 mm Radius at Different Profile Lengths

5.2 Surface Roughness Measurements

The surface roughness of all the twenty seven lenses was measured using a laser interferometer. The surface form was measured to check the quality of the lenses and to make sure that the surface form for all the lenses is consistent. The values measured for the surface form are R_a, R_{RMS} and PV. The surface profile is filtered from a raw profile that is measured using the laser interferometer and a mean line is calculated from this raw profile. As shown below R_a is the arithmetic average of the absolute value of the distance (y_i) in between the mean line and the data points measured. R_{RMS} is the

square root of the sum of squares of y_i (i^{th} data point) divided by the number of data points (n). PV is the maximum peak to valley distance from the measured surface form.

$$R_a = \frac{1}{n}\sum_{i=1}^{n}|y_i| \quad (2)$$

$$R_{RMS} = \sqrt{\frac{1}{n}\sum_{i=1}^{n}(y_i)^2} \quad (3)$$

Table 5.4 shows the surface roughness data of all the lenses. It can be seen that most of the R_a values are under 0.005 microns and most of the R_{RMS} values are under 0.008 microns. But after experiment number 16 the R_{RMS} value of the spherical side of the lens increases due to some damage that occurred to the spherical mold. This damage is the sticking of glass particles to the surface of the mold and is visible with the naked eye.

Figure 5.7 shows imperfections on the spherical side of the lens after the damage on the mold. Figure 5.8 shows the plot of the process parameters of the experiment when the damage occurred. The plot shows the commanded temperature (red dashed line) which is the temperature, the top and bottom temperatures should follow. The machine was programmed to follow a variable average of the top (90%) and bottom (10%) temperatures. Also, these experiments were performed on the 2^{nd} generation machine, which does not have spring loaded thermocouples and the temperature is being measured using the upper and lower surfaces of the top mold and bottom mold, respectively (as show in Figure 3.4). Since the actual temperature close to the glass is unknown, it is difficult to conclude the reason for glass particles getting stuck on the mold.

Table 5.4: Surface Roughness Data for all Lenses

	Spherical Side			Aspherical Side		
EXP #	Ra (microns)	RMS (microns)	PV (microns)	Ra (microns)	RMS (microns)	PV (microns)
1	0.003	0.007	0.926	0.004	0.007	0.612
2	0.004	0.006	0.637	0.003	0.008	1.149
3	0.003	0.006	0.652	0.004	0.007	0.456
4	0.003	0.007	0.914	0.003	0.007	0.683
5	0.003	0.008	0.974	0.004	0.007	0.804
6	0.002	0.004	0.438	0.003	0.004	0.55
7	0.003	0.007	0.580	0.004	0.003	2.721
8	0.002	0.003	0.375	0.003	0.005	0.321
9	0.003	0.006	0.672	0.003	0.006	0.444
10	0.003	0.006	0.762	0.003	0.007	0.74
11	0.003	0.005	0.415	0.003	0.005	0.599
12	0.003	0.008	0.956	0.003	0.005	0.614
13	0.003	0.006	0.875	0.003	0.005	0.582
14	0.003	0.007	0.542	0.004	0.009	0.857
15	0.003	0.006	0.957	0.003	0.006	0.836
16	0.003	0.005	0.401	0.004	0.008	0.726
17	0.003	0.013	0.416	0.003	0.006	0.616
18	0.005	0.014	1.049	0.003	0.005	0.569
19	0.004	0.010	0.950	0.003	0.005	0.566
20	0.006	0.017	0.950	0.003	0.006	0.627
21	0.005	0.016	0.962	0.003	0.005	0.533
22	0.004	0.010	0.972	0.003	0.005	0.578
23	0.004	0.011	0.970	0.003	0.005	0.572
24	0.005	0.017	0.975	0.003	0.005	0.499
25	0.007	0.021	0.960	0.004	0.006	0.597
26	0.006	0.017	0.937	0.003	0.005	0.569
27	0.004	0.012	0.971	0.003	0.005	0.582

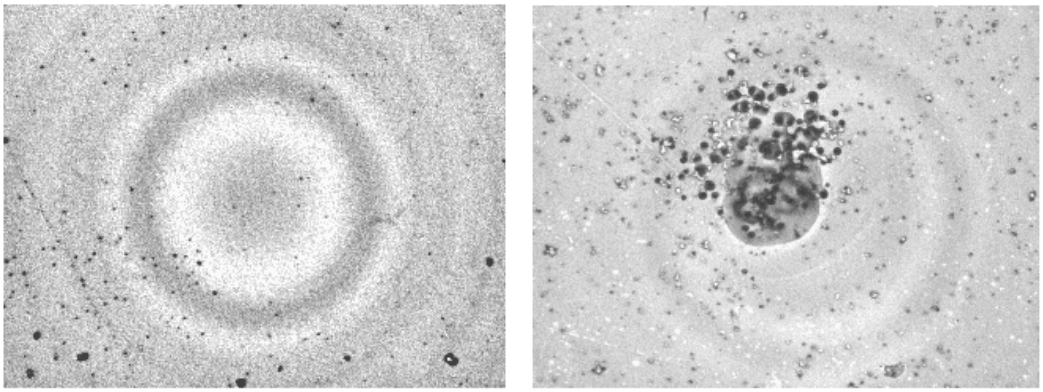

Figure 5.7: Lens Surface before (left) and after (right) Damage on Spherical Mold

Figure 5.8 also shows that there was a force of 325 N applied during the slow cooling cycle for 150 seconds. This force being applied for a long period of 150 seconds when the temperature of the glass is under T_g could be probable cause for glass getting stuck on the spherical mold. The actual temperature close to the glass during the slow cooling cycle is not known, therefore it cannot be concluded that temperature of the glass during the slow cooling stage in experiment number 17 is under T_g.

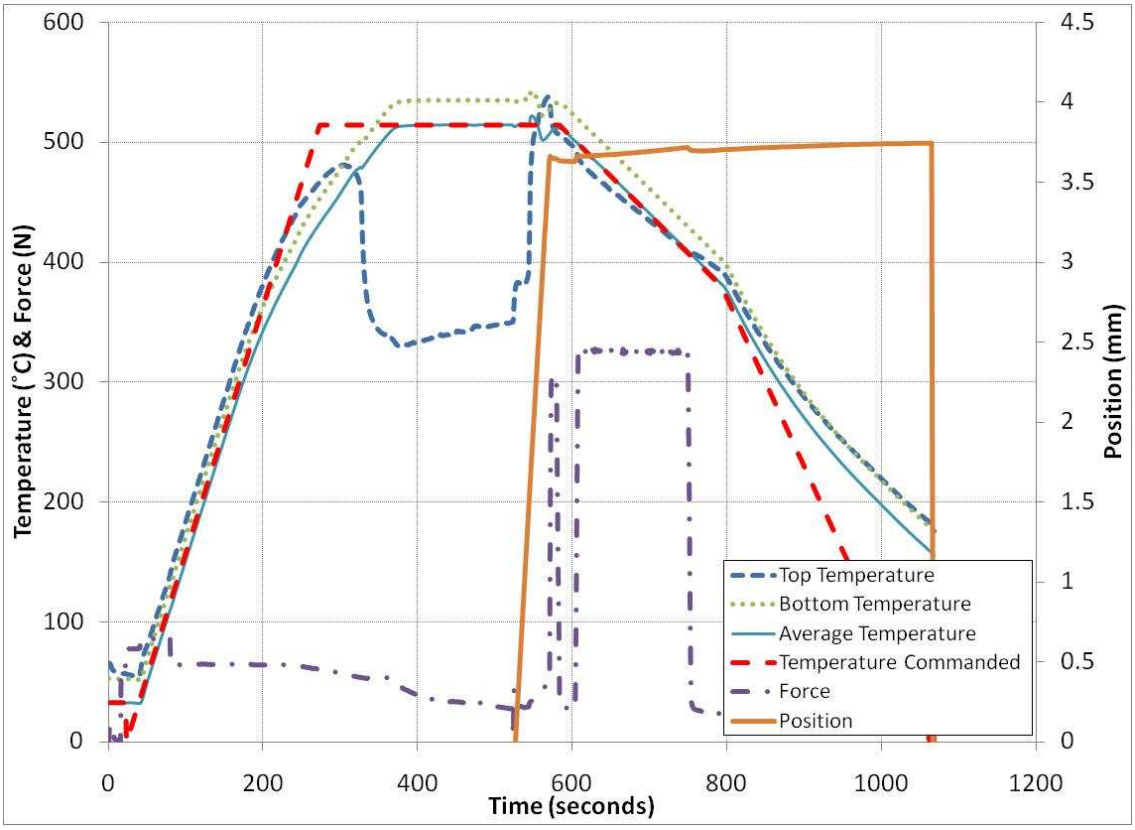

Figure 5.8: Temperature and Force for Experiment 17

5.3 Wear of Mold Coatings

The mold coating used was Tetrahedral Amorphous Carbon (TaC), which is resistant to oxidation at high temperatures up to 700 ˚C. TaC is a shiny metallic coating and a layer with a thickness of 200 nm was used on the molds. When molding

experiments were performed on the first generation machine with this coating, then the coating got damaged within the first five experiments. This happened because the first generation GPM (Glass Press Molding) machine did not have a vacuum attached to the chamber to remove oxygen and prevent oxidation of mold material (Tungsten Carbide). The second generation machine has a very strong vacuum that removes the oxygen from the chamber and nitrogen is purged into the chamber. After running fifty molding experiments using the second generation machine the mold coating are still in perfect condition. The only issue with second generation GPM machine is the sticking of glass which might be due to a temperature control issue.

Table 5.5 shows the surface measurements of the molds after every five experiments at the same position. For the spherical mold it can be seen that the PV (maximum peak to valley distance) increases after every measurement. This means that the after every experiment the surface of the spherical mold keeps getting more glass particles stuck on it due to the temperature issue.

Table 5.5: Surface Roughness Data for Molds

	Spherical Mold			Aspherical Mold		
Measurement after exp. #	Ra (nm)	RMS (nm)	PV (nm)	Ra (nm)	RMS (nm)	PV (nm)
1	1.618	2.110	23.335	2.747	3.624	33.668
5	1.845	2.453	26.212	3.505	4.657	42.161
10	2.437	4.771	178.048	2.021	2.632	76.234
15	2.560	3.878	226.992	2.099	2.766	74.425
20	4.426	14.562	716.512	2.751	3.612	60.691
25	17.602	40.631	945.461	4.010	5.453	125.643

Figure 5.9 shows that the spherical mold had a good surface finish before the damage and the PV value is 26.212 nm. Figure 5.10 shows many glass particles and the PV value goes up to 716.512 nm. Therefore, it can be concluded that it is important to

maintain uniform temperature throughout the top mold and bottom mold during the molding process, otherwise if the temperature of the glass is below T_g then it will get stuck to the surface of the mold cavity.

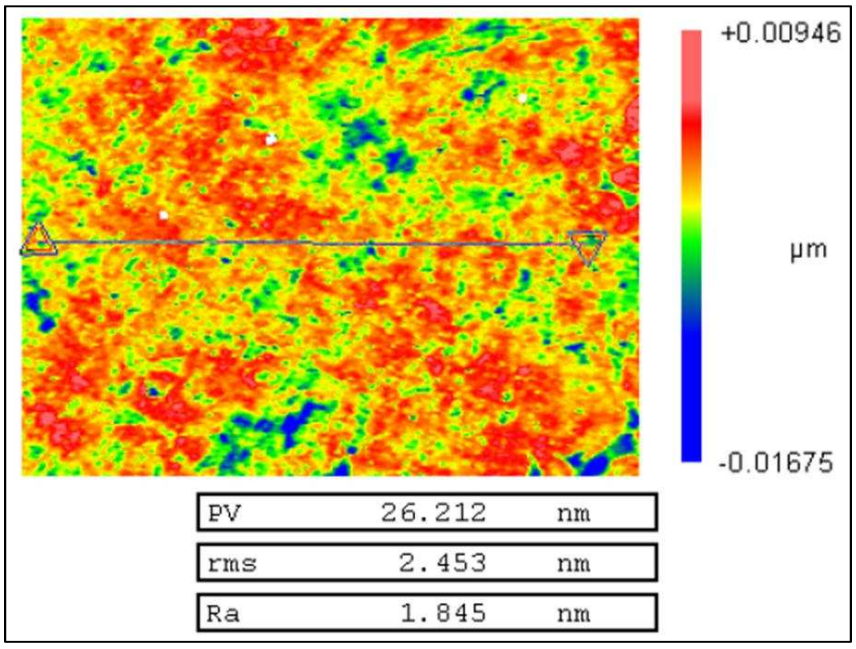

Figure 5.9: Spherical Mold's Surface Scan before Damage

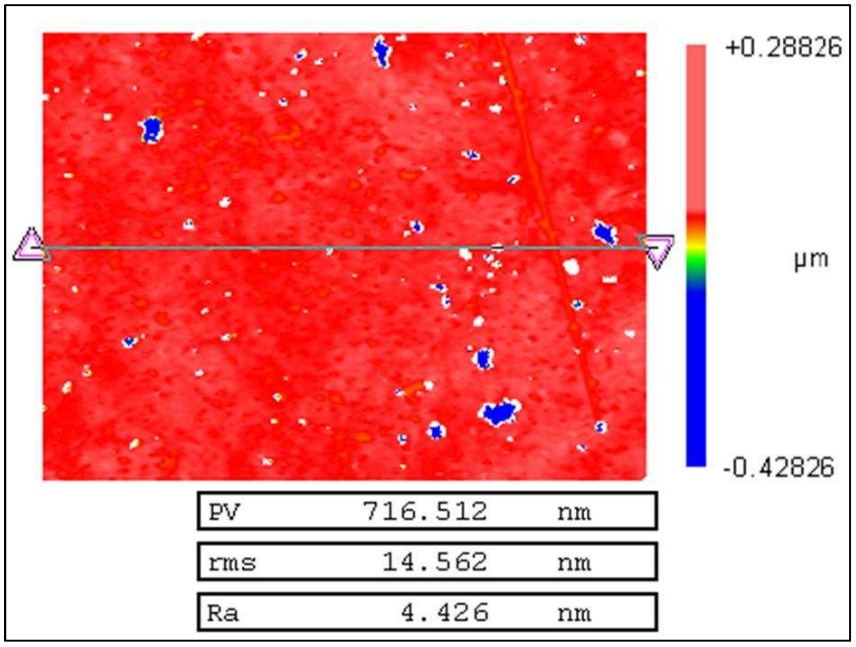

Figure 5.10: Spherical Mold's Surface Scan after Damage

5.4 Sensitivity of Process Parameters when Compared to the Form of Lenses

The process parameters were compared to the different values of radii for each experiment to understand that how the geometry of the lens changes when changes are made to the process parameters. Figure 5.11 compares the time of the heating stage of each experiment to the radius of the spherical side of the lens. The plot shows that there is no trend in between the heating stage time and the radius of the lens. For a heating time of 200 seconds, the range of radii is 53.75-54.42 mm, for a heating time of 250 seconds, the range of radii is 53.86-54.25 mm and for a heating time of 300 seconds the range of radii is 53.88-55.73 mm. A heating time of 300 seconds has the largest range of radii but no conclusions can be drawn from this data. The radii of the spherical side of the lenses were also compared to the other 9 variables, but the plots are similar and inconclusive. The R_{asp} value of the aspherical side of lenses were also compared to the process parameters but the results were similar. Complete results are attached to appendix C and appendix D.

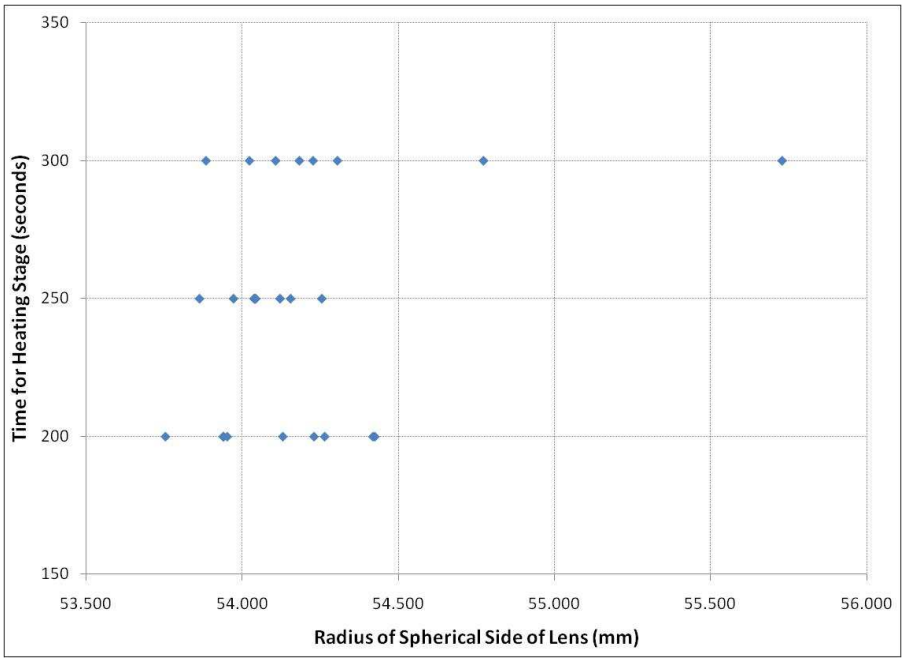

Figure 5.11: Heating Stage Time versus Radius of Spherical Side of Lens

Figure 5.11 shows that there is a non-linear relationship between the variables and the Radius of the spherical side lenses. The relationship in between the variables and the Rasp values of the spherical of the lenses is also non-linear. Since there is non-linear behavior, there is another method that can be used to obtain results from the orthogonal array. This method will be used to determine the effect of the variables from the process parameters on the power error on the aspherical side of the lens only. The power error on the spherical side will not be used because it has a power error has an uncertainty of 21 microns. The power error on the spherical side has an uncertainty of only 2 microns.

Table 5.6: Variables and Power Error for Aspherical Side of Lenses

Exp. #	Heating Time (sec)	Heating Temp (degC)	Soaking Time (sec)	Pressing Time (sec)	Pressing Force (N)	Cooling Cycle 1 Time (sec)	Cooling Cycle 1 End Temp (degC)	Cooling Cycle 1 Press Time (sec)	Cooling Cycle 1 Force (N)	Cooling Cycle 2 Time (sec)	Power Error on Aspherical Side (microns)
1	200	515	120	60	300	120	400	50	100	180	14
2	200	525	120	60	500	120	425	100	300	270	24
3	200	535	120	60	700	120	450	150	500	360	6
4	200	515	185	90	500	210	400	100	300	180	13
5	200	525	185	90	700	210	425	150	500	270	12
6	200	535	185	90	300	210	450	50	100	360	5
7	200	515	250	120	700	300	400	150	500	180	13
8	200	525	250	120	300	300	425	50	100	270	5
9	200	535	250	120	500	300	450	100	300	360	3
10	250	525	120	90	300	300	450	150	300	180	8
11	250	535	120	90	500	300	400	50	500	270	11
12	250	515	120	90	700	300	425	100	100	360	13
13	250	525	185	120	500	120	450	50	500	180	4
14	250	535	185	120	700	120	400	100	100	270	6
15	250	515	185	120	300	120	425	150	300	360	20
16	250	525	250	60	700	210	450	100	100	180	18
17	250	535	250	60	300	210	400	150	300	270	5
18	250	515	250	60	500	210	425	50	500	360	25
19	300	535	120	120	300	210	425	100	500	180	16
20	300	515	120	120	500	210	450	150	100	270	15
21	300	525	120	120	700	210	400	50	300	360	19
22	300	535	185	60	500	300	425	150	100	180	3
23	300	515	185	60	700	300	450	50	300	270	4
24	300	525	185	60	300	300	400	100	500	360	13
25	300	535	250	90	700	120	425	50	300	180	24
26	300	515	250	90	300	120	450	100	500	270	10
27	300	525	250	90	500	120	400	150	100	360	2

Table 5.6 shows the power error on the aspherical side for each lens and the value of the variables that was used for each experiment. In experiments 1 through 9 the heating time is kept constant at the lower value of 200 seconds, while different combinations of other variables are used. In experiments 10 through 18 the heating time is kept constant at the medium value 250 seconds, and once again different

combinations of other variables are used. This is same case for experiments 19 through 27 where the value of heating time is high. This characteristic of orthogonal arrays makes it possible to quantify the effects of changing the heating time on the overall system. In this method first the overall mean of the numerical results for all the experiments is calculated:

$$\mathrm{m} = \frac{1}{27}\sum_{i=1}^{27} \mathrm{n_i} \tag{4}$$

Where, m is the overall mean and ni is the numerical result for each experiment. In our case, n is the power error.

To determine the effect of each variable on power error, it is necessary to find the deviation of heating time (V1) at each level from the overall mean. From Table 5.6, it can be seen that the heating time is low for the first nine experiments, medium for the next nine experiments, and high for the last nine experiments. Therefore, the means for each level of V1 would be found using equations 5 through 7.

$$m(V1_L) = \frac{1}{9}(n_1 + n_2 + n_3 + n_4 + n_5 + n_6 + n_7 + n_8 + n_9) \tag{5}$$

$$m(V1_L) = \frac{1}{9}(n_{10} + n_{11} + n_{12} + n_{13} + n_{14} + n_{15} + n_{16} + n_{17} + n_{18}) \tag{6}$$

$$m(V1_L) = \frac{1}{9}(n_{19} + n_{20} + n_{21} + n_{22} + n_{23} + n_{24} + n_{25} + n_{26} + n_{27}) \tag{7}$$

Where m(V1L), m(V1M), and m(V1H) are the means of the three levels of V1. The rest of the nine variables follow the same pattern with different combinations of experiments. The means of each level for each variable, according to the results listed in Table 5.6, can be seen in Table 5.7. These individual means can be used to find the effect each variable has on the overall result by finding the deviation of each variable level from the overall mean. The effect of V1 at the low level can be found by the deviation v1L=m(V1L) – m. The effects of the other two levels can be found using the same method. The deviation of each variable level from the overall mean can be seen in

Table 5.8. The variables that deviate the most from the mean have the strongest effect on the results and are therefore the most influential to the optimization of the design.

Table 5.7: Mean of Each Variable Level

Variable	Low	Medium	High
Heating Time	10.6	12.2	11.8
Soaking Time	14.0	8.9	11.7
Pressing Time	12.4	10.9	11.2
Cooling Stage 1 Time	12.2	14.2	8.1
Cooling Stage 2 Time	12.6	10.2	11.8
Heating Temp	14.1	11.7	8.8
Pressing Force	10.7	11.1	12.8
Cooling Cycle 1 Press Force	9.0	13.3	12.2
Cooling Cycle 1 Press Duration	12.3	12.9	9.3
Cooling Cycle 1 End Temp	10.7	15.8	8.1
Total Mean	11.5		

Table 5.8: Deviations from Overall Mean of Power Error

Variable	Low	Medium	High	Max. Difference
Heating Time	-0.9	0.7	0.3	**1.7**
Soaking Time	2.5	-2.6	0.2	**5.1**
Pressing Time	0.9	-0.6	-0.3	**1.6**
Cooling Stage 1 Time	0.7	2.7	-3.4	**6.1**
Cooling Stage 2 Time	1.1	-1.3	0.3	**2.3**
Heating Temp	2.6	0.2	-2.7	**5.3**
Pressing Force	-0.8	-0.4	1.3	**2.1**
Cooling Cycle 1 Press Force	-2.5	1.8	0.7	**4.3**
Cooling Cycle 1 Press Duration	0.8	1.4	-2.2	**3.6**
Cooling Cycle 1 End Temp	-0.8	4.3	-3.4	**7.7**

In Table 5.8, the difference in between the maximum and minimum value for each variable is calculated and the variables with the highest difference have the most effect on the power error on the aspherical side of the lens. Cooling Stage 1 Time and Cooling Cycle 1 End Temperature have the largest effect on the power error. Soaking Time, Heating Temperature, and Cooling Stage 1 Press Force have a mediocre effect on the power error and the rest of the variables have a lower effect. The levels that are

shaded in table 5.8 have the maximum negative deviation and a combination of all variables that have the maximum negative deviation would result in an experiment which produces lenses with minimum power error. Therefore, such an experiment will produce lenses that have radii and Rasp values close to the molds.

CHAPTER 6

CONCLUSION AND FUTURE WORK

6.1 Conclusion

A set of experiments was designed that was used to find the best process parameters that would produce lenses with minimum cycle time, repeatable form error and minimum form error. Three experiments are chosen as shown in Table 6.1, experiment number 1 has the minimum cycle time, experiment 15 has the best repeatability when compared to process repeatability for experiment 13 and 27 and a third experiment was generated using the orthogonal arrays. This third experiment has optimized process parameters which result in lenses that would minimize the power error of the aspherical side of the lens.

Table 6.1: Process Parameters for Experiments 1, 15 and Experiment with Optimized Power Error

	Exp. # 1	**Exp. # 15**	**Min. Aspherical Power Error**
Heating Time (seconds)	200	250	200
Soaking Time (seconds)	120	185	185
Pressing Time (seconds)	60	120	90
Cooling Stage 1 Time (seconds)	120	120	300
Cooling Stage 2 Time (seconds)	180	360	270
Heating Temperature (degC)	587	587	607
Cooling Stage 1 End Temp (degC)	400	425	450
Pressing Stage Force (N)	300	300	300
Cooling Stage 1 Force (N)	100	300	100
Cooling Stage 1 Press time (seconds)	50	150	150
Total Cycle Time (min)	**11.3**	**17.3**	**17.4**

Experiment number 1 has the minimum cycle time of 11.3 minutes. Experiment number 15 which has the best repeatability has a total cycle time of 17.3 minutes. The

lenses produced have a spherical side and an aspherical side. The uncertainty of power error on the spherical side is ±33 microns and the uncertainty of power error on the aspherical side is ±2 microns. The reason for having high uncertainty on the spherical side was proven to be a metrology issue. The optimized experiment has a cycle time of 18.3 minutes.

In the course of this research project there were two machines that were used for glass press molding. The first machine was used to get a better understanding of the GPM process and there were many modifications made to machine. The machine had issues due to non-uniform heating of the molds and measuring temperature at the incorrect position. These issues were solved using by changing the position of the induction heater and by installing spring loaded thermocouples. But, these modifications did not help to make the machine functional for molding experiments because of oxidation that damaged the surface of the molds. This oxidation occurred due to lack of a good vacuum system that would remove oxygen from the molding chamber.

The second machine was used to perform the twenty seven experiments that were generated using design of experiments. This machine used infrared lamps for heating the molds but it did not have spring loaded thermocouples which resulted in damage to one of the molds. Even though the machine had some issues, it was able to produce good lenses and the surface form and surface profile of these lenses were measured to evaluate repeatability. All the results acquired in this research could be used to validate the glass molding simulations and make the simulation more accurate.

6.2 Future Work

It would be recommended to make modifications to the 2nd generation machine and perform more experiments with molds that have lower radii. The modifications that need to be made on the second machine are installing the spring loaded or laser thermocouples and changing the programming of the PLC such that both the bottom and top plate are always touching the upper and lower molds, respectively. When both the molds are touching the plates at all times, then there will be an even conduction path throughout the molds which will help in maintaining a uniform temperature in both the molds.

Since it is very difficult to measure the radius of lenses with large radii and small profile lengths, it is very important to determine the relation between radius and the length of the lenses which are easy to measure with minimum uncertainty. Therefore, it is recommended to perform molding experiments on lenses which have diameters greater than 10 mm. If the profile length of lens is longer then there will less uncertainty in the fitting of the radius on a curve.

It would also be recommended to perform the same twenty seven experiments with molds that have different radii and compare the results to the experiments performed in this research. If the power error between the molds and lenses used in this research is similar if different mold geometries are used than the data acquired in this project could be very useful. Glass press molding has great a future and further research could prove glass molding to be a very effective method to produce glass lenses on a large scale.

APPENDICES

Appendix A

Form Results

Table A-1: Form Measurements for 27 Experiments from DOE

	Spherical Side			Aspherical Side		
Exp. #	Curve Fit Radius (mm)	Form Error within Fit Radius (Microns)	Total Power Error Compared to Mold (mm)	Curve Fit Radius (mm)	Form Error within Fit Radius (Microns)	Total Power Error Compared to Mold (mm)
1	54.425	0.018	0.286	9.370	0.056	0.014
2	54.419	0.020	0.280	9.360	0.056	0.024
3	53.939	0.090	0.200	9.390	0.063	0.006
4	53.940	0.060	0.199	9.371	0.083	0.013
5	54.130	0.032	0.009	9.372	0.048	0.012
6	54.230	0.038	0.091	9.379	0.111	0.005
7	53.952	0.036	0.187	9.371	0.066	0.013
8	54.264	0.060	0.125	9.379	0.089	0.005
9	53.754	0.037	0.385	9.387	0.081	0.003
10	54.038	0.034	0.101	9.392	0.074	0.008
11	54.121	0.047	0.018	9.395	0.063	0.011
12	54.040	0.045	0.099	9.371	0.037	0.013
13	54.155	0.042	0.016	9.380	0.043	0.004
14	54.043	0.110	0.096	9.378	0.071	0.006
15	53.863	0.057	0.276	9.364	0.071	0.020
16	53.972	0.027	0.167	9.366	0.051	0.018
17	54.042	0.028	0.097	9.389	0.088	0.005
18	54.255	0.063	0.116	9.359	0.070	0.025
19	54.107	0.035	0.032	9.368	0.038	0.016
20	54.227	0.110	0.088	9.369	0.043	0.015
21	54.183	0.025	0.044	9.365	0.051	0.019
22	54.305	0.071	0.166	9.381	0.105	0.003
23	55.730	1.224	1.591	9.388	0.050	0.004
24	54.023	0.034	0.116	9.371	0.023	0.013
25	54.773	0.052	0.634	9.360	0.094	0.024
26	53.884	0.047	0.255	9.374	0.026	0.010
27	54.071	0.188	0.068	9.382	0.034	0.002

Table A-2: Repeatability Results from Experiment Number 13

	Spherical Side			Aspherical Side		
Lens #	Fit Radius (mm)	Form Error within Fit Radius (Microns)	Total Power Error Compared to Mold (mm)	Fit Radius (mm)	Form Error within Fit Radius (Microns)	Total Power Error Compared to Mold (mm)
1	54.087	0.038	0.052	9.365	0.240	0.019
2	54.133	0.026	0.006	9.381	0.067	0.003
3	53.698	0.085	0.441	9.382	0.052	0.002
4	54.121	0.044	0.018	9.370	0.076	0.014
5	54.278	0.092	0.139	9.369	0.083	0.015
6	54.208	0.045	0.069	9.367	0.072	0.017
7	53.926	0.076	0.213	9.368	0.098	0.016
8	54.309	0.056	0.170	9.366	0.089	0.018
9	54.103	0.049	0.036	9.372	0.062	0.012
10	54.032	0.089	0.107	9.379	0.195	0.005
Average	**54.090**	**0.060**	**0.125**	**9.372**	**0.103**	**0.012**
Std. Dev.	**0.178**	**0.024**	**0.130**	**0.006**	**0.062**	**0.006**

Appendix A (continued)

Table A-3: Repeatability Results from Experiment Number 15

	Spherical Side			Aspherical Side		
Lens #	Fit Radius (mm)	Form Error within Fit Radius (Microns)	Total Power Error Compared to Mold (mm)	Fit Radius (mm)	Form Error within Fit Radius (Microns)	Total Power Error Compared to Mold (mm)
1	53.891	0.023	0.248	9.366	0.059	0.018
2	53.955	0.034	0.184	9.363	0.044	0.021
3	53.878	0.023	0.261	9.365	0.060	0.019
4	53.891	0.040	0.248	9.368	0.068	0.016
5	53.945	0.022	0.194	9.367	0.054	0.017
6	53.882	0.032	0.257	9.369	0.055	0.015
7	53.901	0.039	0.238	9.364	0.070	0.020
8	53.934	0.020	0.205	9.367	0.066	0.017
9	53.869	0.035	0.270	9.362	0.049	0.022
10	53.965	0.041	0.174	9.365	0.051	0.019
Mean	**53.911**	**0.031**	**0.228**	**9.366**	**0.058**	**0.018**
Std Dev	**0.033**	**0.008**	**0.033**	**0.002**	**0.008**	**0.002**

Table A-4: Repeatability Results from Experiment Number 27

	Spherical Side			Aspherical Side		
Lens #	Fit Radius (mm)	Form Error within Fit Radius (Microns)	Total Power Error Compared to Mold (mm)	Fit Radius (mm)	Form Error within Fit Radius (Microns)	Total Power Error Compared to Mold (mm)
1	54.107	0.049	0.032	9.379	0.107	0.005
2	54.045	0.042	0.094	9.372	0.115	0.012
3	54.014	0.072	0.125	9.372	0.048	0.012
4	54.064	0.048	0.075	9.382	0.076	0.002
5	53.913	0.059	0.226	9.378	0.065	0.006
6	54.233	0.014	0.094	9.373	0.037	0.011
7	54.098	0.076	0.041	9.375	0.044	0.009
8	54.225	0.196	0.086	9.380	0.112	0.004
9	54.142	0.021	0.003	9.374	0.031	0.010
10	54.092	0.034	0.047	9.371	0.041	0.013
Mean	**54.093**	**0.061**	**0.082**	**9.376**	**0.068**	**0.008**
Std. Dev	**0.086**	**0.047**	**0.056**	**0.003**	**0.030**	**0.003**

Appendix B

Temperature, Force and Position Data of 27 Experiments from Taguchi Method

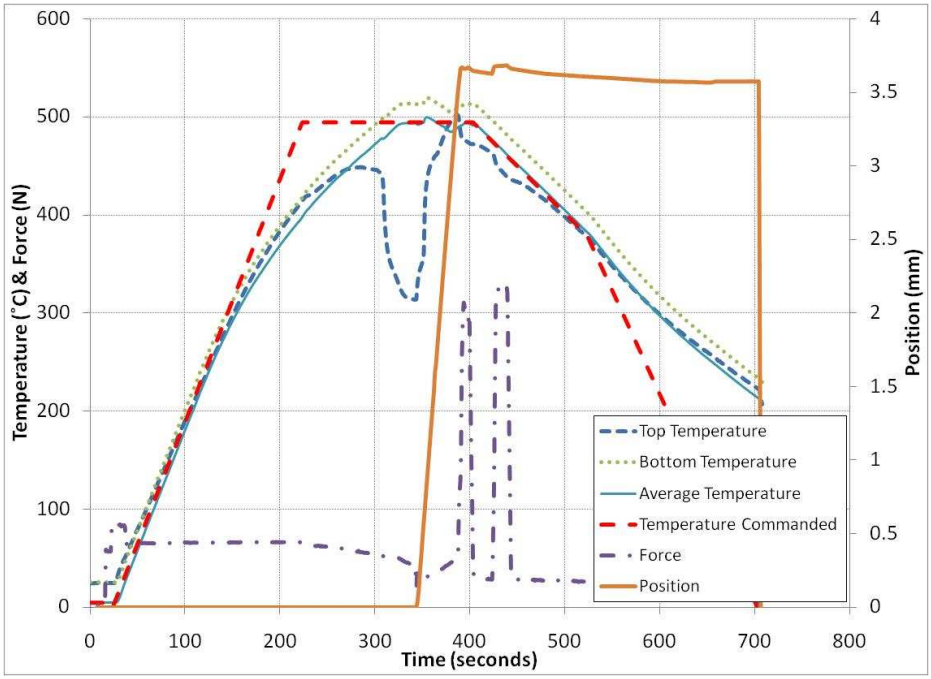

Figure B-1: Experiment 1

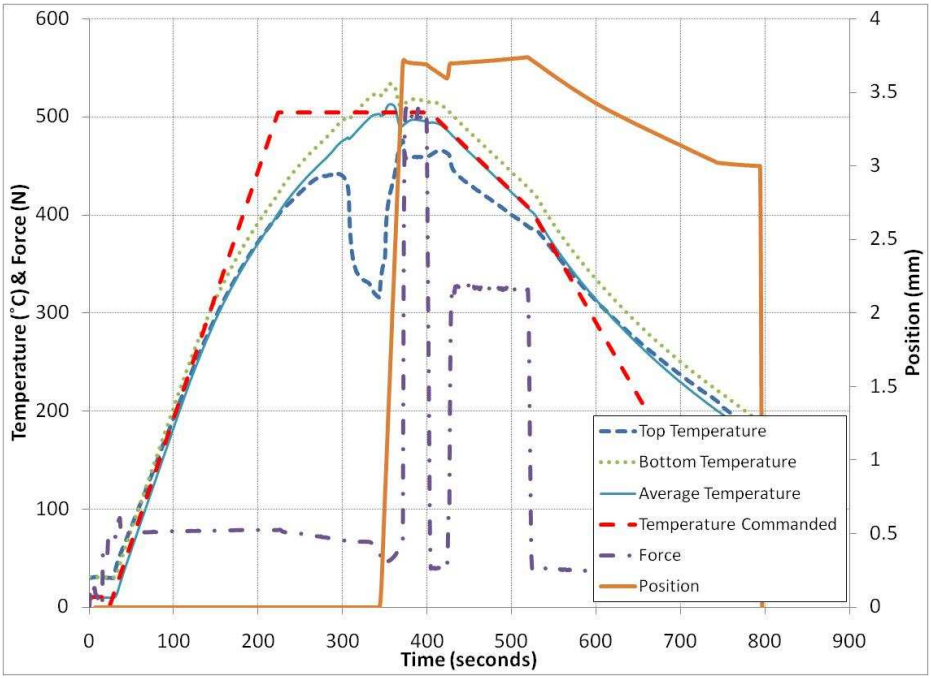

Figure B-2: Experiment 2

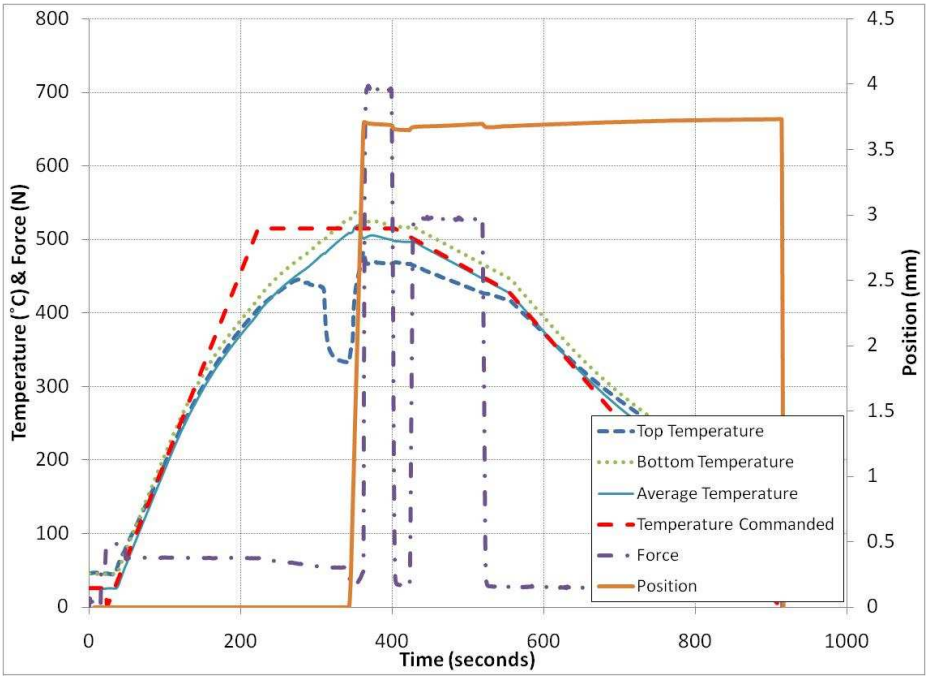

Figure B-3: Experiment 3

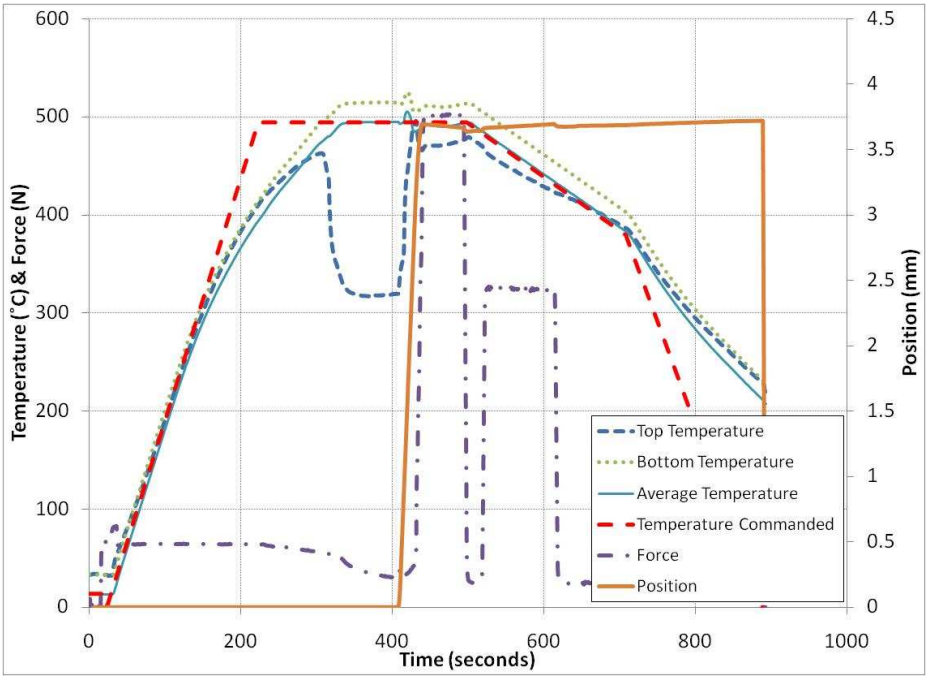

Figure B-4: Experiment 4

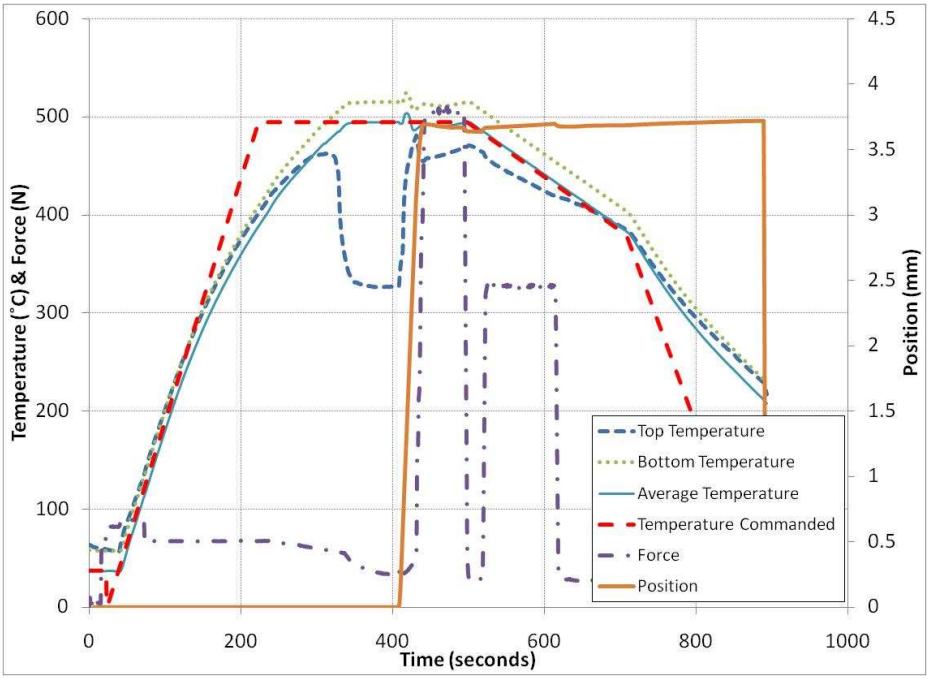

Figure B-5: Experiment 5

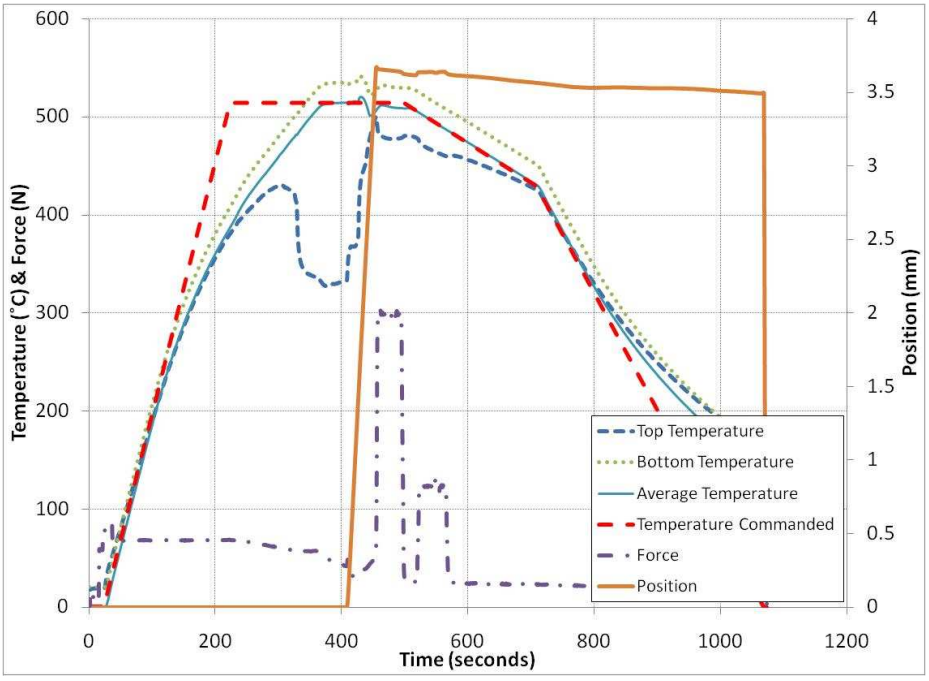

Figure B-6: Experiment 6

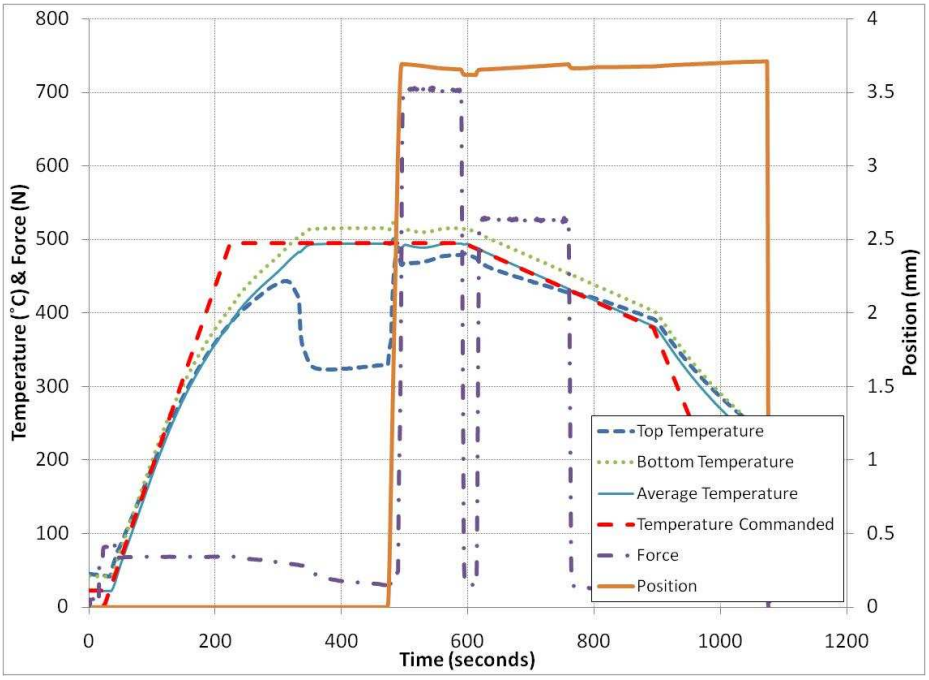

Figure B-7: Experiment 7

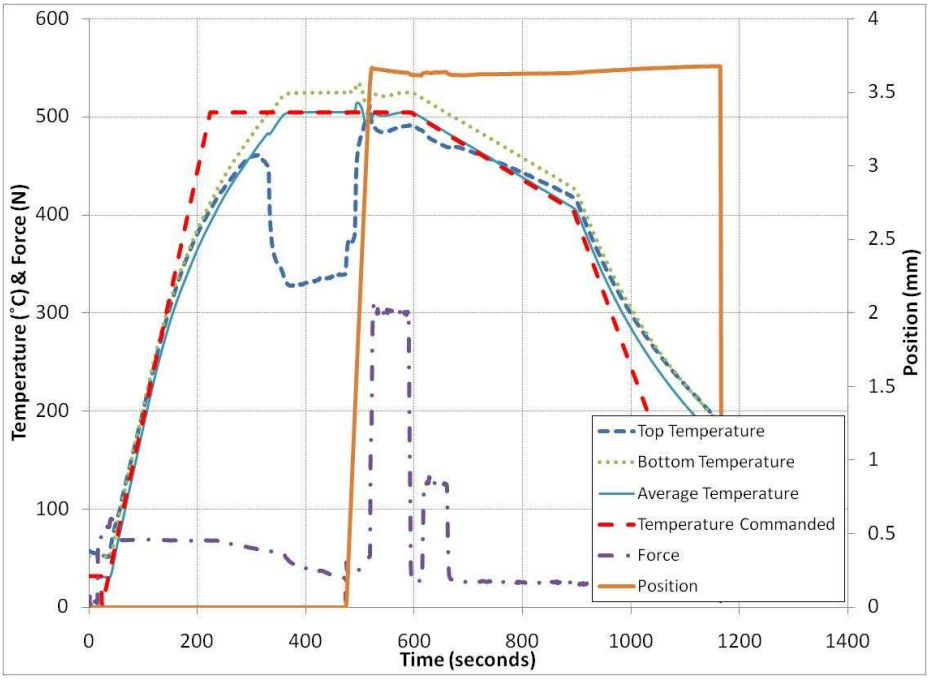

Figure B-8: Experiment 8

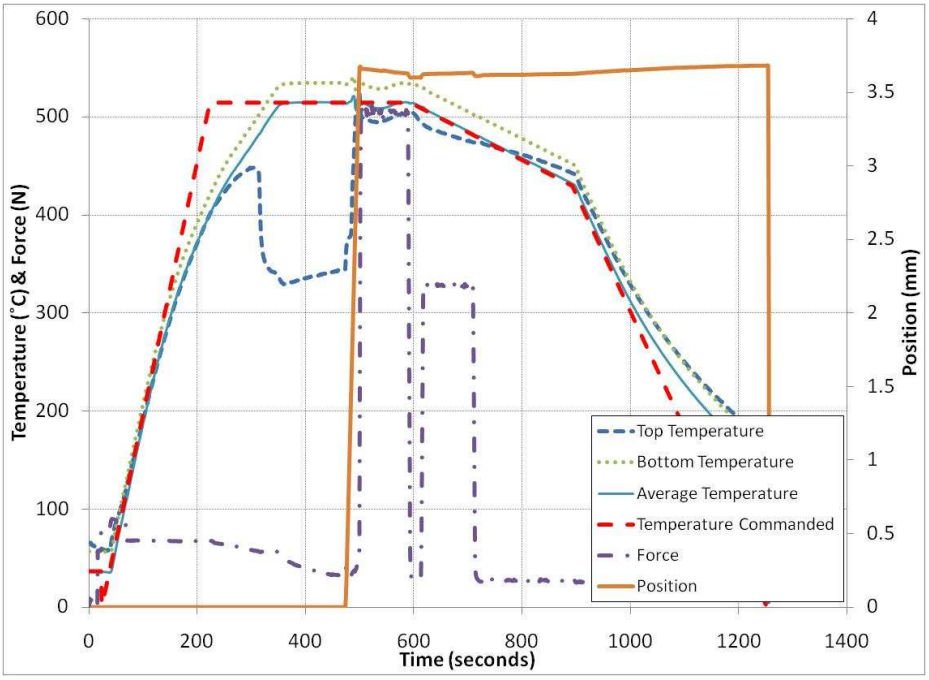

Figure B-9: Experiment 9

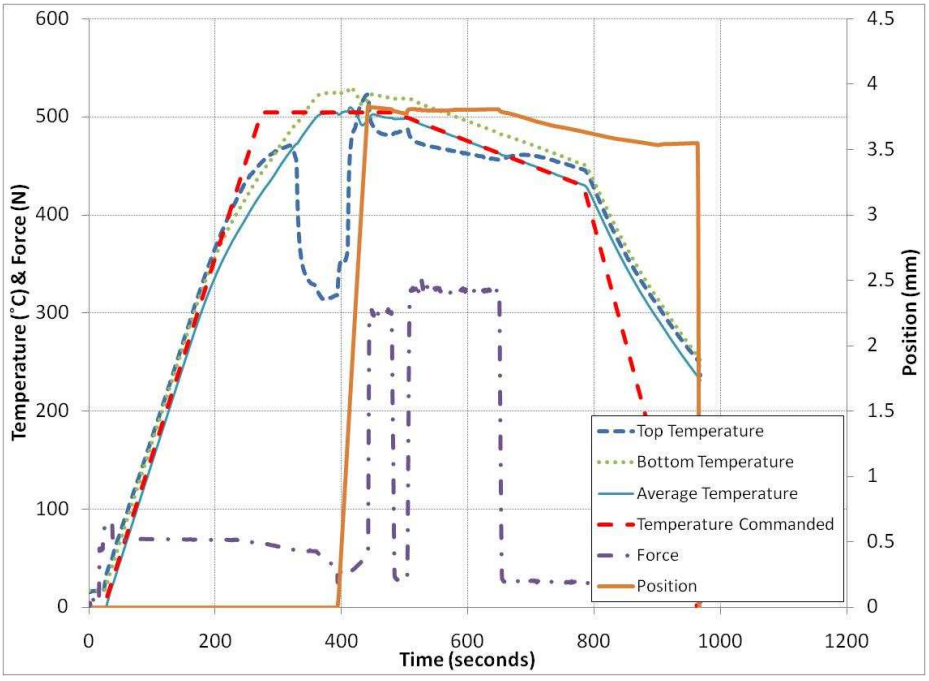

Figure B-10: Experiment 10

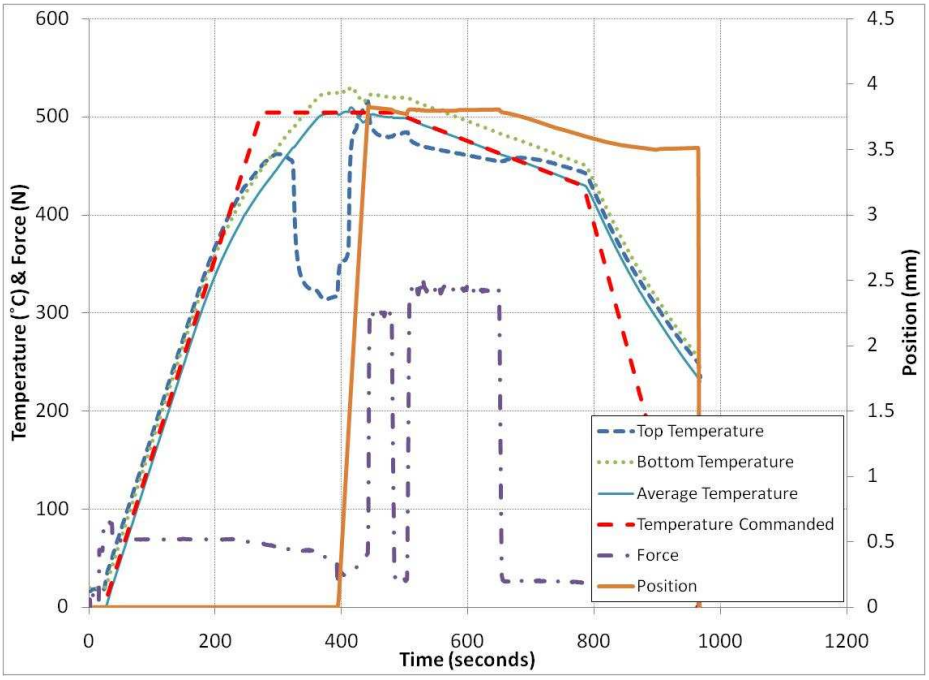

Figure B-11: Experiment 11

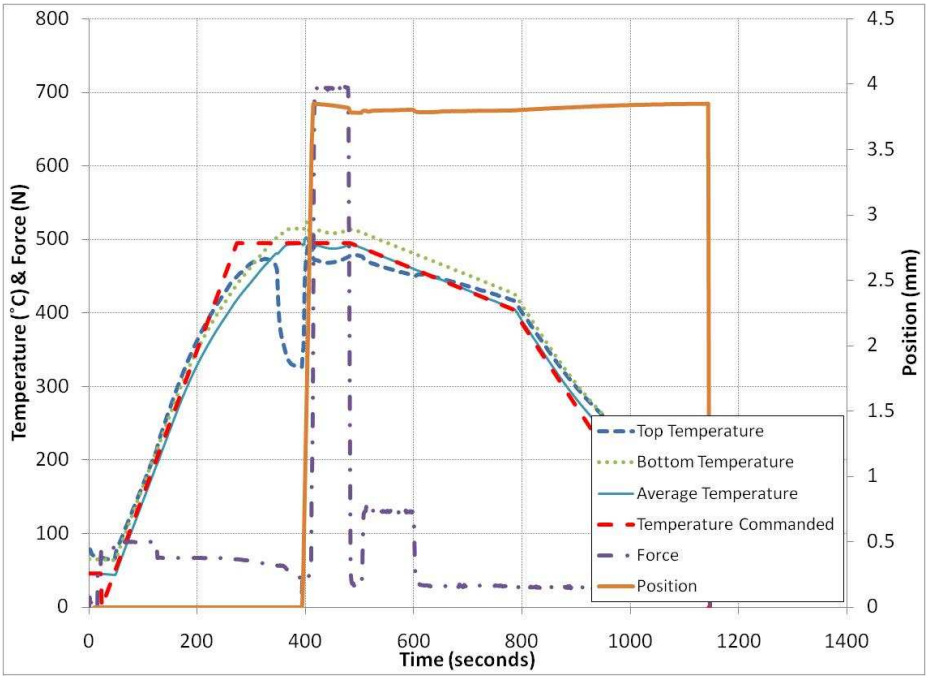

Figure B-12: Experiment 12

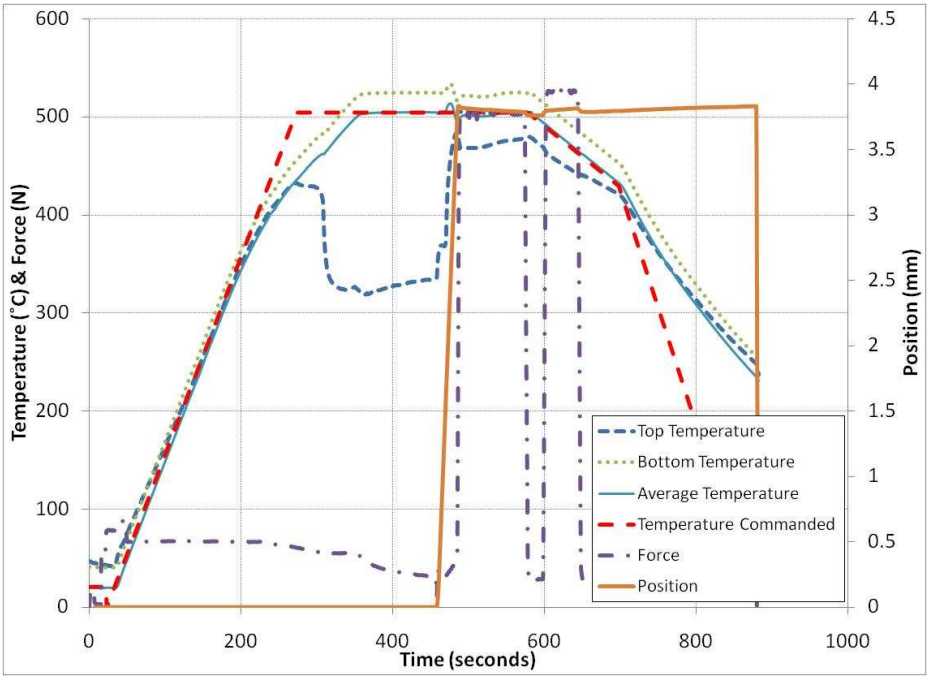

Figure B-13: Experiment 13

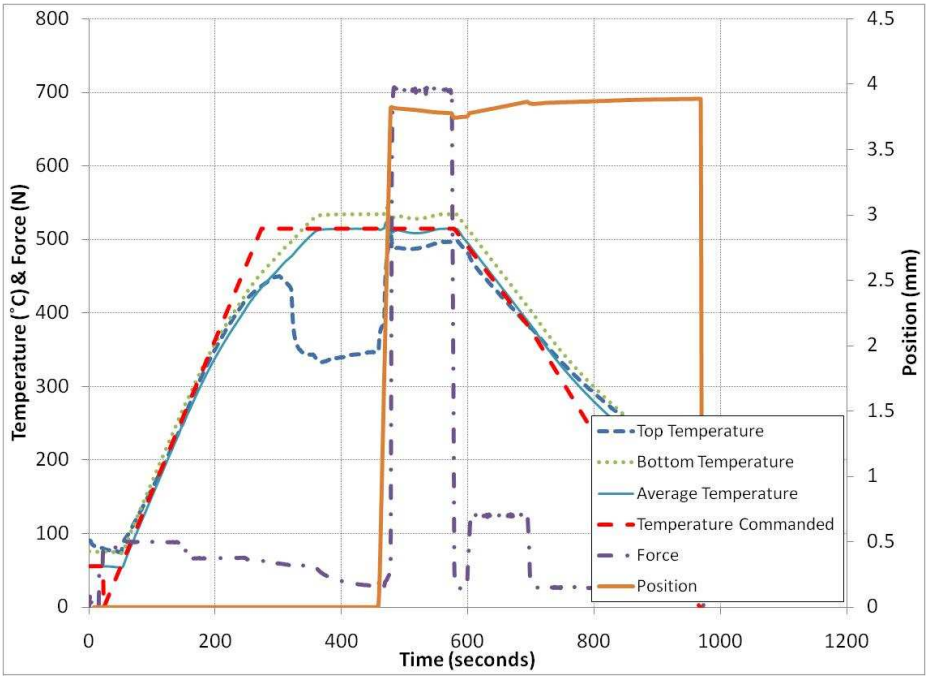

Figure B-14: Experiment 14

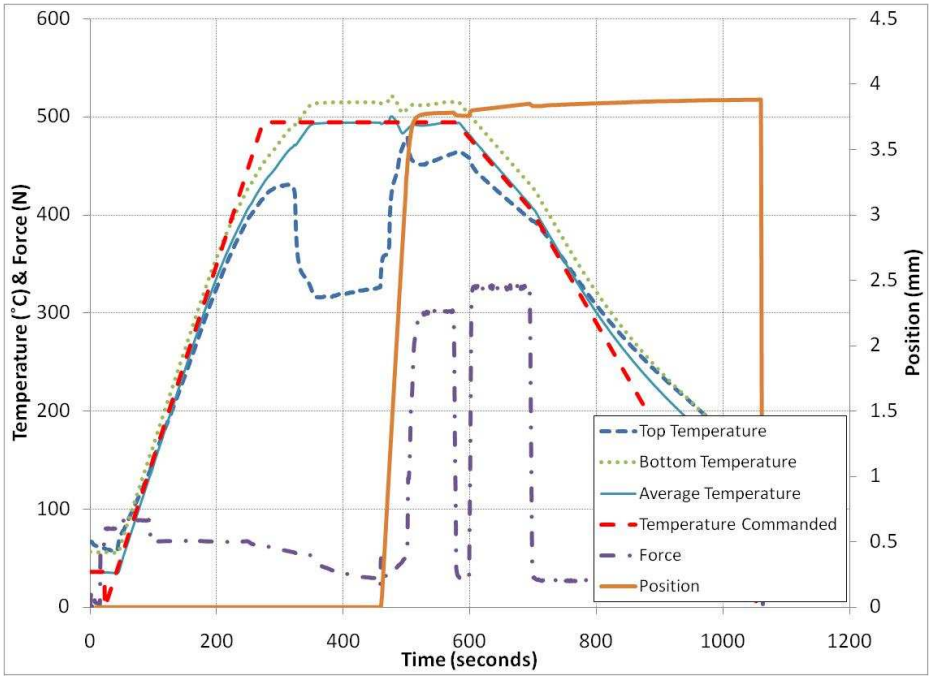

Figure B-15: Experiment 15

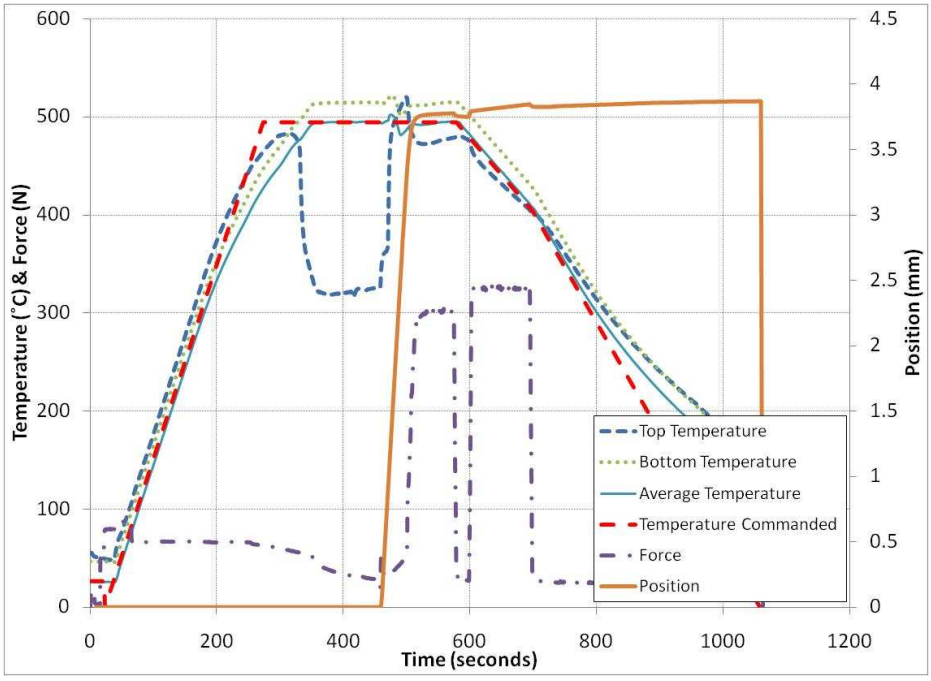

Figure B-16: Experiment 16

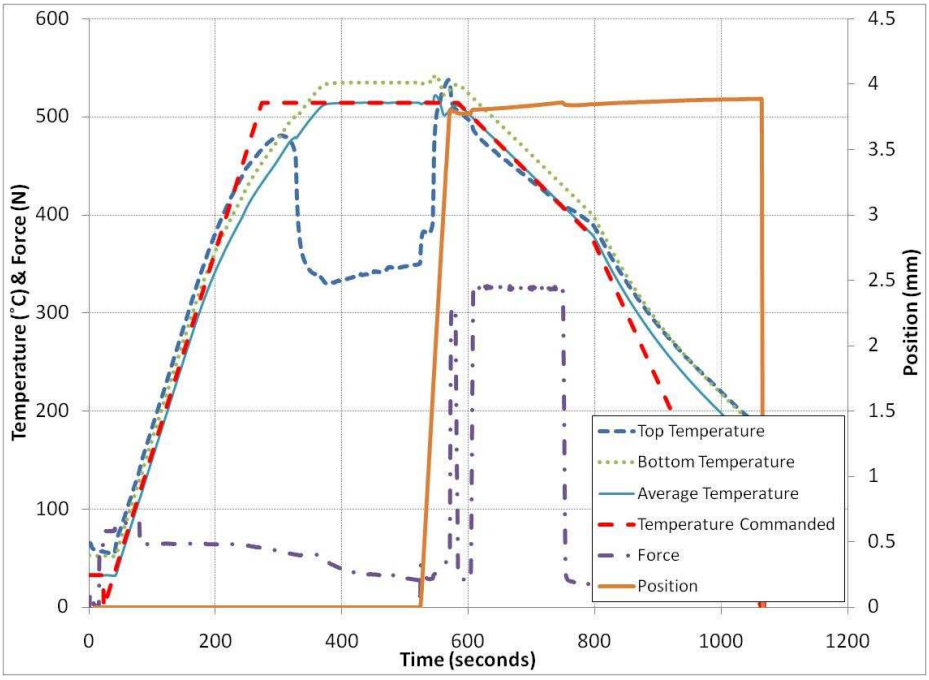

Figure B-17: Experiment 17

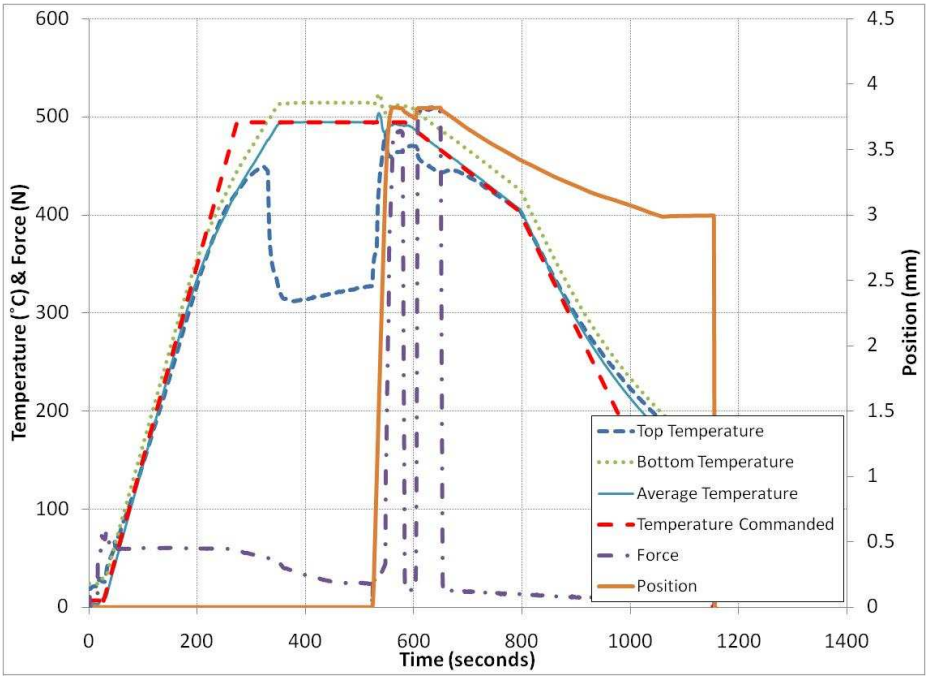

Figure B-18: Experiment 18

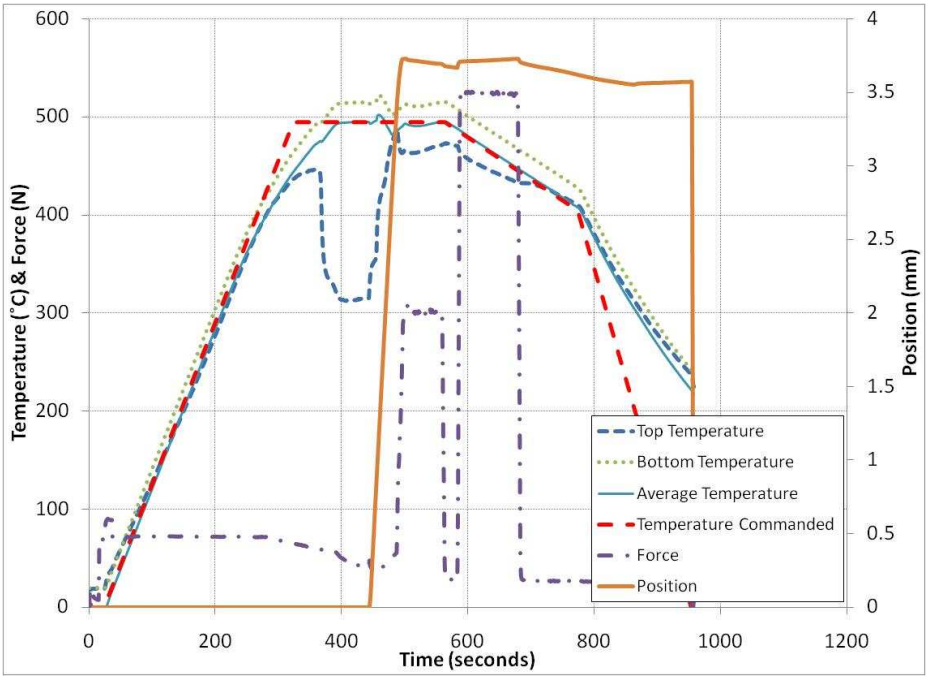

Figure B-19: Experiment 19

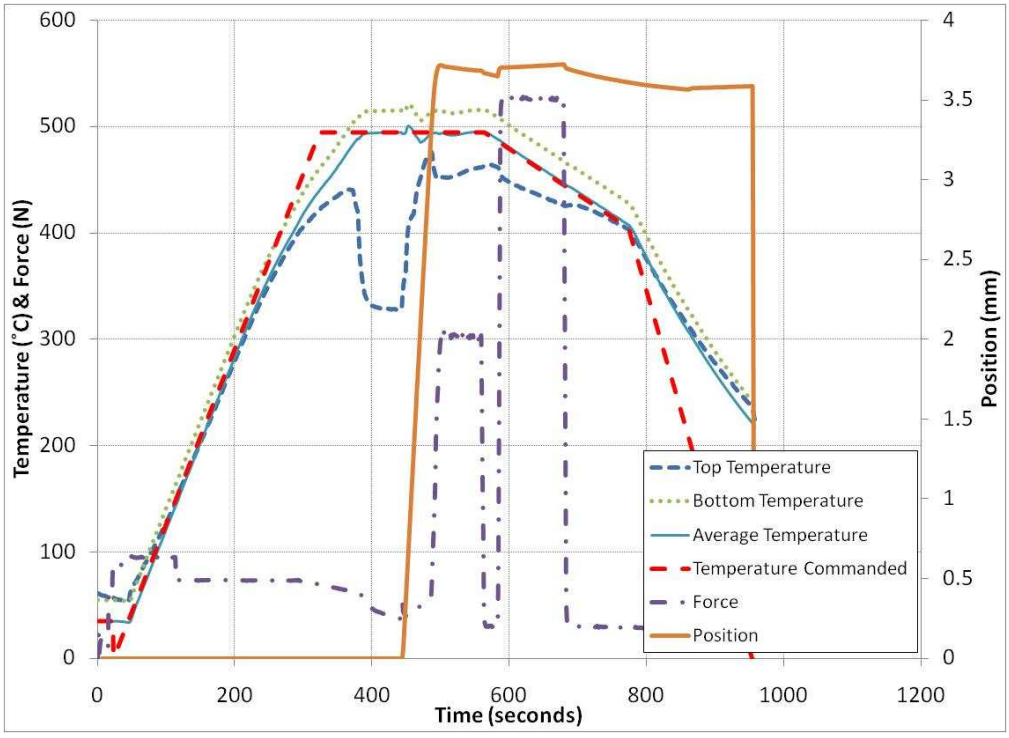

Figure B-20: Experiment 20

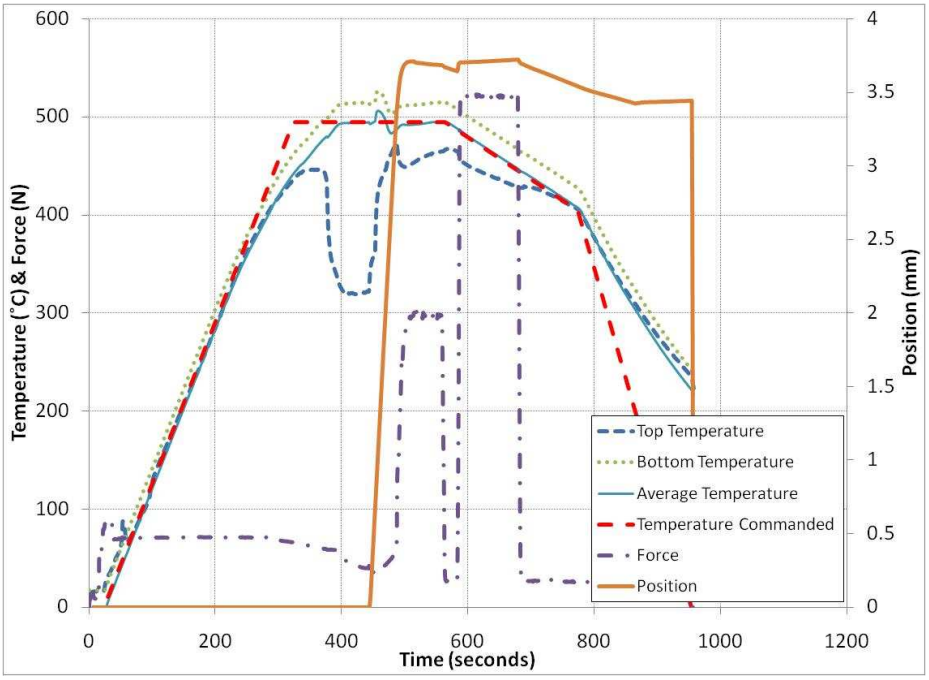

Figure B-21: Experiment 21

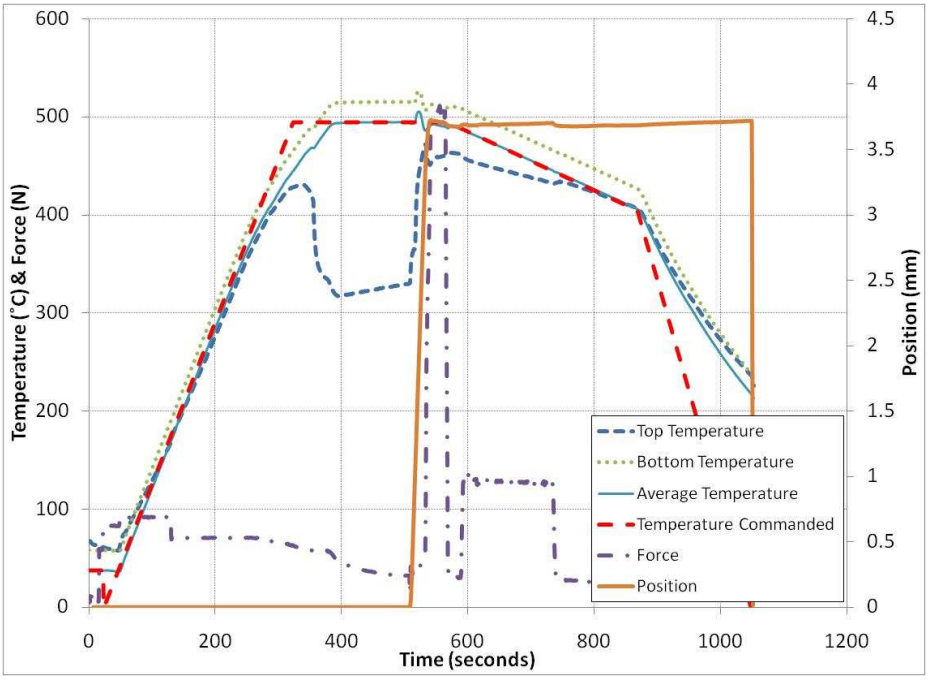

Figure B-22: Experiment 22

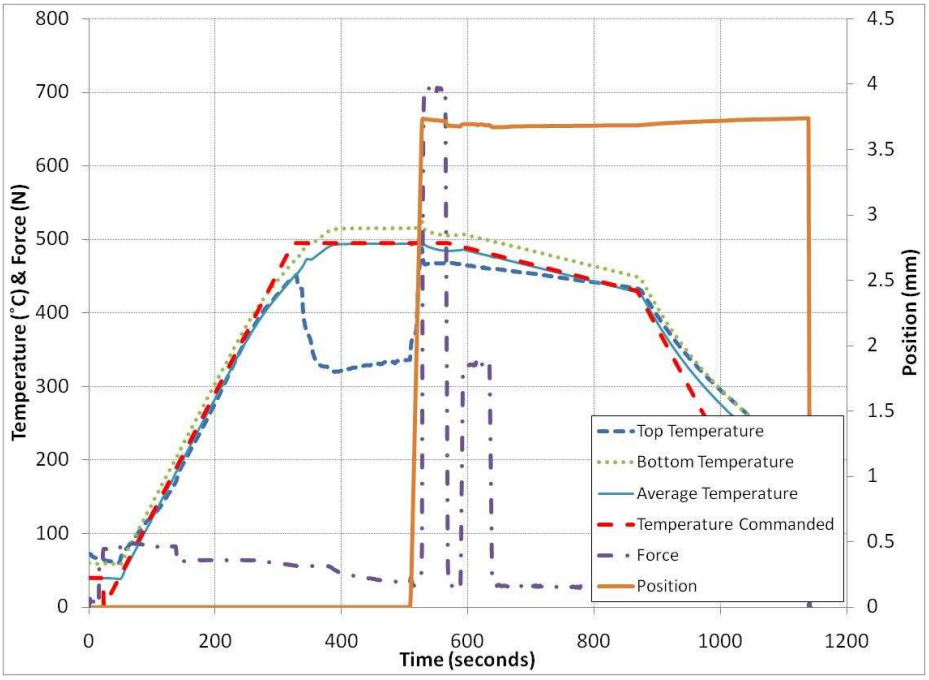

Figure B-23: Experiment 23

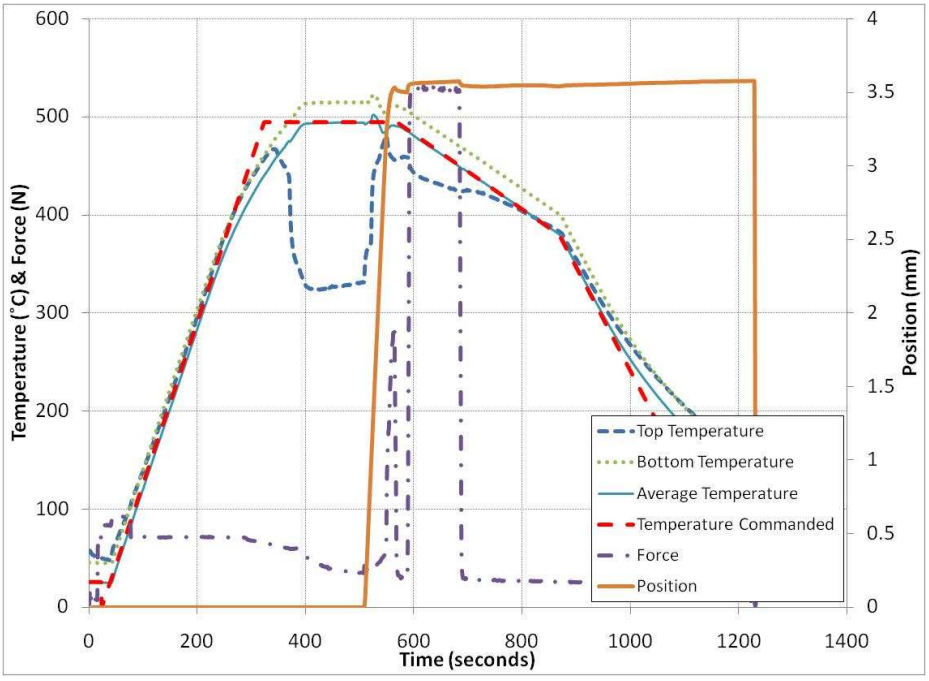

Figure B-24: Experiment 24

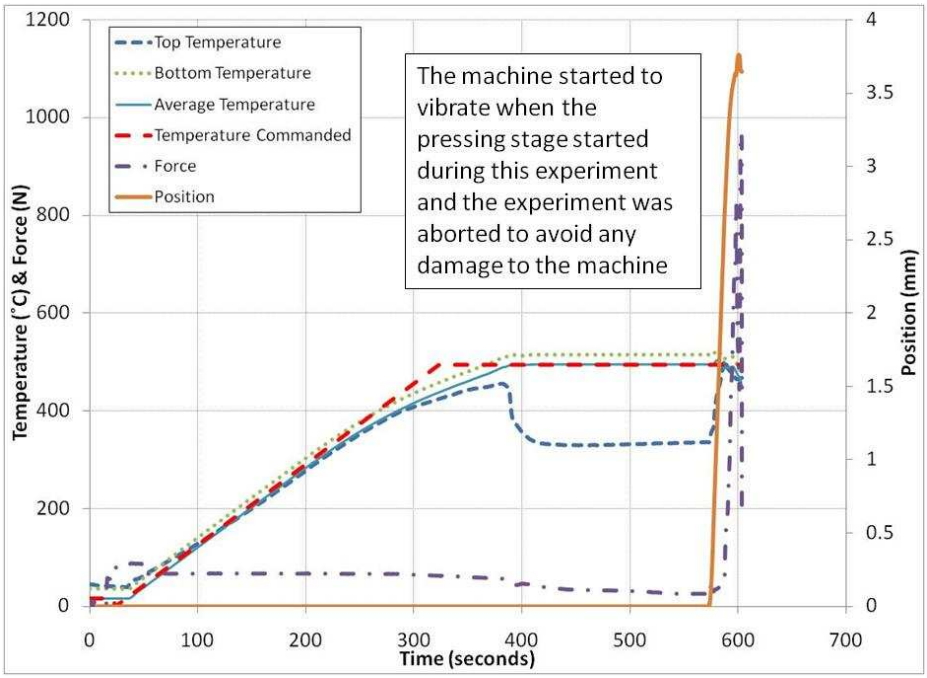

Figure B-25: Experiment 25

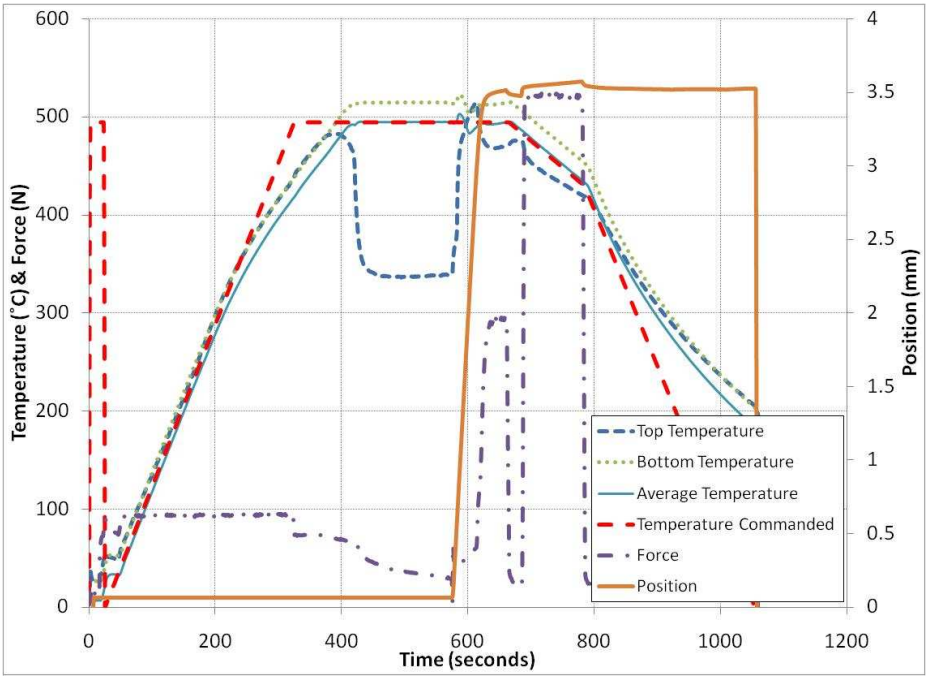

Figure B-26: Experiment 26

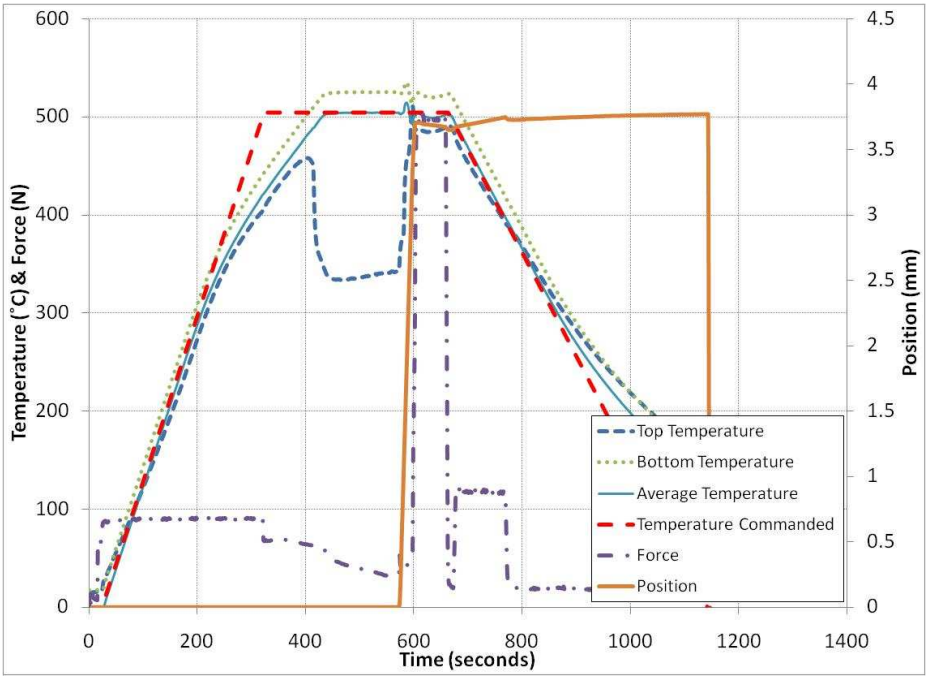

Figure B-27: Experiment 27

Appendix C

Input Variables compared to Radius of Spherical Side of Lens

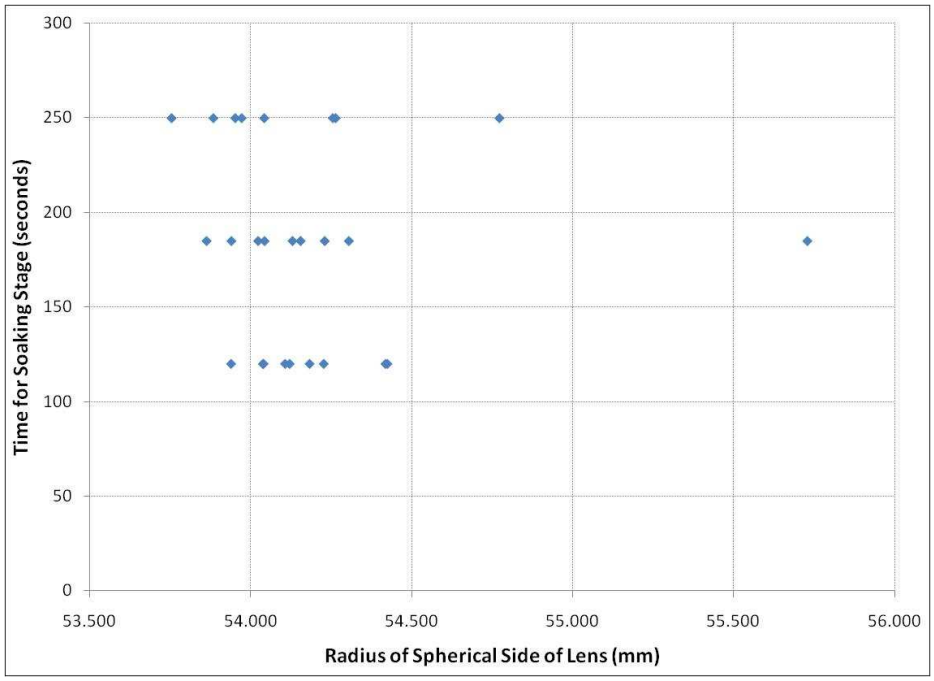

Figure C-1: Radius of Spherical Side of Lens versus Time for Soaking Stage

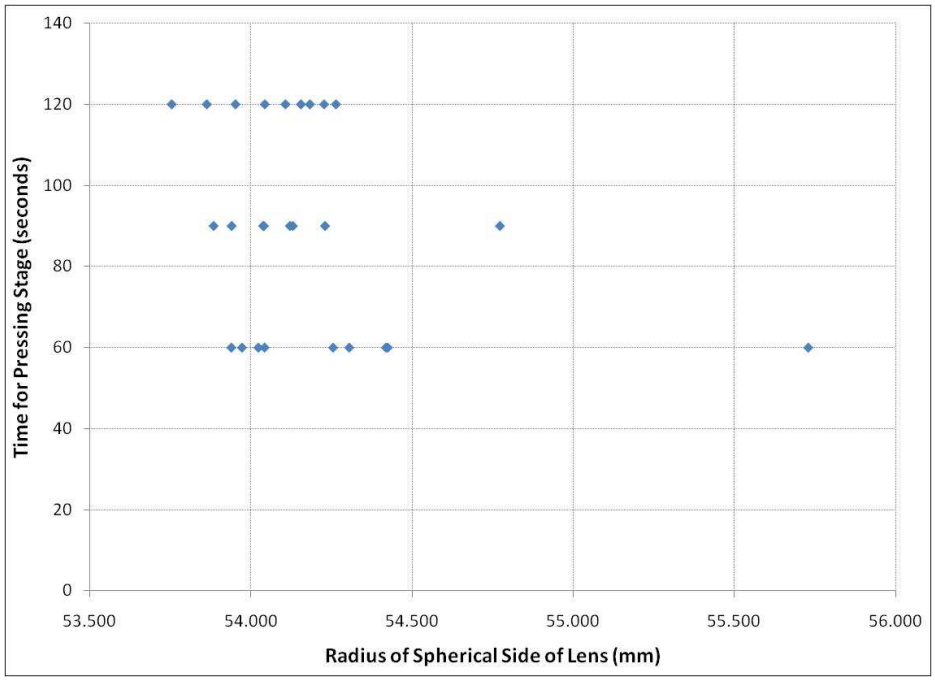

Figure C-2: Radius of Spherical Side of Lens versus Time for Pressing Stag

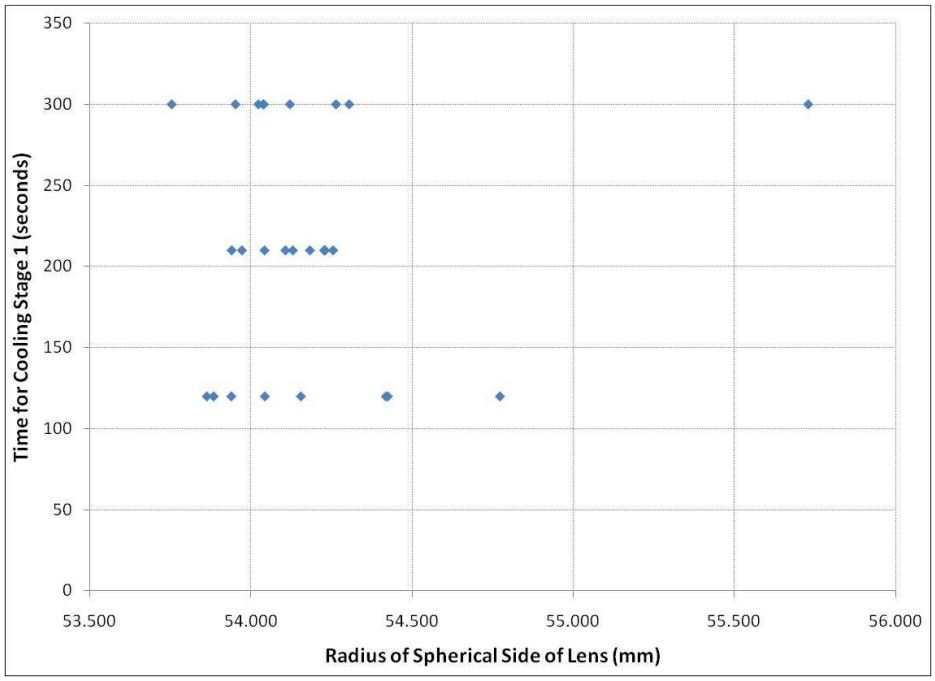

Figure C-3: Radius of Spherical Side of Lens versus Time for Cooling Stage 1

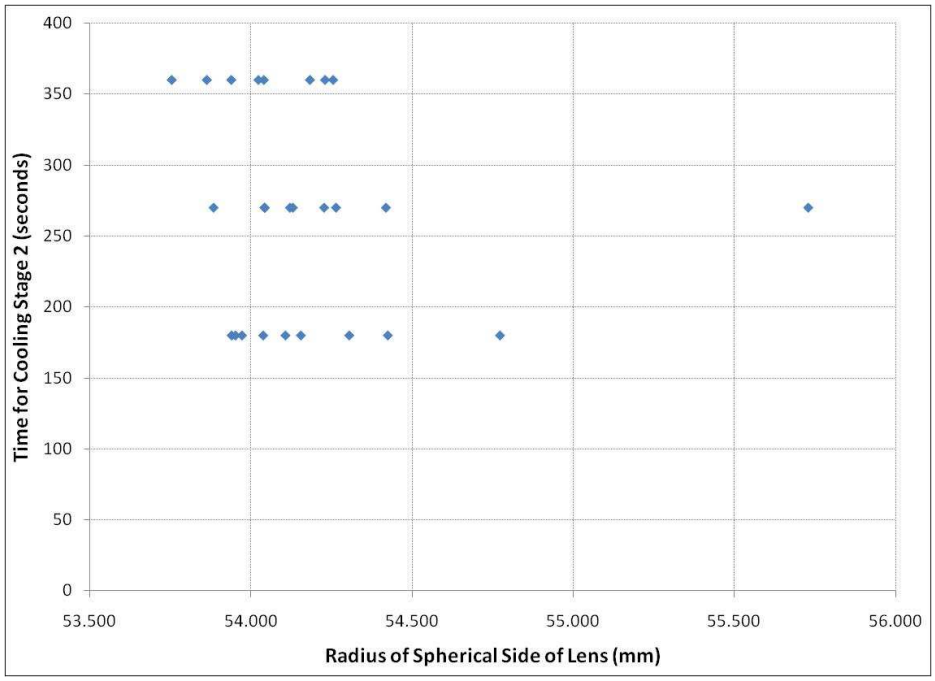

Figure C-4: Radius of Spherical Side of Lens versus Time for Cooling Stage 2

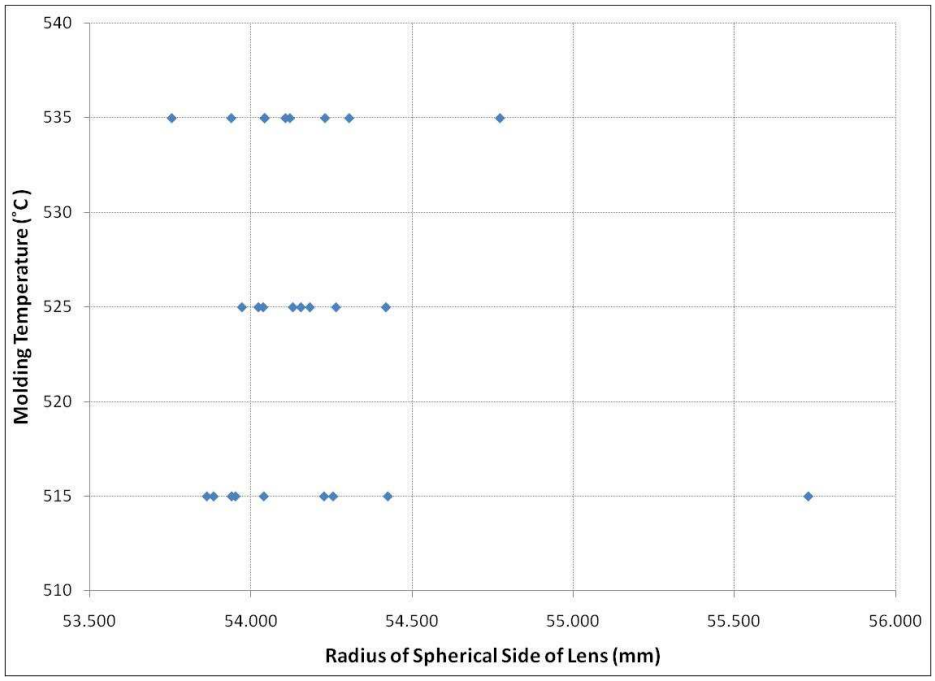

Figure C-5: Radius of Spherical Side of Lens versus Molding Temperature

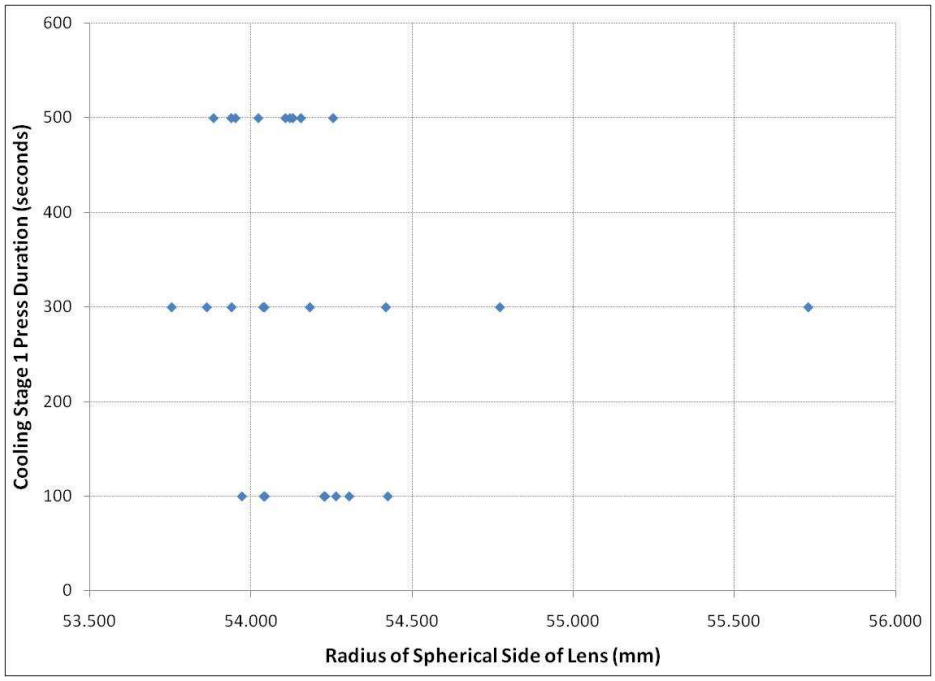

Figure C-6: Radius of Spherical Side of Lens versus Cooling Stage 1 Press Duration

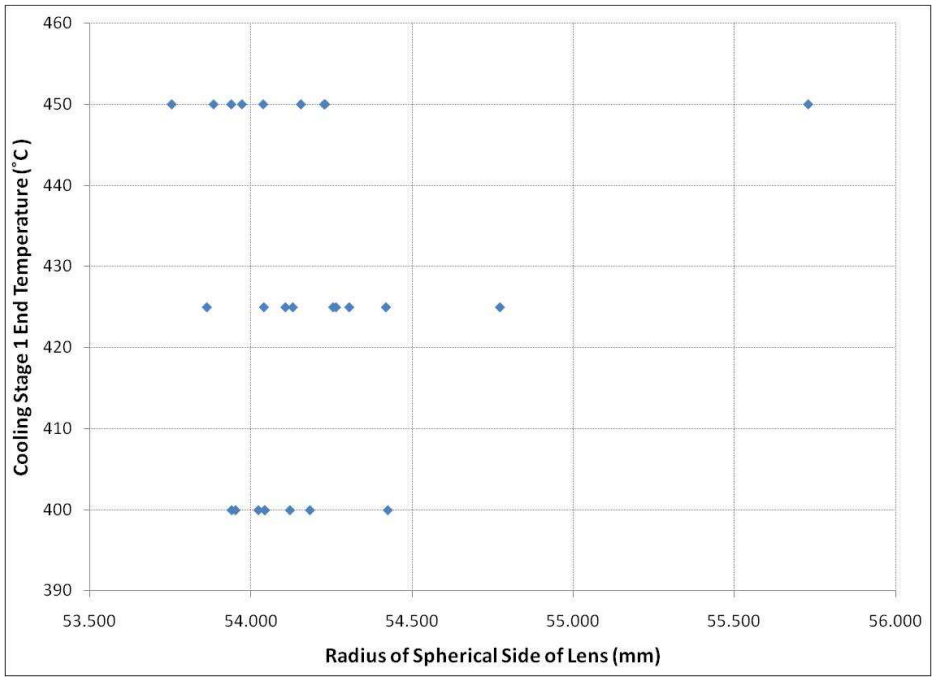

Figure C-7: Radius of Spherical Side of Lens versus Cooling Stage 1 End Temperature

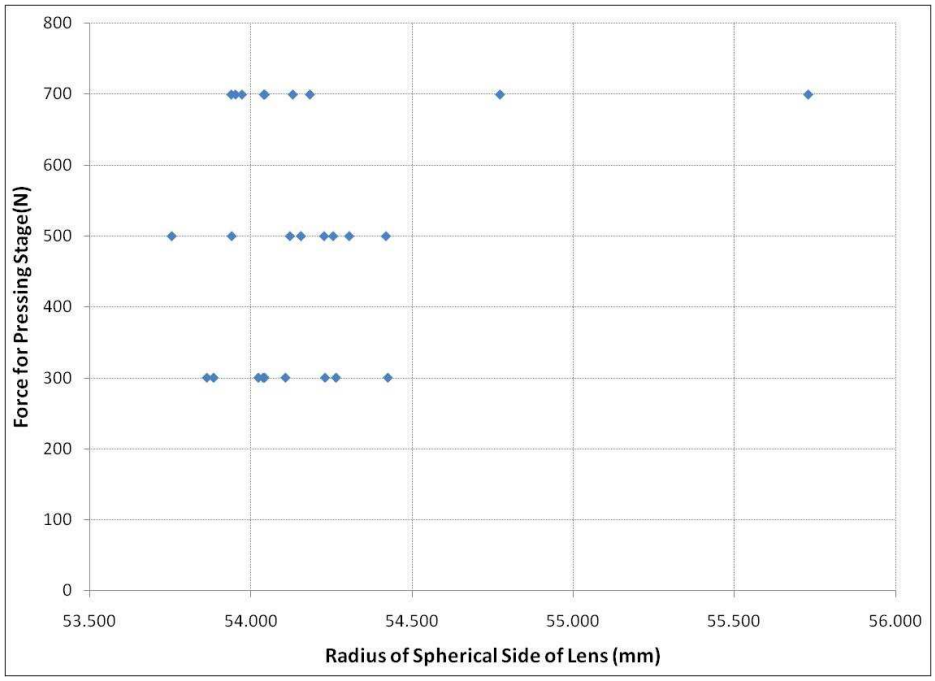

Figure C-8: Radius of Spherical Side of Lens versus Force for Pressing Stage

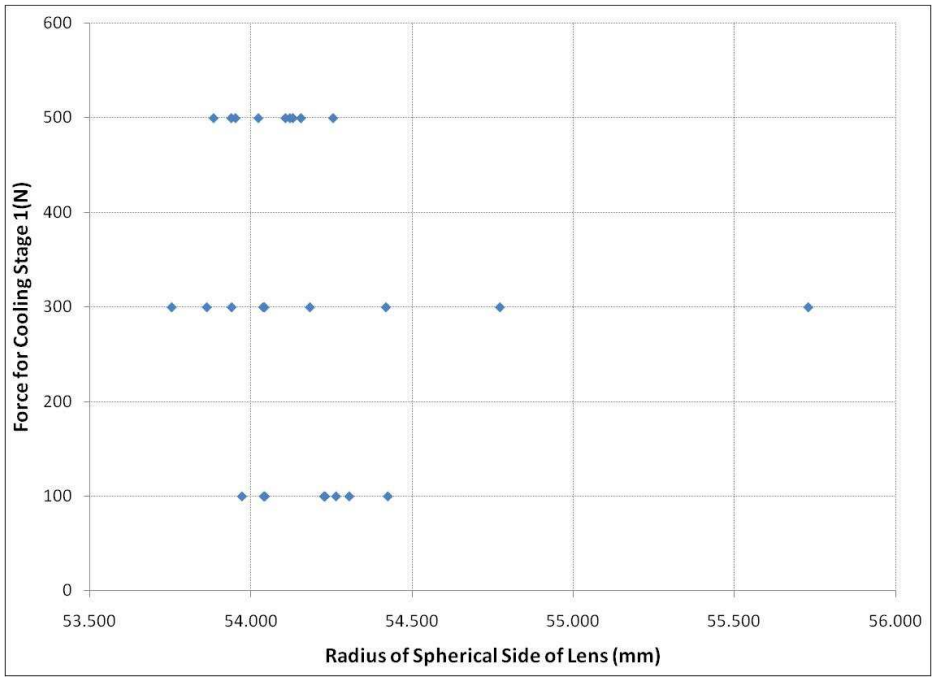

Figure C-9: Radius of Spherical Side of Lens versus Cooling Stage 1 Force

APPENDIX D

Input Variables compared to R_{asp} value of Aspherical Side of Lens

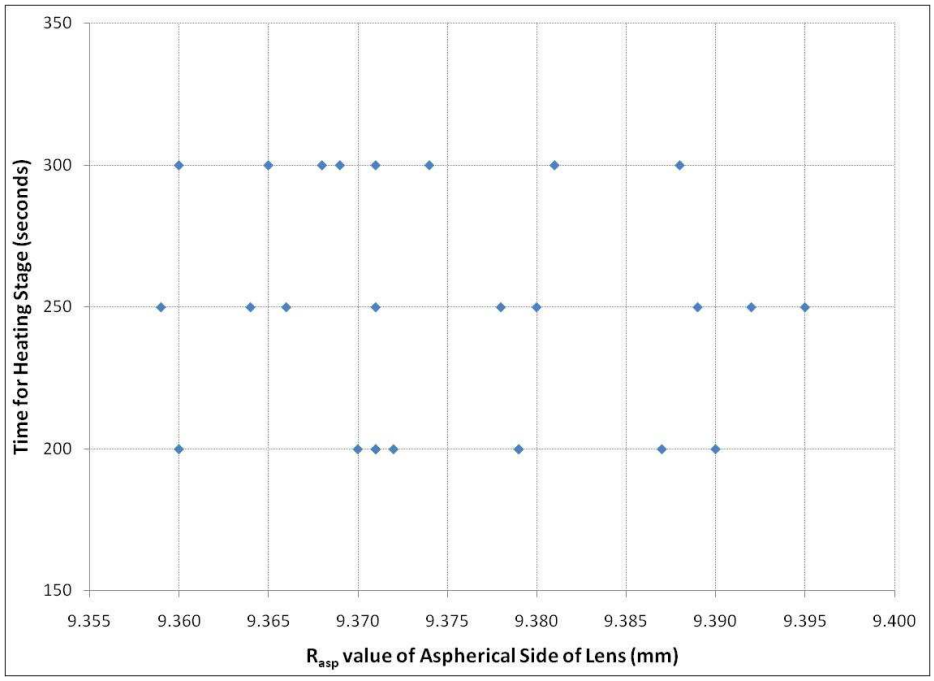

Figure D-1: R_{asp} value of Aspherical Side of Lens versus Time for Heating Stage

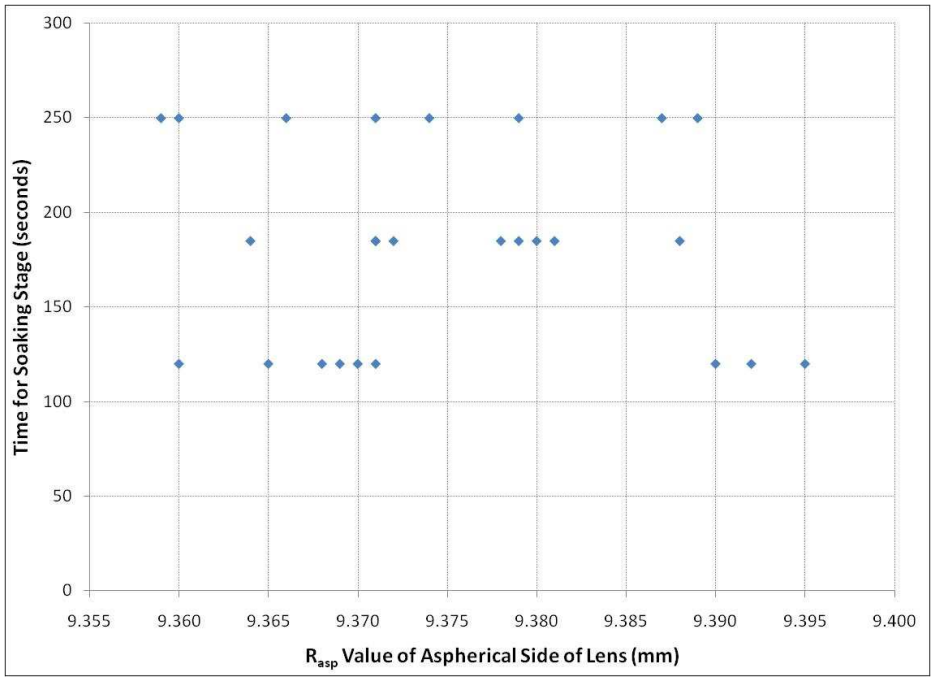

Figure D-2: R_{asp} value of Aspherical Side of Lens versus Time for Soaking Stage

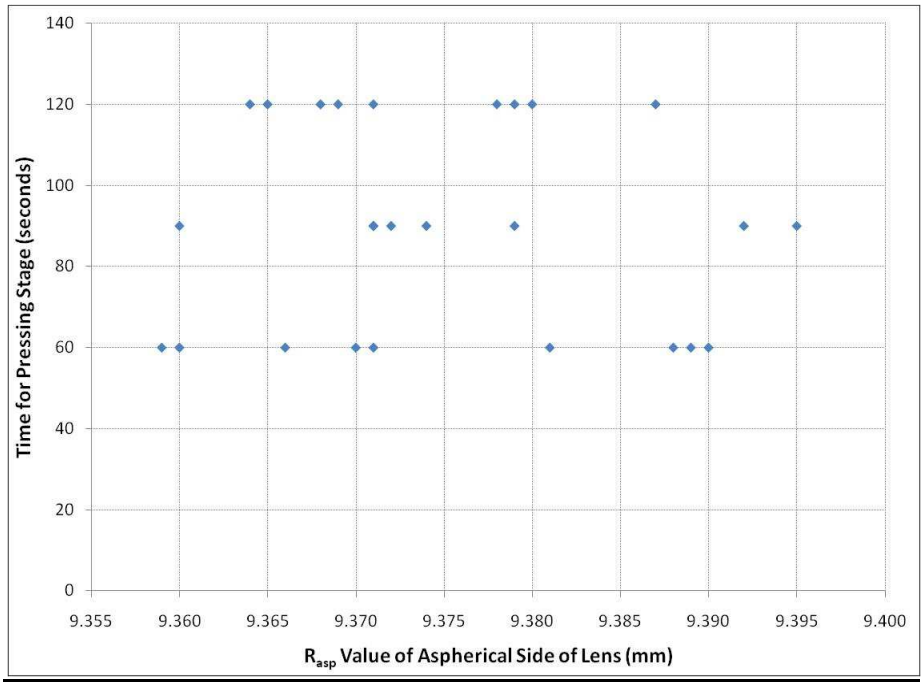

Figure D-3: R_{asp} value of Aspherical Side of Lens versus Time for Pressing Stage

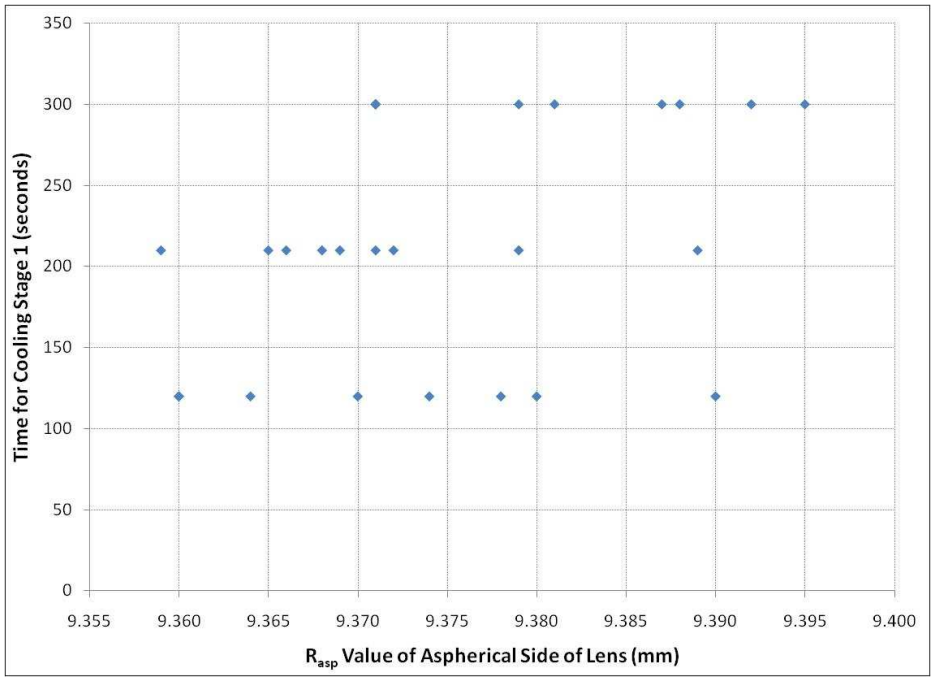

Figure D-4: R_{asp} value of Aspherical Side of Lens versus Time for Cooling Stage 1

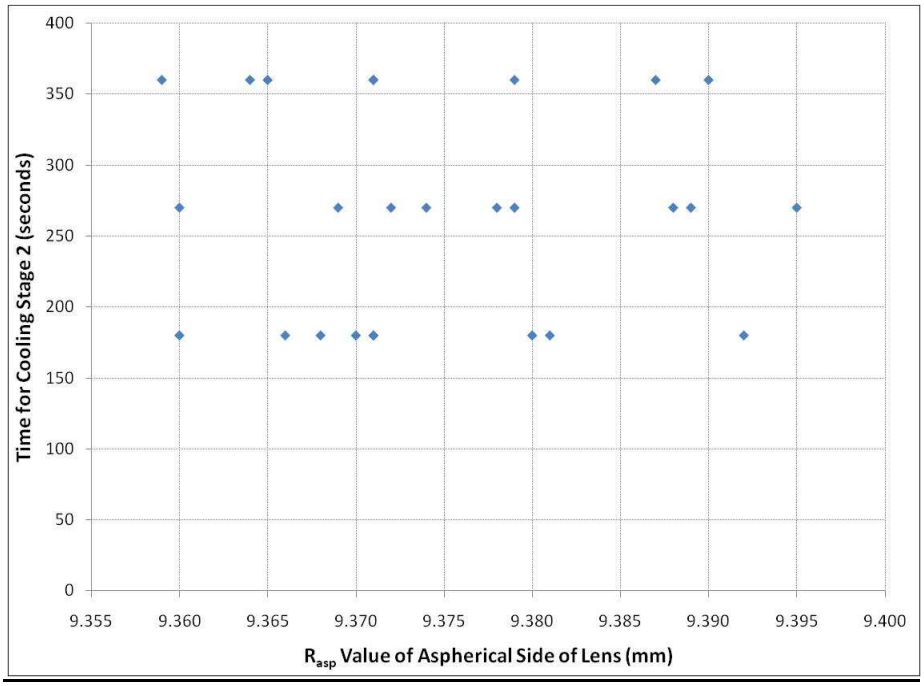

Figure D-5: R_{asp} value of Aspherical Side of Lens versus Time for Cooling Stage 2

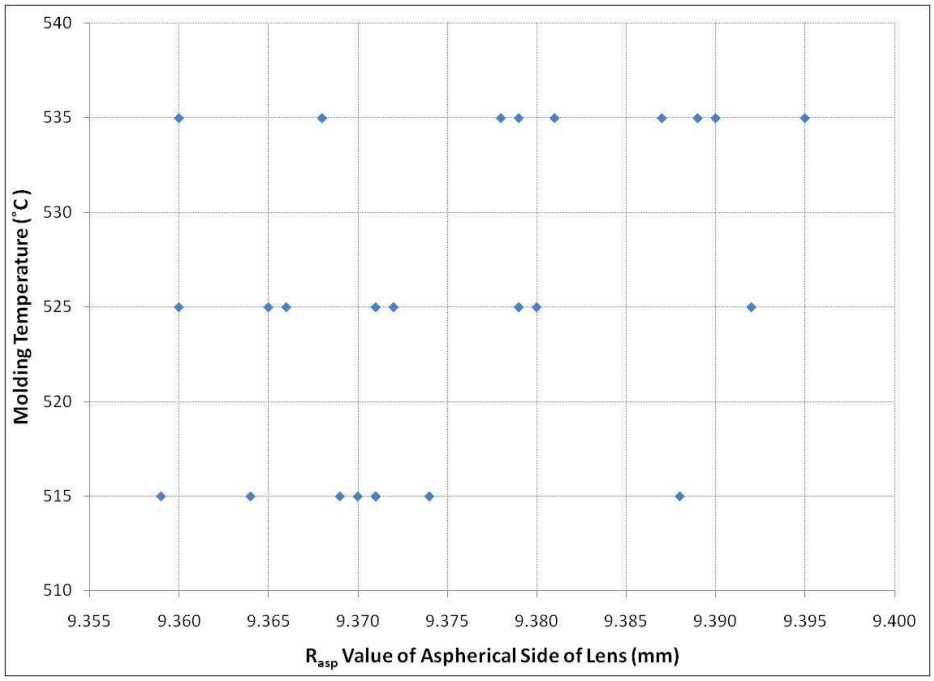

Figure D-6: R_{asp} value of Aspherical Side of Lens versus Molding Temperature

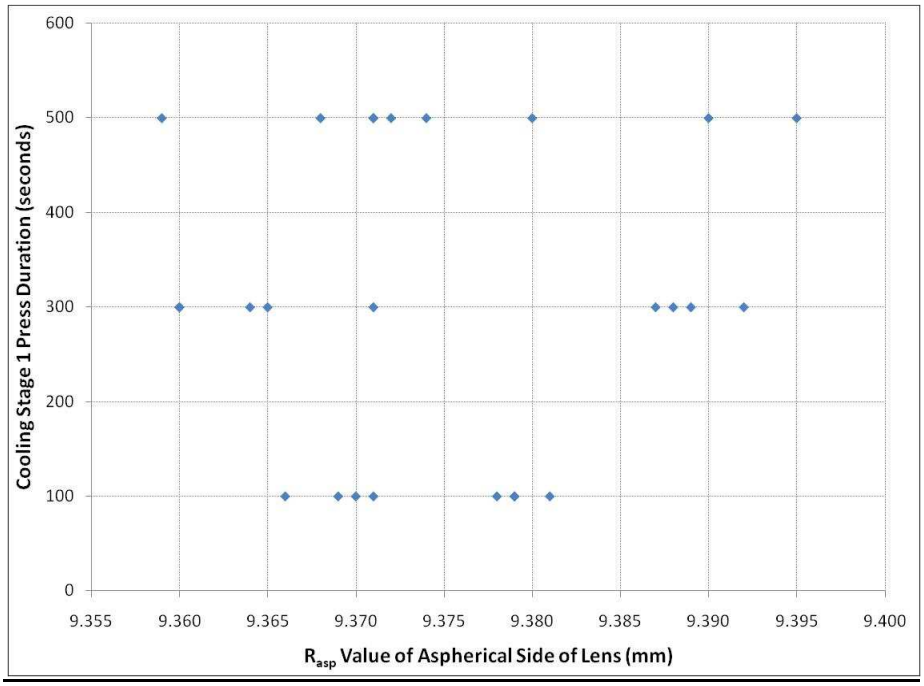

Figure D-7: R_{asp} value of Aspherical Side of Lens versus Cooling Stage 1 Press Duration

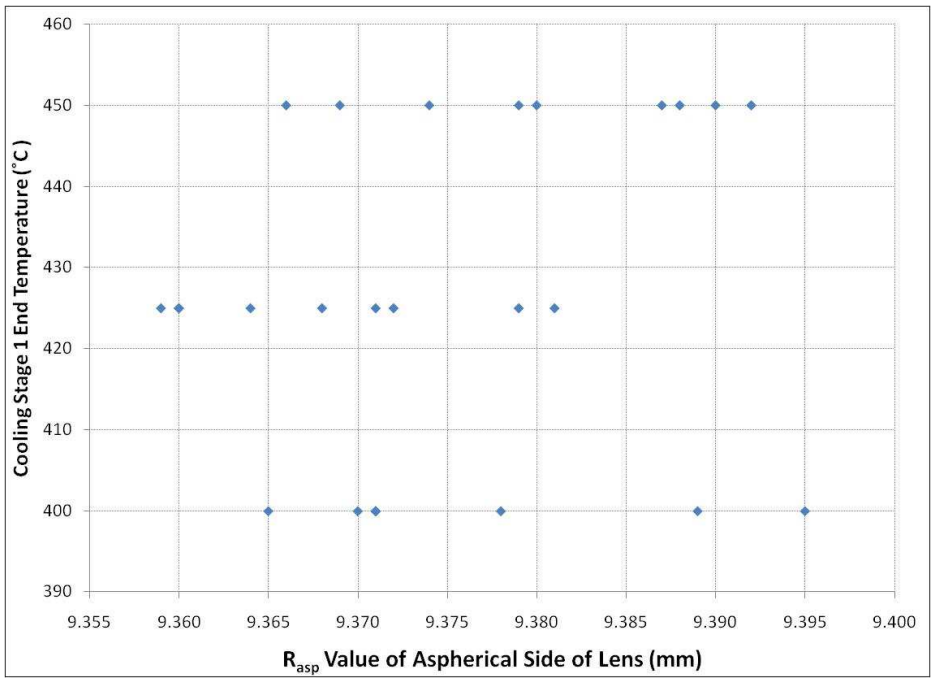

Figure D-8: R_{asp} value of Aspherical Side of Lens versus Cooling Stage 1 End Temperature

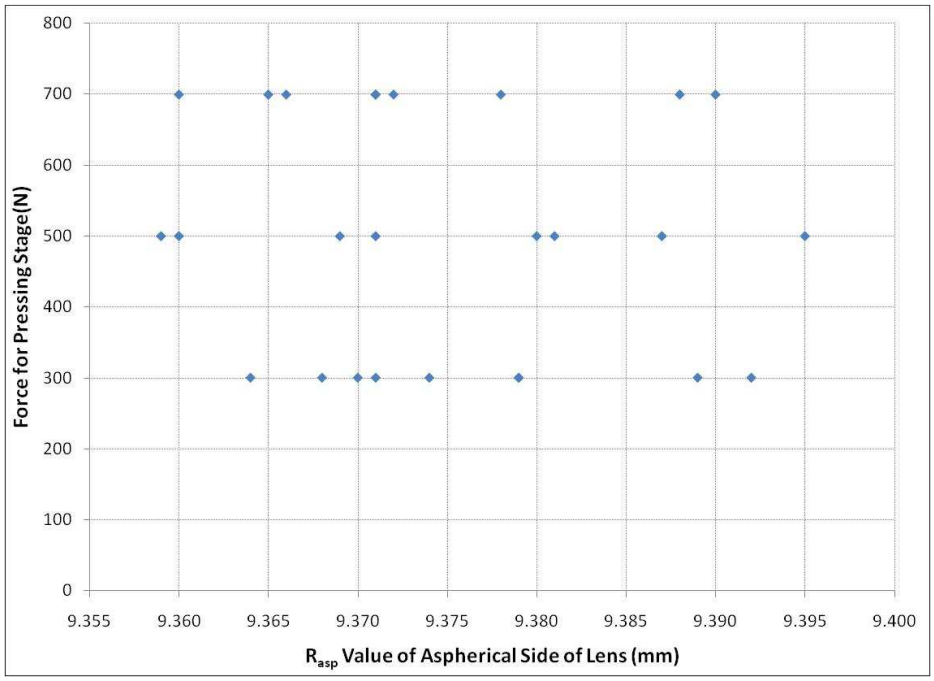

Figure D-9: R_{asp} value of Aspherical Side of Lens versus Force for Pressing Stage

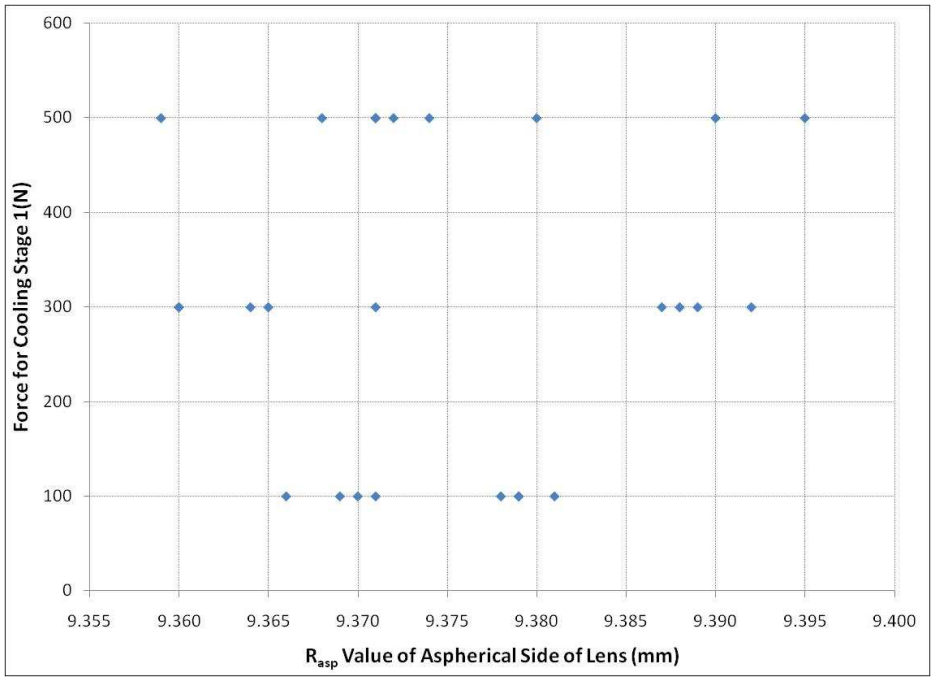

Figure D-10: R_{asp} value of Aspherical Side of Lens versus Cooling Stage 1 Force

REFERENCES

1. Carson, F., 1969, 'Basic Optics and Optical Instruments', General Publishing Company, Ltd., Toronto, Ontario, Canada.

2. Toshiba, 'High Precision Optical Glass Mold Press Machine', Toshiba Machine Co. Ltd, 2008, <http://www.toshiba-machine.co.jp>.

3. Yi, A., Firestone, G., and Jain, A., 2005, 'Precision Laboratory Apparatus for High Temperature Compression Molding of Glass Lenses', Review of Scientific Instruments, Columbus, Ohio.

4. Tsai, Y., Hung, C., and Hung, J., 2008, 'Glass Material Model for the Forming Stage of the Glass Molding Process', Journal of Materials Processing Technology, Vol. 201, Pages 751-754.

5. Quartz, 'Properties of BK7', Quartz Unlimited LLC, Boca Raton, 2001, <http://www.qullc.com/BK7.html>

6. Jain, A., Firestone, G., and Yi, A., 2005, 'Viscosity Measurement by Cylindrical Compression for Numerical Modeling of Precision Lens Molding Process', Journal of American Ceramic Society, Vol. 88, No. 9, Pages 2409-2414, 2005.

7. Yi, A., and Huang, C., 2006, 'Development of a Compression Molding Process for Three-Dimensional Tailored Free-From Glass Optics', Applied Optics, September 2006, Vol. 45, No. 25., Page 6511-6518.

8. Klocke, F., Dambon, O and Pongs, G., 2008 'Finite Element Analysis of Glass Moulding', Proceedings of IMechE, Vol. 222, Pages 101-106, 2008.

9. Katsuki, M., 2007, 'Glass Molding and Mold Machining for Optical Elements', Toshiba Machine Co. Ltd., IMOC 2007.

10. Jain, A., Li, L., and Yi, A., 2005, 'A Collaborative Research in Experimental Study and Numerical Simulation of Compression Molding of Precision Glass Optical Elements', ASPE Annual Meeting, Norfolk, VA, October 9-14, 2005.

11. Yi, A., and Chen, Y., 2008, 'Numerical Simulation and Experimental Study of Residual Stresses in Compression Molding of Precision Glass Optical Components', Journal of Manufacturing Science and Engineering, October 2008, Vol. 130.

12. Yi, A., and Jain, A., 2005, 'Compression Molding of Aspherical Glass Lenses-A Combined Experimental and Numerical Analysis', Journal of the American Society, Vol. 88, No. 3, Pages 579-586, 2005.

13. Jain, A., and Yi, A., 2005, 'Numerical Modeling of Viscoelastic Stress Relaxation During Glass Lens Forming Process', Journal of American Ceramic Society, Vol. 88, No. 3, Pages 530-535, 2005.

14. Zhao, W., Chen, Y., Shen, L., and Yi, A., 2009, 'Refractive Index and Dispersion Variation in Precision Optical Glass Molding by Computed Tomography', Applied Optics, Vol. 48, No. 19, Pages 3588-3595, 1 July 2009.

15. Yi, A., 2008, 'Economically Feasible Net Shape Manufacturing of Micro and Macro Glass Optics', Proceedings of 2008 NSF Engineering Research and Innovation Conference, Knoxville, Tennessee.

16. Deegan, J., 2007, 'Precision Glass Molding Technical Brief', Rochester Precision Optics, March 2007.

17. Su, L., Chen, Y., Yi, A., and Klocke, F., 2008, 'Refractive Index Variation on Compression Molding of Precision Glass Optical Components', Applied Optics, Vol. 47, No. 10,Pages 1662-1667, 1 April 2008.

18. Chen, Y., Yi, A., and Yao, D., 2008, 'A reflow Process for Glass Microlens Array Fabrication by use of Precision Compression Molding', Journal of Micromechanics and Microengineering, Vol. 18, 2008.

19. Zhao, W., Chen, Y., and Shen, L., 2009, 'Investigation of the Refractive Index Distribution in Precision Compression Glass Molding by use of 3D Tomography', Measurement Science and Technology, Ver. 20, No. 5, 2009.

20. Yang, C., Yi, A., Fritz, K., and Guido, P., 2007, 'Manufacturing of Glass Diffractive Optical Elements by use of Precision Compression Molding Process', Proceedings of the ASME International Manufacturing Science and Engineering Conference 2007, Pages 191-196.

21. Tohme, Y., 2008, 'Glass Molding Machine Phase 2', Moore Precision Tools Nanotech Systems, Keene, New Hampshire.

22. Dixon, J., 1995, 'Engineering Design and Design for Manufacturing', Field Stone Publishers, Conway, Massachusetts.

23. Taguchi, G., and Konishi, S., 'Orthogonal Arrays and Linear Graphs', American Supplier Institute, 1987.